5-2009

The mechanical characterization of polymeric sandwich materials for marine applications

Akawut Siriruk
University of Tennessee

To the Graduate Council:

I am submitting herewith a dissertation written by Akawut Siriruk entitled "The mechanical characterization of polymeric sandwich materials for marine applications." I have examined the final electronic copy of this dissertation for form and content and recommend that it be accepted in partial fulfillment of the requirements for the degree of Doctor of Philosophy, with a major in Civil Engineering.

Dayakar Penumadu, Major Professor

We have read this dissertation and recommend its acceptance:

Accepted for the Council:

Carolyn R. Hodges

Vice Provost and Dean of the Graduate School

(Original signatures are on file with official student records.)

To the Graduate Council:

I am submitting herewith a dissertation written by Akawut Siriruk entitled "The Mechanical Characterization of Polymeric Sandwich Materials for Marine Applications." I have examined the final electronic copy of this dissertation for form and content and recommend that it be accepted in partial fulfillment of the requirements for the degree of Doctor of Philosophy, with a major in Civil Engineering.

Dayakar Penumadu
_____
Major Professor

Y. Jack Weitsman
_____
Co-advisor

We have read this dissertation
and recommend its acceptance:

Edwin G. Burdette
_____

John Landes
_____

Accepted for the Council:

Carolyn R. Hodges
_____
Vice Provost and
Dean of the Graduate School

THE MECHANICAL CHARACTERIZATION OF POLYMERIC SANDWICH MATERIALS FOR MARINE APPLICATIONS

A Dissertation
Presented for the
Doctor of Philosophy
Degree
The University of Tennessee, Knoxville

Akawut Siriruk

May 2009

DEDICATION

I dedicate this dissertation to my parents, Dr. Pisit and Kultanee Siriruk, and my brother, Pavee Siriruk, for their unending love, support, and encouragement. Together they have inspired me to live a life with integrity.

ACKNOWLEDGEMENTS

My heartfelt thanks and deepest appreciation go to my advisor, Dr. Dayakar Penumadu, and co-advisor, Dr. Jack Y. Weitsman, for their guidance, patience, and support throughout the course of my study. Many thanks indeed for giving me the opportunity, many wonderful ideas, and invaluable knowledge. Their expertise and superb abilities as researchers and professors are widely known. No need to say how proud I am to have had the privilege of being one of their students. My wholehearted thanks also go to the distinguished members of the Committee, Dr. John Landes and Dr. Edwin G. Burdette, for showing me the way in the course of my study and taking time off of their busy schedules to review this dissertation. Many hearty thanks go especially to Dr. Edwin G. Burdett for admitting me to this program and kindly introducing me to Dr. Penumadu.

I am most thankful also for the unwavering support from my family, especially my brother, Pavee, who I believe successfully makes a better academic person out of me.

I would like to express my gratitude to several other people, especially Ken Thomas, and Larry Roberts for providing material support and the equipment needed to carry out my research projects. Without their inestimable assistance, my experiments would not have been possible. Many sincere thanks, of course, go to my beloved friends and colleagues, including Alan Tackie, Curtis Nordin, David Lane, Lungui Li, Matthew Kant, Peng Zhu, Robin Woracek, and William Ragland for always being there when I need them to discuss problems, help with research, and bolster the bonds of friendship. Together they

make graduate study a memorable experience. Lastly, my profound and heart-to-heart thanks, of course, go to Anupont Thaicharoenporn, Panya Klongassornkul, Pannatorn Boonmahitisud, and Patara Hongladarom for being such good company that makes my postgraduate years as educational and challenging as they are entertaining. Their genuine friendship and moral support are much appreciated.

This project is supported by the Office of Naval Research (ONR), which is managed by Dr. Yapa Rajapakse. Testing materials are kindly made available by Dr. K.N. Shivakumar of North Carolina A&T University. Their support is greatly appreciated.

ABSTRACT

The growing use of foam core composite sandwich structures has increased considerably in order to reduce the costs of acquisition and maintenance and to improve the operational performance for naval vessels.

This study, which is the only one of its kind, focuses on understanding the properties and response of H100 PVC foam and carbon fiber vinyl/ester facing sandwich layups to static, dynamic, and cyclic loads in the presence of sea water, moisture, low temperature, and hydrostatic pressure. Several mechanical properties of both component materials have been identified. The degradations induced by sea water on foam, facing and sandwich were investigated, characterized and quantified. These included the Mode I fracture toughness of foam as well as the interfacial delamination fracture toughness at the foam/facing interface.

In addition, the thermal properties of foam and facings were investigated as well as the effects of cryogenic temperatures. This dissertation presents several novel experimental techniques and computational schemes.

TABLE OF CONTENTS

LIST OF TABLES

LIST OF FIGURES

Figure **Page**

CHAPTER 1

INTRODUCTION

The understanding of the behavior and properties of materials underpins most major technology. Of especial importance are material properties such as strength, stiffness, and thermal conductivity, as well as hygrothermal expansion, creep, and failure mechanisms.

For naval applications, one particularly interesting approach is to investigate the effects of sea water on composites, such as sorption processes and water induced swelling as well as possible sea water induced degradations. Sandwich composite structures have unique advantages offering high strength to weight ratio, excellent insulation properties, low water absorption, and good corrosion resistance. Sandwich structures consisting of carbon fiber facing and polyvinyl chloride (PVC) foam were examined in this study (Shivakumar, Swaminathan, and Sharpe, 2006; Daniel and Abot, 2000). The PVC foam is extensively used as a core material for sandwich lay-up employed in marine, public transportation, and wind energy applications where light weight and high strength are the primary considerations (DERAKANE, 2004). In addition, sandwich structures increase the buoyancy of submersible marine craft and enhance the stability of surface ships by lowering their center of gravity.

This dissertation focuses on the effects of sea water on polymeric facing/foam core sandwich composites since only a limited amount of information is available on this subject.

Since PVC foams are being used for marine craft, they cannot avoid exposure to sea water environment. It was established in a previous work (Li and Weitsman, 2004) that most of the permeated water in foams was confined within a boundary layer adjacent to the exposed surfaces and that this interaction with moisture resulted in expansional strain. This mechanism was estimated to reduce the stiffness and integrity of the foam material. Moreover, the performance of composite structures under immersion and exposure to simulated sea water showed a reduction in its original properties (Ionita and Weitsman, 2007). The water soaked portion of foam can lead to unexpected structural failure and should be carefully evaluated for long term exposure to sea water. To improve the durability and safety of composite structures, the critical properties affected by sea water exposure must be studied.

Any water-induced reduction in the interfacial strength between the different components of the composite sandwich lay-up may lead to the peeling of the facing, which eventually leads to failure. Indeed, the delamination that occurs either at the facing-core interface or within the core material is one of the important structural failures observed during the life span of marine craft (Kolat et al., 2007). Mode I fracture is considered to play a significant role in the failure process (Papanicolaou and Bakos, 1996). In this study, a comparative study regarding fracture toughness (G_c) was investigated to determine the effects of the sea environment and low temperature on its degradation. The defects arising from sea water ingress, as well as from extreme temperatures, can grow and eventually bring about the separation of the facing from the PVC core. An evaluation of this phenomenon is of great importance because such a seperation may lead to the failure

of the entire structure. After the experimental data were corrected, both analytical and numerical approaches were employed to evaluate delamination processes. The deformation and shape distortion of sandwich layups due to the effect of one sided exposure to sea water and temperature are also analyzed in this work.

In view of the specific geometry of the sandwich structure, where both top and bottom fiber-reinforced facings are much thinner than the thickness of the foam core, enabled the assessment of the effect of one sided exposure to sea water by means of the shear lag method (Gin-Boay et al., 1999).

CHAPTER 2

BACKGROUND FOR RESEARCH

The use of composites continues to expand at a rapid pace, and the current study is motivated by novel performance requirements. This study is part of an extensive Office of Naval Research (ONR) program and concerns various aspects of the response of composites to the effects of sea water and temperature. Specifically, this study focuses on sandwich structural components that consist of a 25 mm thick PVC foam core and 1.5 mm carbon fiber reinforced/vinyl ester facings. Novel concepts for measuring the mechanical properties of both foam and facing materials are included.

It is well known that polymers and polymeric composites absorb moisture and fluids from both atmospheric and ocean environments. The purpose of this work is to determine the effects of sea environment on PVC foam and carbon fiber reinforced/vinyl ester facings. For that purpose, specimens were pre-conditioned, as necessary, by immersing them within simulated sea water for predetermined periods of time until reaching saturation. Tensile and torsional tests were employed to establish the basic mechanical properties of the materials at hand. Comparative values were obtained by performing similar tests under dry conditions. Since naval environments vary around the globe, material data were collected over the range of -10 °C to 40 °C, both in the presence and absence of sea water.

It was already established (Li and Weitsman, 2004) that delamination is a critical failure mode occurring in sandwich structures. Therefore, an experimental study was undertaken to determine the interfacial fracture toughness of sandwich composites pre-conditioned with sea water and data compared to results evaluated for the dry state. To quantify the amount of degradation due to sea water, the critical strain energy release rate, G_c, was compared. This comparison utilized both global and detailed finite element method (FEM) techniques, to investigate and compare the values of various G_c against each other.

This study also seeks to verify that shear lag analysis is suitable for determining the extent of deformation in sandwich layups exposed to the expansional effects of sea water. Analytical, numerical, and experimental methods were used to investigate the usefulness of the simplified shear lag method. Another aspect of this study presents a new approach to measuring the shear modulus of PVC foams, a method that turned out to be superior to the technique based on the ASTM C 273 standard. The ASTM device may not be suitable for the testing of the very soft foam core material in shear because it involves a heavy and slanted mechanism that gives rise to friction that could well interfere with the shearing process.

This study also addresses freezing and thawing effects since temperature fluctuations play a significant role in the response of sandwich composite.

2.1 Composite materials

The term “composite” originally arose in engineering to refer to when two or more materials were combined in order to rectify a shortcoming of a particular useful component. Nowadays, the term “advanced composite” means specifically the combination of very strong and stiff fibers embedded within a matrix designed to hold the fibers together. This type of composite combines the very high strength and stiffness of the individual fibers with their coalescence provided by the matrix, resulting in a much greater toughness than would otherwise be obtainable (Kelly, 1994).

The best-known composite materials are designed for high strength, high stiffness, and low weight. Carbon fiber composites, particularly those with polymeric matrices, have become the dominant advanced materials in the aerospace, automotive, and sporting goods industries. The price of carbon has been decreasing since the utilization of polymeric composite in the construction industry, which substantially increased its production volume (Chung, 1994).

It should be borne in mind that uni-directionally reinforced composites are transversely isotropic about the fiber directions, with highly disparate material properties in the longitudinal and transverse directions.

2.2 Sea water and thermal environment

Engineering materials exposed to sea water are subjected to various deteriorating reactions throughout their time life. Chemical reactions that take place in sea water can

be attributed to the sorption of water by the polymeric phase caused by means of ion-ion and ion-water interactions. A comprehensive list of the properties of sea water is available in the literature (Wiesenburg and Little, 1987).

The absorption of sea water in composite materials has been studied intensively in recent years (Mouritz et al., 2004). In several studies (Chung 1994; Kootsookos and Mouritz 2004; Weitsman, 2006) it was shown that sea water absorption leads to a decrease of the mechanical properties of composites or induces damage within. The extent of the above effects depends on the characteristics of the fibers and the matrix materials and, most significantly, on the quality of the interfaces between those components. It is the interface that determines load transfer across the resin and within the composites; therefore, the possibility exists that overall properties may dramatically deteriorate due to environmental exposure, even though both the matrix and the reinforcement individually offer good environmental resistance.

More specifically, the presence of water molecules at the fiber-matrix interface can lead to the diminishing of the chemical bonding that assures the adhesion from fibers to matrix. Such degradation could well be irreversible and strikes at the basic mechanism of fiber reinforcement since it removes the ability of the matrix to transfer load among fibers. The above concerns are of particular importance for applications where composites are immersed in water for long periods. In such a case it is necessary to know if the composites will establish an equilibrated balance with their environment or if will be degraded by it.

Water ingress causes both swelling and plasticization of the resin. In addition, a composite structure consisting of several layers of differing orientations of fiber reinforcement, often with thick resin interlayers, is susceptible to water being trapped in a particular layer or at the interface between layers. This effect may be irreversible because of osmosis, and blistering may result (Tucker and Brown, 1989). To overcome such a problem it is necessary to choose very carefully both the resin materials and manufacturing techniques. The presence of water at the material surface may lower surface energy and promote the growth of micro cracks. Water trapped at the interface may also dissolve certain components of the resin, and an acidic environment is known to degrade glass fibers. Fibers such as the aramid family can absorb considerable quantities of water, and although this does not lead to a deterioration of fiber properties, the resulting swelling of the fibers may be a cause of composite degradation (Upadhyay and Prucz, 1992).

Among other studies it was shown (Adams and Singh, 1995) that immersion in sea water led to a loss of material stiffness. In addition to changes in mechanical properties, modification of other physical characteristics may occur, such as changes in dielectric properties.

The properties of carbon fibers vary widely depending on the structure of fibers. In general, the most important properties of carbon fibers include low density, high tensile modulus and strength, low thermal expansion coefficient, thermal stability in the absence of oxygen up to 3000 ˚C, excellent creep resistance, chemical stability, even when

exposed to strong acids, biocompatibility, low electrical resistivity, availability in a continuous form, and cost that deceases with time. On the other hand, the disadvantages of carbon fibers are their anisotropy in the axial versus transverse directions, low strain to failure, a low compressive strength when compared to tensile strength, a tendency to be oxidized and evaporate upon heating in air above about 400 ˚C, and oxidation of carbon fibers that is catalyzed by an alkaline environment (Chung, 1994).

The degradation of carbon fiber composites under hygrothermal environment conditions is mostly due to the swelling of the polymeric phase and to a decrease in the fiber matrix adhesion. For unidirectional carbon fiber matrix composites, this degradation is essentially confined to the transverse, rather than the longitudinal, properties. The deterioration becomes more severe as the temperature increases. The fatigue resistance is particularly sensitive to moisture, as the fatigue life is significantly lowered even for less than 2% moisture content in epoxy matrix composite (Selvarathinam and Weitsman, 1998).

High temperatures may degrade the mechanical properties of carbon fiber composites due to the oxidation of both matrix and carbon fibers. The extent of degradation is smaller when the fiber matrix bonding is strong, as air could permeate a weak fiber-matrix interface. Among composites with high-temperature polymer matrices, the key to thermal stability is the selection of compatible fibers that afford a strong fiber-matrix bonding; such compatibility is more important than the selection of fibers which are oxidation resistant by themselves. In fact, the degradation in shear strength of carbon

fiber/polyimide matrix composites that follows their exposure to air at high temperature for an extended period of time is not due to the weight loss but rather to changes in fiber-matrix interaction, perhaps caused by small changes in resin composition or by chemical changes at the fiber matrix interface.

The inspection of fiber composites focuses on observing the fiber arrangement and various kinds of defects, as such structural features strongly affect the properties of the composites. These defects may be matrix cracks or voids, fiber cracks, interface cracks (debonding), and delaminations (splitting between lamina and a laminate).

In many circumstances, composite materials are utilized during extreme winter temperatures, under significant temperature transitions over relatively short periods of time, sustaining exposure to freeze-thaw cycles. In order to increase the reliability of the carbon fiber/matrix use, the mechanical behavior of polymeric matrix composites at low temperatures was investigated in this study. Experiment data indicate that tensile strengths were generally higher at cryogenic temperatures than at ambient temperature (Nordin, 2007; Kim et al., 2007). Nevertheless, microscopic examination of the surface morphology showed evidence of degradation within the polymeric phase at cryogenic temperatures (Gates et al., 2003; Kang et al., 2007).

In this study, the basic cryogenic mechanical properties of composites were determined experimentally at various temperature levels as well as under cyclic thermal exposures. It should be borne in mind that in a multi-directionally reinforced laminate, the mismatch in

thermal expansion coefficients has to be taken into consideration, not only between the matrix and fibrous phase, but also between the various individual piles. Altogether, it is necessary to account for the effects of low temperature, material degradation due to temperature cycling, and freeze/thaw of sea water due to cryogenic cycling (Kim et al., 2008).

2.3 Fluid ingress processes

Diffusion is a mechanism which, in the present case, involves the penetration of fluids into solids by a process of random molecular motions. This mechanism is modeled by means of diffusion equations that were first proposed by Fick and elaborated upon by a multitude of other researchers. A detailed explanation is available in several books (e.g. Crank, 1980; Cussler, 1997). It is generally acknowledged that water and moisture penetrate polymers and polymeric composites by a diffusion process. Note, however, that non-Fickian diffusion processes occur rather frequently, which complicate both modeling efforts and the understanding of the role of the water on material degradation, that in many cases may become irreversible. For instance, water ingress can occur by capillary action along the fiber-matrix interface, and some resin system can be dissolved by water.

A more detailed discussion of the classical diffusion equation (Fick's law) is presented in Chapter 6 of this dissertation. At the present stage it suffices to list the fundamental results (Crank, 1980) for the mass of water, M_t, absorbed at time t across a unit surface area of an infinite plate of thickness h, in proportion to the mass of water absorbed at saturation, M_∞, as given by:

$$\frac{M_t}{M_\infty} = 1 - \frac{8}{\pi}\sum_{n=0}^{\infty}\frac{1}{(2n+1)^2}\exp\left[-D(2n+1)^2\pi^2 t/h^2\right] \tag{2.3}$$

Where D denotes diffusivity

For $\frac{Dt}{h^2} < 0.05$, the relationship describing absorption reduces to

$$\frac{M_t}{M_\infty} = \frac{4}{\pi}\cdot\sqrt{\frac{Dt}{h^2}} \tag{2.4}$$

Therefore, it is possible to determine D from early weight-gain data plotted against $\sqrt{t}$. In some cases the simple Fickian model proves inadequate, such as when two plateaus are observed in the absorption curve of mass of water absorbed vs. square root of time or where it is found that the absorption depends on the specimen thickness in manners that differ from those listed above. It is sometimes useful to consider a more complex model of Langmuir type fluid ingress, which is viewed as consisting of two fluid phases, one free to diffuse and the other trapped within the absorbing medium. However, this type of sorption process will not be considered herein.

Environmental exposure can induce various forms of mechanical response in composite structure such as internal stress and warping of laminates due to the mismatch of material

parameters between adjacent layers. Fick's model of one-dimensinal diffusion can be used to predict hygrothermal strains of carbon/epoxy laminates at different levels of relative humidity (Chung, Wang, and Tsai, 2008). In an ocean environment, moisture and temperature fluctuations affect the response of polymeric composites in an analogous way and may similarly degrade material properties.

This implies that micro cracks can then grow in the composites due to the different coefficients of water-induced expansion between different orientations of layers.

CHAPTER 3

POLYMERIC FOAMS AND SANDWICH COMPOSITES: MATERIAL PROPERTIES, ENVIRONMENTAL EFFECTS, AND SHEAR-LAG MODELING

This chapter is a slightly revised version of a paper with the same title accepted for the Journal of Composites Science and Technology in 2008 by Akawut Siriruk, Y. Jack Weitsman, and Dayakar Penumadu:

Siriruk, A., Weitsman, Y.J., and Penumadu, D. "Polymeric foams and sandwich composites: Material properties, environmental effects, and shear-lag modeling." *Composites Science and Technology*
In Press, Corrected Proof doi:10.1016/j.compscitech.2008.02.034.

Abstract

Marine composite sandwich structural materials comprising of low density PVC foam core and vinyl ester based resin composite facings with carbon fiber are studied for associated degradation in mechanical behavior with a sea water environment. This paper presents experimental and analytical results concerning the properties and response of closed cell polymeric foams (PVC H100) and their sandwich composites. Data regarding the elastic properties of foam (shear and Young's modulus) are collected by means of novel custom made devices and interpreted by means of displacement based analytical models. Emphasis is placed on environmental effects and a novel approach of using

expansional strain analogy to study the effects of both sea water and temperature is proposed.

It is shown that the custom-made shear testing apparatus employed herein offers a significant improvement over the device recommended by ASTM. Using torsional testing, the values of shear modulus in the water-saturated outer shell of soaked foam samples are obtained, and they show a degradation of 72% with long-term exposure to sea water.

***Keywords**:* A. Polymer-matrix composites, B. Mechanical Properties, C. Modeling, D. Torsional Testing, E. Resin Transfer Molding

3.1 Introduction

The utilization of sandwich structures in naval craft is of current interest to the US and several European navies. Their light weight lowers the center of gravity of naval vessels when incorporated in the super structure and similarly increases the buoyancy of submersibles.

Exposure to sea ambience induces environmental effects into both polymeric facings and polymeric foams. It has been already established in earlier works that the ingress of sea water is essentially confined to the outer, exposed, facing of the sandwich structure and to just a few adjacent cells of the foam core (Li and Weitsman, 2004; Ionita and Weitsman, 2007). Similarly, it was found that the effect of exposure to external temperature remains delimited to the outer facings for a significant time due to the high thermal insulation

provided by the foam. Consequently, both foregoing environmental effects induce an essentially one-sided expansion into the sandwich lay-up that tends to distort its shape. Though both temperature and sea water reduce the foam's moduli, this effect is not considered herein due to the insignificant role of the foam material in resisting the above distortions.

The effects of sea water on mechanical properties, which are most pronounced within the cellular foam, were investigated experimentally by means of custom made shear apparatus and test specimens. It was shown that the shear testing device proposed herein has several significant advantages over that recommended by ASTM (ASTM C 273). The experimental settings followed herein are guided by an elementary shear-lag analyses, which proved to be in good agreement with FEM computational values. Comprehensive presentations of the shear lag method can be found in two textbooks (Kuhn, 1956; Megson, 1999).

The main advantages of the shear-lag formulation are that they provide a direct means for dimensional scaling and demonstrate the presence of a straightforward analogy between one-sided loading and one-sided environmental exposure. It is also worth noting that the effects of hydrothermal exposure were discussed by Frotig (Frostig, 1997), though - in the absence of data - it was assumed that water was uniformly distributed within the core domain. Such an assumption, which is contradicted by experiments, also disregards the ensuing bending caused by environment.

3.2 Elementary consideration of the shear-lag model and some FEM comparison

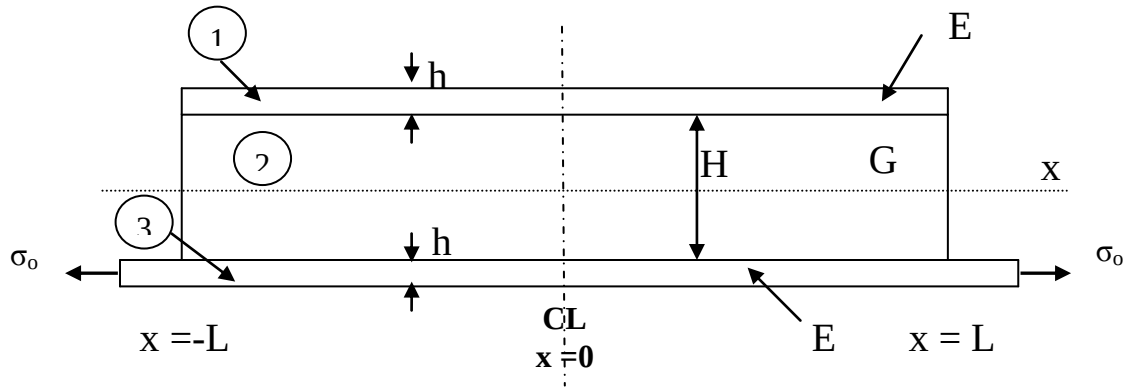

Figure 3.1: Configuration for tensile loading on bottom facing "3".

Consider the sandwich layup and loading shown in Figure 3.1, where *E* denotes the Young's modulus of the facing regions "1" and "3" and *G* is the shear modulus of the core material in region "2". Let σ_i and u_i (i = 1,3) denote the normal stresses and displacements parallel to the x axis, in regions "1" and "3", respectively, and τ the shear stress in the core material in region "2". The well known shear lag formulation (Cox, 1952; Camps et al., 2000) for the present case is given by:

$$h\frac{d\sigma_1}{dx} = -h\frac{d\sigma_3}{dx} = \tau \tag{3.1}$$

$$\tau = G\frac{u_1 - u_3}{H} \tag{3.2}$$

$$\sigma_i = E\frac{du_i}{dx} \qquad i = 1,3 \tag{3.3}$$

Straightforward manipulations of the foregoing expression yield

$$\begin{pmatrix}\sigma_1\\ \sigma_3\end{pmatrix} = \frac{\sigma_o}{2}\left(1 \mp \frac{\cosh\alpha x}{\cosh\alpha L}\right) \tag{3.4}$$

where $\alpha^2 = \dfrac{2G}{hHE}$

The disparity between σ_1 and σ_3 will cause a bending moment

$$M \cong \sigma_3 - \sigma_1 \; hH = \sigma_o hH \frac{\cosh \alpha x}{2 \cosh \alpha L} \tag{3.5}$$

Since $E >> G$ and $H >> h$, the moment of inertia of the sandwich layup is

$$I \approx 2h\left(\frac{H}{2}\right)^2 = \frac{1}{2} hH^2$$

Thus, the out of plane displacement, v, is obtained from

$$\mathrm{v}'' = \frac{M}{EI} \cong k^2 \cosh \alpha x$$

where $k^2 = \dfrac{\sigma_o}{EH \cosh \alpha L}$

Symmetry and boundary conditions require that v′ (0) = 0 and v (±L) = 0. Hence

$$\mathrm{v} = -\frac{k^2}{\alpha^2}(\cosh \alpha L - \cosh \alpha x) \tag{3.6}$$

and $$\mathrm{v}(0) = -\frac{k^2}{\alpha^2}(\cosh \alpha L - 1) \tag{3.7}$$

The strain ratio at the center of the panel, as given by shear lag alone, is

$$r = \frac{\varepsilon_1(0)}{\varepsilon_3(0)} \sim \frac{\cosh \alpha L - 1}{\cosh \alpha L + 1} \tag{3.8}$$

while, upon including bending, it is given by

$$r = \frac{\dfrac{\sigma_o}{2} - \dfrac{M(0)}{I}\left(\dfrac{H}{2} + h\right)}{\dfrac{\sigma_o}{2} + \dfrac{M(0)}{I}\left(\dfrac{H}{2} + h\right)} \tag{3.9}$$

The aforementioned results are amenable to experimental and computational verification.

Accordingly, a finite element analysis employing ABAQUS CAE software was used to verify the stress distribution in the aforementioned sandwich layup. As may be seen from Figure 3.2 a finer mesh was used over the much stiffer upper and lower facing (regions "1" and "3") in order to better capture the stress variation. The mesh used in this analysis consisted of 8-node biquadratic quadrilateral elements (CPEG8R) in 2D for all regions and a state of plane strain was assumed to hold in this analysis with simply supported conditions $u_y = 0$ at $x = L$ and $u_x = u_y = 0$ at $x = -L$.

The following value were employed in both analytical and numerical calculations we employed the following values G_{core} = 25 MPa, E_{facing} = 80 GPa, h = 1.5 mm, H = 25.4 mm, $2L$ = 350 mm and P = 40 MPa.

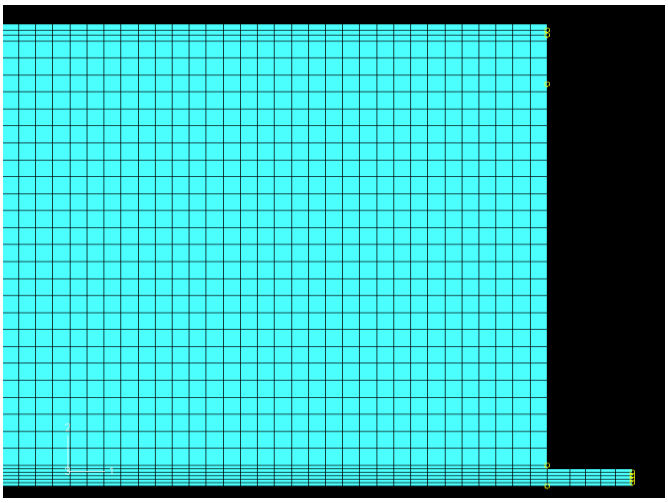

Figure 3.2: ABAQUS CAE finite element mesh utilized in the computation.

A very good agreement was obtained for the value of the central for the deflection Δ between those predicted by expression (3.6) and the FE model, those where Δ = 0.3 mm and 0.27 mm respectively. Eqn. (3.8) shows that the axial stresses within the bottom facing were reduced by about 10% from the edge to center of the sandwich beam, which were transferred through shear to the top layer.

Regarding the strain ratio $r = \frac{\varepsilon_1(0)}{\varepsilon_3(0)}$, it is worth noting that the FEM calculation yielded a value of 0.02, while the analytical Eqns. (3.8) and (3.9) gave r = 0.11 and r = 0.06, respectively. The range of experimental data falls within the above values. Data scatter can be attributed to variability in the facings' thicknesses.

Note also that within the foam layer the maximal value of the shear stress was τ = 0.07 MPa, while that of normal stress was σ = 0 (1) Pa. Both those values were much smaller than their corresponding values at failure, namely $\tau_f = 1.4\,\text{MPa}$ and $\sigma_f = 2\,\text{MPa}$. The reason for the exceedingly small value of the normal stress is that in the loading in the current problem acts in plane.

3.3 The expansional strain analogy for environmental effects

As noted earlier, experimental evidence suggests that, when exposed to external environment, sandwich layups undergo a one-sided expansion for substantial time durations. Consider the same geometry as in Figure 3.1 but instead of the applied stress

σ_o let the lower facing be subjected to an expansional strain e_o, which may be due to the ingress of water or to the effect of temperature under one-sided exposure.

The analysis follows the same steps outlined in expressions (3.1) through (3.6), except that Eqn. (3.3) is replaced by

$$\sigma_1 = E\frac{du_1}{dx}, \text{ while } \sigma_3 = E\left(\frac{du_3}{dx} - e_0\right) \tag{3.3a}$$

where the expansional strain e_o is considered to be constant. It can be readily shown that expression (3.4) through (3.9) remain valid by replacing σ_o with $E\varepsilon_o$.

It is important to note that while experiments to assess the validity of the results predicted in section 2 are simple to conduct, such tests are extremely difficult to perform for one sided environmental exposure. Hence the significance of the analogy.

FEM computations for the same geometry shown Figure 3.1 with $\sigma_0 = 0$, but where uniform internal expansional strain $\varepsilon_0 = \alpha\Delta T$ was distributed along the bottom layer, were performed following the same scheme outlined in the previous section. The values of α and ΔT were 11.5 με/1 °C and 50 °C, respectively. These values correspond to $\varepsilon_o E = 40\,\text{MPa}$ of the previous section. The results for Δ and r were Δ =0.3 mm and r = 0.05, thus agreeing very well with the corresponding values of 0.3 mm and 0.05 for $\sigma = 40\,\text{MPa}$.

3.4 Test fixtures and foam material data

3.4.1 Tensile modulus

It was necessary to employ small amplitude load cells and a special mechanism for load introduction through interfacial shear alone to test foam in tension, in view of its exceedingly low modulus. The details of the specimen design and loading fixture are shown in Figure 3.3 (a, b), with stress-strain data exhibited in Figure (3.3c). These data yielded a value of E = 60 MPa for H100 foam, within the initially linear range. It was nevertheless impossible to record the effect of immersion in sea water on E. As noted earlier, the ingress of sea water into polymeric foams is confined to the near vicinity of the exposed boundaries, thus the major portions of the test samples remained dry after exposure and no significant effect could be detected under tensile loading.

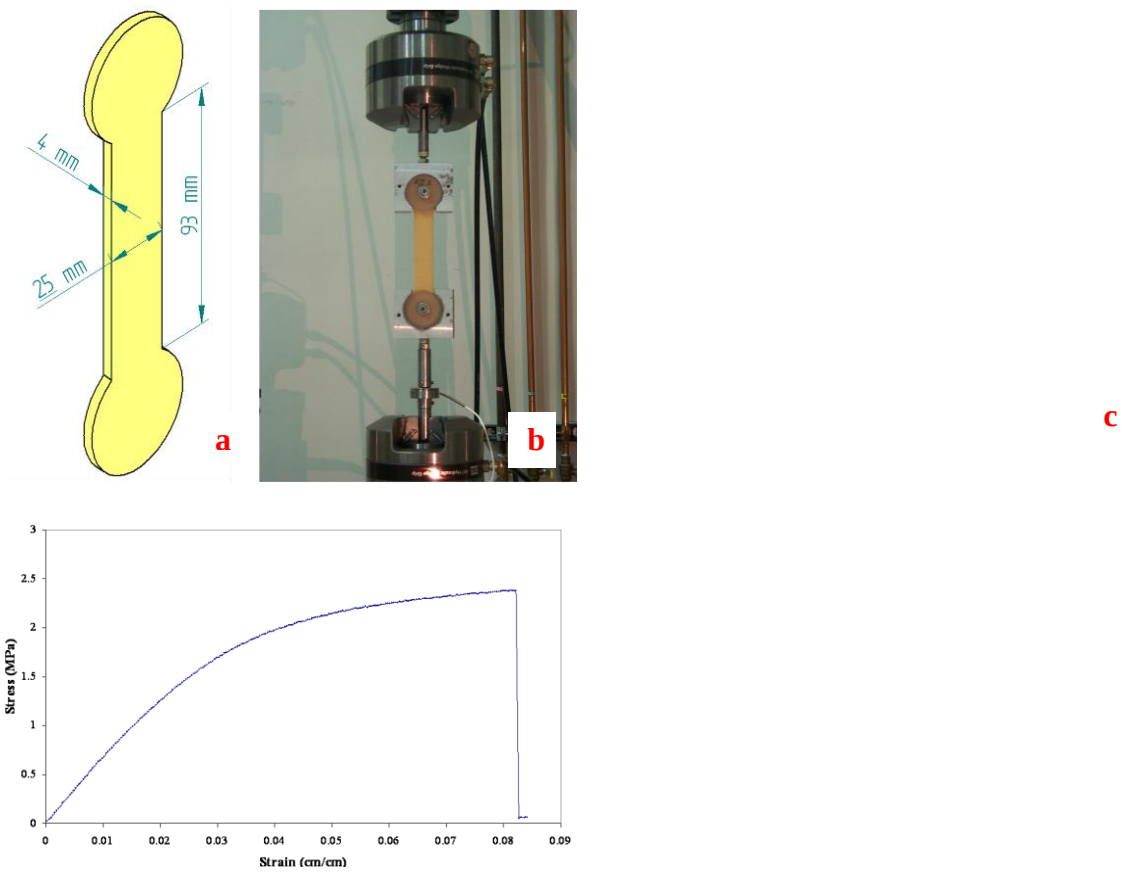

Figure 3.3 a: Specimen shape, b: Loading system in tension,

Figure c: Tensile stress-strain data ($E_{\text{initial.}}$= 60MPa).

3.4.2 Shear modulus

The shear modulus of polymeric foams was tested by means of the custom-made fixture shown in Figure 3.4[①]. The dimensions and materials selected in the design of the fixture were guided by the requirement that dead weight effects should be negligible. Accordingly, aluminum was selected for the yoke material due to its relatively low

① The authors are indebted to Dr. Leishan Chen for suggesting the design of this device.

weight, and the value of the shear modulus G was inferred from the displacements $u(0)$ recorded at the loading point, which was located at the bottom of the device.

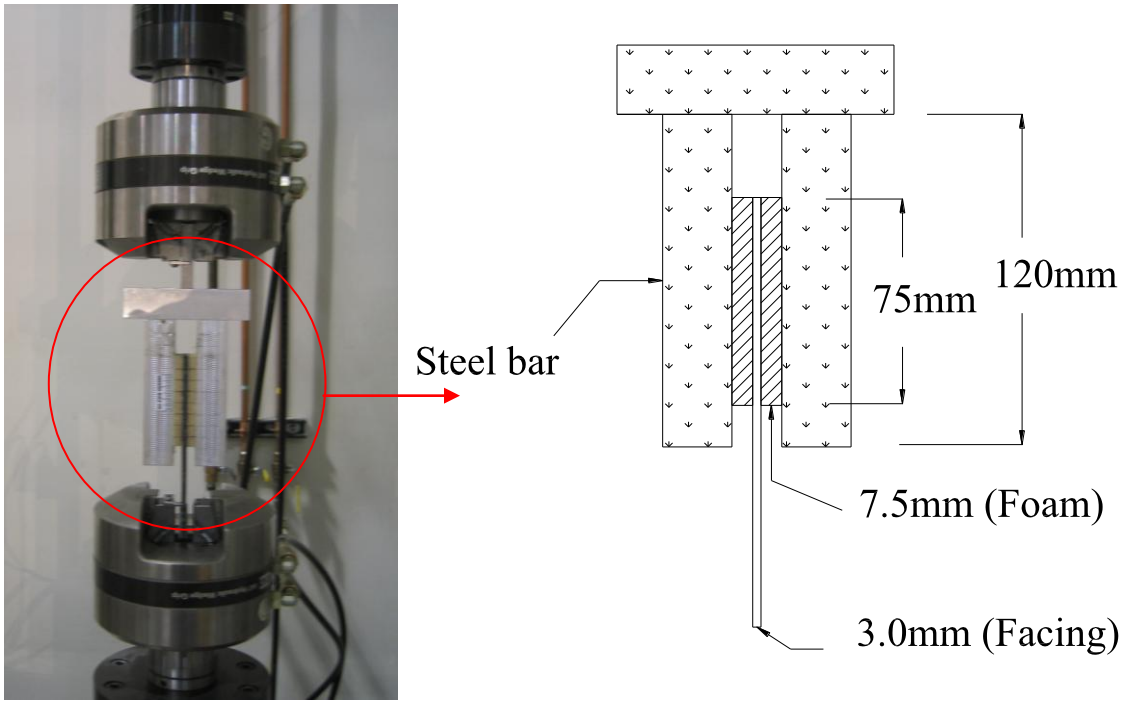

Figure 3.4: Shear modulus experimental set up.

Results are given in Figure 3.5, whereby it was determined that G = 26.5 MPa. Discarding the fact that foams may exhibit a rather slight degree of anisotropy, it was nevertheless assumed that material isotropy holds, thereby yielding a poisson ratio of v = 0.13. Note that direct measurements of v were impossible to conduct.

As can be seen in Figure 3.5, the relation between $\gamma = \frac{u(0)}{h}$ and τ deviated from linearity. It is therefore preferable to utilize the fixture shown in Figure 3.4 rather than that recommended by ASTM (As shown in Figure 3.6). Besides its slanted configuration, the ASTM device also introduces an unavoidable friction due to the several joints involved in the manner of load introduction.

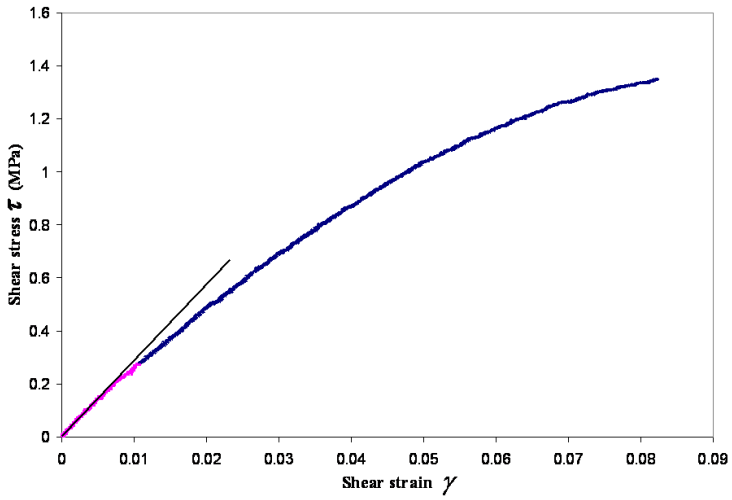

Figure 3.5: Stress-strain data in $G_{initial}$ = 26.5 MPa. (Left)

Figure 3.6: Recommended ASTM shear system. (Right)

3.4.3 Torsional data and effect of sea water

Unlike the circumstance of tension, torsional loading data are much more sensitive to the presence of fluids, since in this case maximal shear strains occur near the outer boundaries of the test sample- where most of the fluid is indeed located. Custom made fixtures were developed to test soft foam samples under large rotations as shown in

Figure 3.7a. A specially designed transducer with a capacity to measure a full-scale range of 0 to 0.7 N-m torque was incorporated within the bottom grip to provide very precise values of torsional shear stress on thin rectangular samples with a thickness of 4 mm.

Torsional test data for rotation θ vs. torque T are shown in Figure 3.7b for dry and saturated samples of H100 foam coupons[*], which can be readily converted to a relation between the shear strain and stress γ and τ. The saturated condition was achieved by immersing the samples in sea water at 40 ˚C for up to three months, at which stage water weight gain reached an equilibrium level. Tests were performed on a MTS 858 torsional testing machine with a 0.7 N-m torsional load cell. It can be noted that the initial shear modulus of the saturated samples was $G_{\text{saturated}}$ 20.4 MPa, a reduction of about 20% when compared to the dry value G_{dry} 24.3 MPa. Note, however, that the aforementioned "saturated" value is obtained for samples with dry interiors.

The initial slopes of the curves shown in Figure 3.7b are 2.04×10^{-3} and 1.71×10^{-3}, respectively. It can be seen that for increasing rotation the above slopes are convex, which agrees with the prediction of finite elasticity theory stating that $G = G(0; \gamma^2)$. The large hysteresis loops observed upon unloading can be attributed to the fact that since the loading mechanism constrains the vertical motion of the grips, they induce compressive stresses in the test coupons. These compressive stresses, that are the bi-product of large twisting rotations, may cause irreversible damage through buckling within the thin walls

[*] Data scatter is noticeable, and varies from batch to batch. The 20% reduction in $G_{\text{saturated}}$ represents the most severe case recorded in several replicate tests.

of the outer cells of the foam, thereby reducing its shear stiffness and resulting in permanent deformation upon total unloading (Ashyby, 2005).

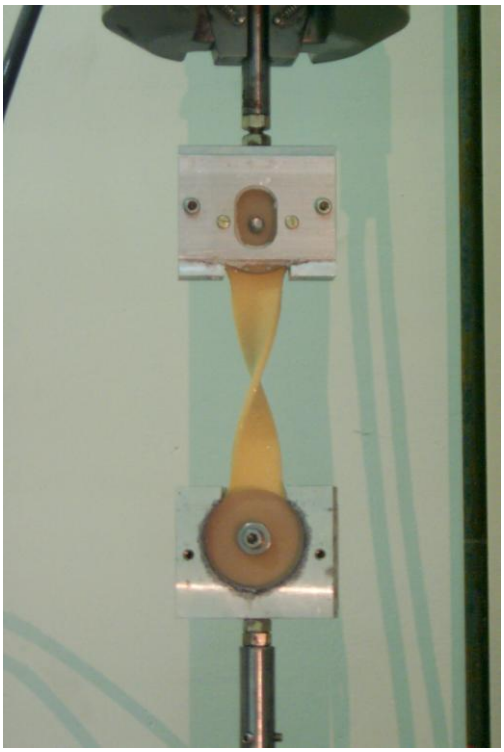

Figure 3.7a: Foam sample undergoing large rotation (Rotary actuator at the top).

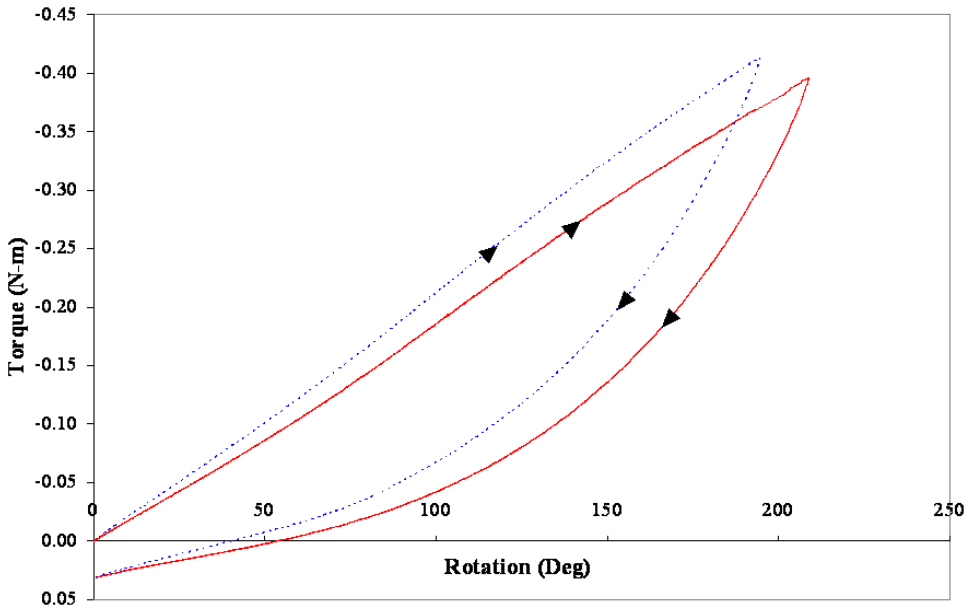

Figure 3.7b: Torque vs. rotation angle for dry (---) and saturated (—) samples.

3.5 Evaluation of wet moduli

Weight gain data on 4 mm thick H100 foam samples of specific weight 0.1 indicated that they absorbed sea water about 1.1 times their dry weight (110%) (Li and Weitsman, 2004). Figure 3.8 shows that most of the fluid was concentrated in the outer cells.

Desorption data collected from 2 mm thin slices in the interior of a $(25\ mm)^3$ foam cube subsequent to its saturation are shown in Figure 3.9. Accordingly, the interior region absorbs about 4 % of sea water, thereby implying an enhanced foam density of about 0.14 g/cm^3. It has been shown independently that H100 contains a certain degree of porosity, which suggests that sea water penetrated the interior region due to its permeability. Diffusion through the polymeric cellular wall is much too slow to account for this phenomenon during the time frame employed herein.

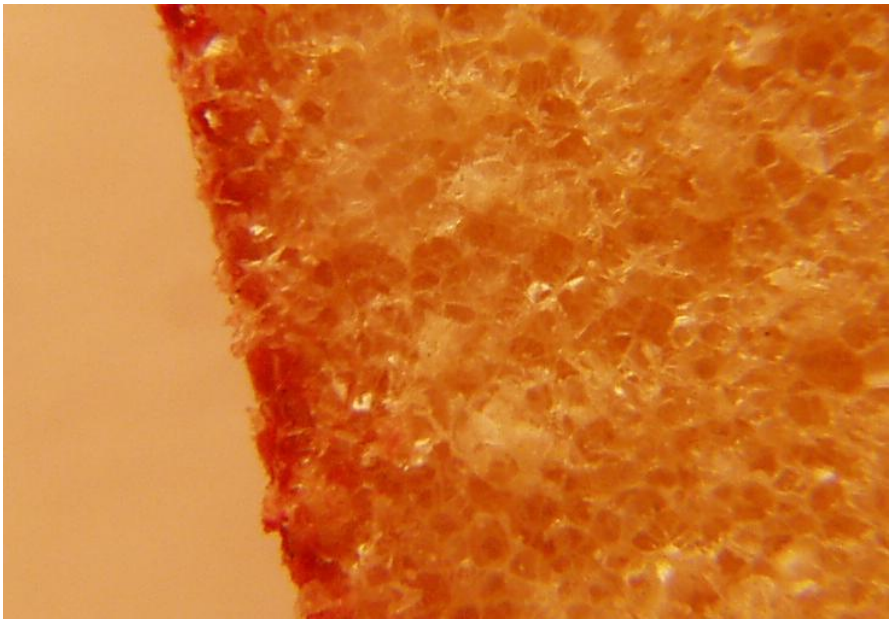

Figure 3.8: A micrograph of an immersed foam, showing that the penetration of sea water remains confined near the exposed boundary after three years of immersion.

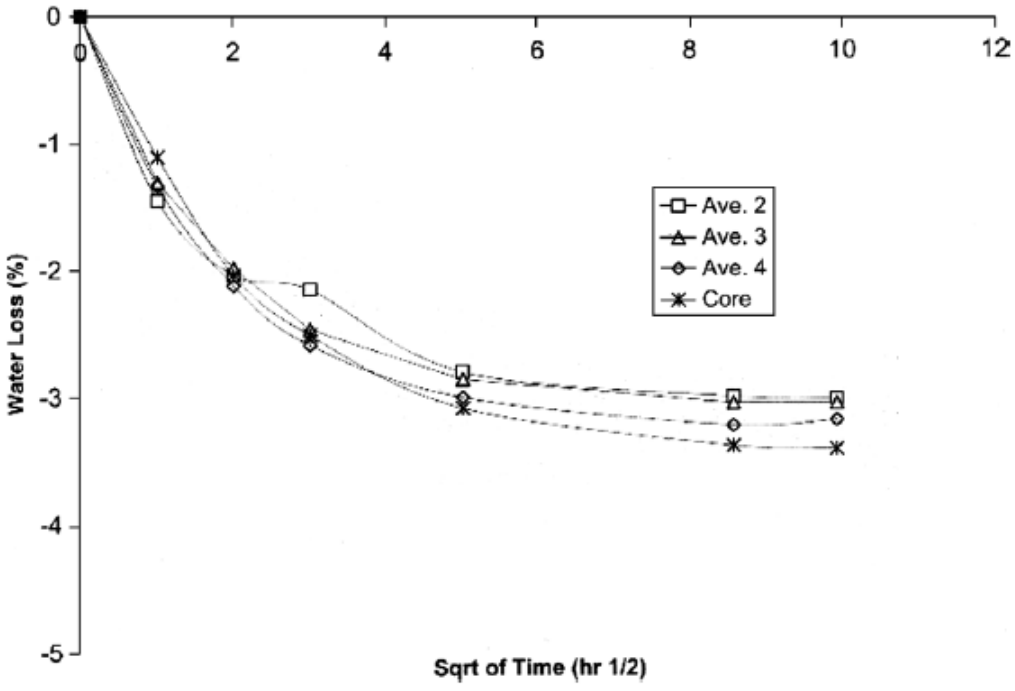

Figure 3.9: Weight loss data for 2 mm thin slices cut from interior layers of a $(25\ mm)^3$ H100 foam. (Number indicate slice location away from exposed surface)

The above observations enable the assessment of the average thickness δ of the water filled outer layer, where most of the fluid is concentrated. Let h denote the coupon's thickness; it follows that $\frac{2\times 1.1\delta_T + 0.14(h-2\delta_T) - 0.1h}{0.1h} = 1.1$. Thus, δ_T ~0.145 mm.

With δ_T at hand, it is possible to employ the dry and saturated torsional data to assess the wet shear modulus of the foam G_w.

For this purpose, consider the geometry shown in Figure 3.10, where all dimensions and materials properties are known, except the shear modulus G_w of the outer wet regions. This is done by employing the well-known expression relating the torsional behavior of a solid rectangular section of height D and width W and a similar relationship for a hollow rectangular tube of the same outer dimension and thickness δ_T (Timoshenko and Goodier, 1951).

These are $\left[\frac{M_T^{(s)}}{\theta}\right]_{solid} = \frac{1}{3}H_s h_s^3 G_s$ and $\left[\frac{M_T^{(o)}}{\theta}\right]_{hollow} = \frac{4A^2 G\delta}{L}$ (3.10)

where $A = (D-\delta_T)(W-\delta_T)$ and $L = 2(D+W-2\delta_T)$

Let the saturated sample consist of an inner, essentially dry, core of modulus G and dimensions $H_s = D - 2\delta_T$ and $h_s = W - 2\delta_T$. This core is encased within a thin saturated tube of thickness δ_T and the yet unknown "wet modulus" G_w.

Denote by R the ratio $\left(\frac{M_T}{\theta}\right)_{dry} \Big/ \left(\frac{M_T}{\theta}\right)_{wet}$. One obtains

$$R = \left(\frac{H_s}{D}\right)\left(\frac{h_s}{W}\right)^3 + \frac{12A^2\delta_T}{LDW^3}\frac{G_w}{G_{dry}} \tag{3.11}$$

For D = 25 mm, W = 4 mm, δ_T = 0.145 mm, H_s = 24.71 mm and h_s =3.71 mm and with $R = \frac{1.71}{2.04} = 0.838$. It follows that $G_w \sim 0.28G = 7.3\,\text{MPa}$.

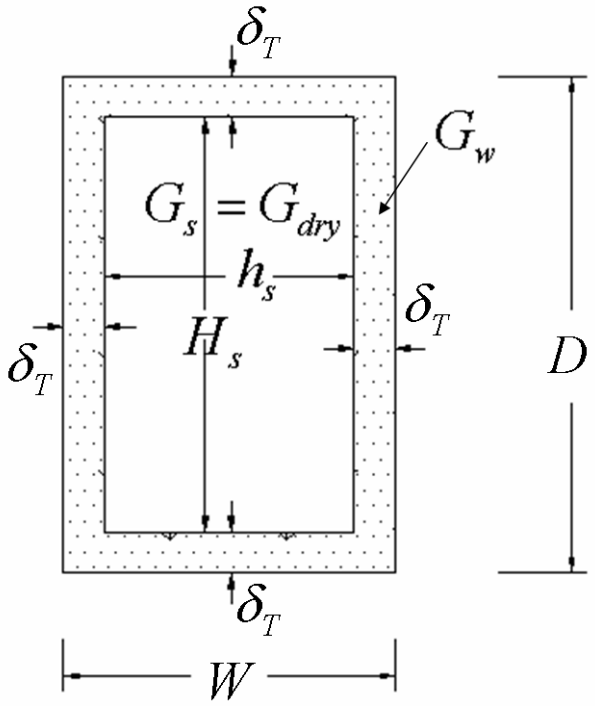

Figure 3.10: A sketch of the cross section subjected to torsion.

Note that G_{dry} and the overall torsional resistance are experimentally determined.

The only unknown is G_w of the saturated region.

Due to the incompressibility of water, it is reasonable to assume $\nu_w = 0.5$ for the fully saturated foam hence $E_w \sim 22\,\text{MPa}$. This explains why with the aforementioned value of the wet and dry tensile data are indiscernibly close to each other, falling within data scatter. The aforementioned values of G_w and E_w are required for the evaluation of the fracture energy at the foam/facing interface when exposed to sea water.

3.6 Moisture shrinkage and thermal expansion of H100 PVC foam

The purpose of this part is to evaluate the hygrothermal effects from sea water on deformation and damage of sandwich layups and on closed cell polymeric foams. This is part of ongoing research to evaluate the effect on sea water induced property degradation for composite facings and foam core material after a pre-determined amount of time soaking. The experiments involved the measurement of reliable data related to the diffusion of temperature and corresponding thermal strain across the thickness of polymeric sandwich materials. Experimental results associated with the effect of physical aging for these polymeric composites are also considered for the interpretation of data associated with specimens subjected to extended periods of soaking

A foam specimen with 4mm in thickness was soaked in sea water at 40 °c for 4 months to reach a saturated state. Specimens of rectangular dimension of 25 mm × 67 mm were attached to an extensometer then desiccated for the duration of about 200 hours necessary to reach an equilibrium state.

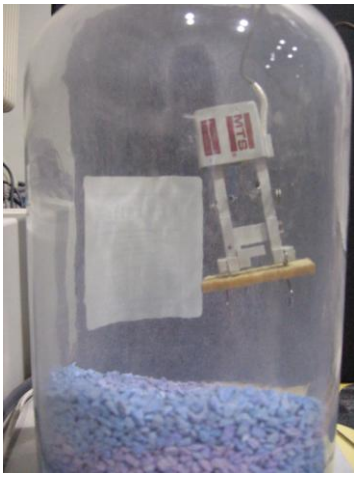

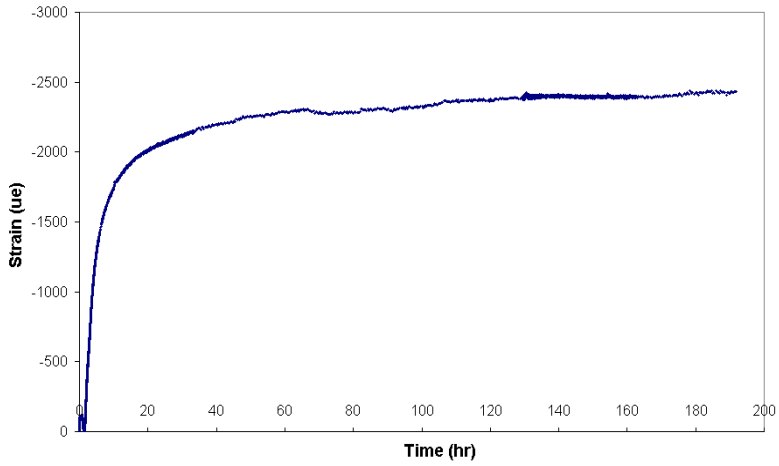

Figure 3.11: Experimental setup; Fig. 3.12: Typical shrinking strain data (με) vs. time (hr)

Shrinkage strains caused by the withdrawal of sea water from the pre-saturated foam were recorded during drying means of extensometer, resulting in ε_H = 2200 με at saturation. It was assumed that this value corresponds to that of the expansional strain as well.

The experimental investigation of thermal properties consisted of measuring the thermal conductivity and linear expansion coefficient of the foam. Data were obtained by employing a novel technique that uses transient plane thermal source input with

equipment obtained from HotDisk®. In addition, a unique experimental setup was developed to obtain temperature measurements at various locations across the thickness of a sandwich lay-up as shown in Figure 3.13.

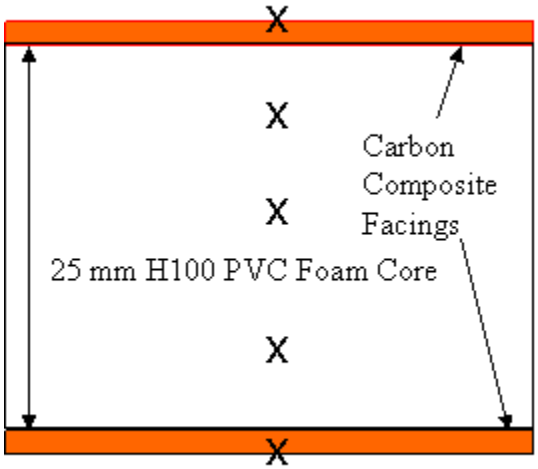

X Thermocouple Locations

Figure 3.13: Layout of thermocouples places across the thickness.

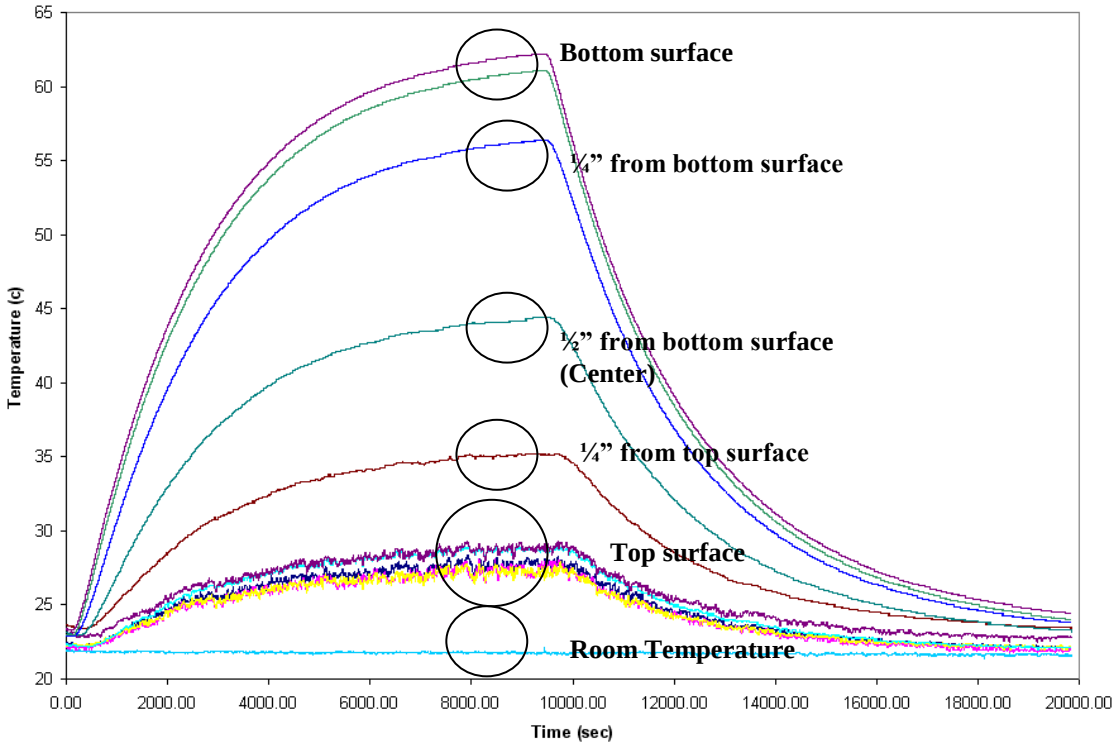

Figure 3.14: Temperature variation across the thickness.

Figure 3.14 shows the results from a typical test with bottom facing exposed to a temperature increase from room temperature to approximately 63 °C. The data indicate a non-linear increase of temperature as heat diffuses through the thickness from bottom to top of the sandwich structure. It is very significant to note that using the aforementioned experimental set up corresponds to realistic interfacial bonding of PVC foam core and carbon fiber/vinyl ester composite facing consequent to a VARTM process, thus providing on-site thermal diffusion data for ship structures. These data, together with those for the thermal expansion coefficients reported later, enable to computation of anticipated strains and corresponding stresses in sandwich structure for various environmental conditions that is essential for the prediction of geometric distortions and joint stresses of sandwich structures.

Due to inherent variations in PVC foam properties from various batches of manufacturing, it is important to measure the actual linear expansion coefficient of core materials. For that purpose the experimental setup was modified as shown in Figure 3.15. To obtain thermal expansion, 11 thermocouples at different locations were used to interpret temperature data across the thickness and an extensometer was placed directly on PVC foam surface to obtain thermal expansional strains. Five thermocouples were placed on the top surface to record temperatures at various locations surrounding the extensometer. Two thermocouples were used at the bottom surface to obtain data from the heating source, and one thermocouple was used to measure ambient room temperature. Figure 3.15 shows typical temperature data across the thickness and top surface of a foam panel in relation to an increasing temperature input at the bottom surface. The thermal expansion coefficient was determined by means of the temperature data from the five thermocouples that surrounded the extensometer on the top surface. Typical results are shown in Figures 3.16 and 3.17. Thermal conductivity was recorded means of a one sided heating imposed on a 25 mm thick foam slab and a careful recording of temperatures across its thickness vs. time. Thermal expansion was recorded by means of an extensometer. The resulting was $\alpha = 70\ \mu\varepsilon/1^{\circ}C$.

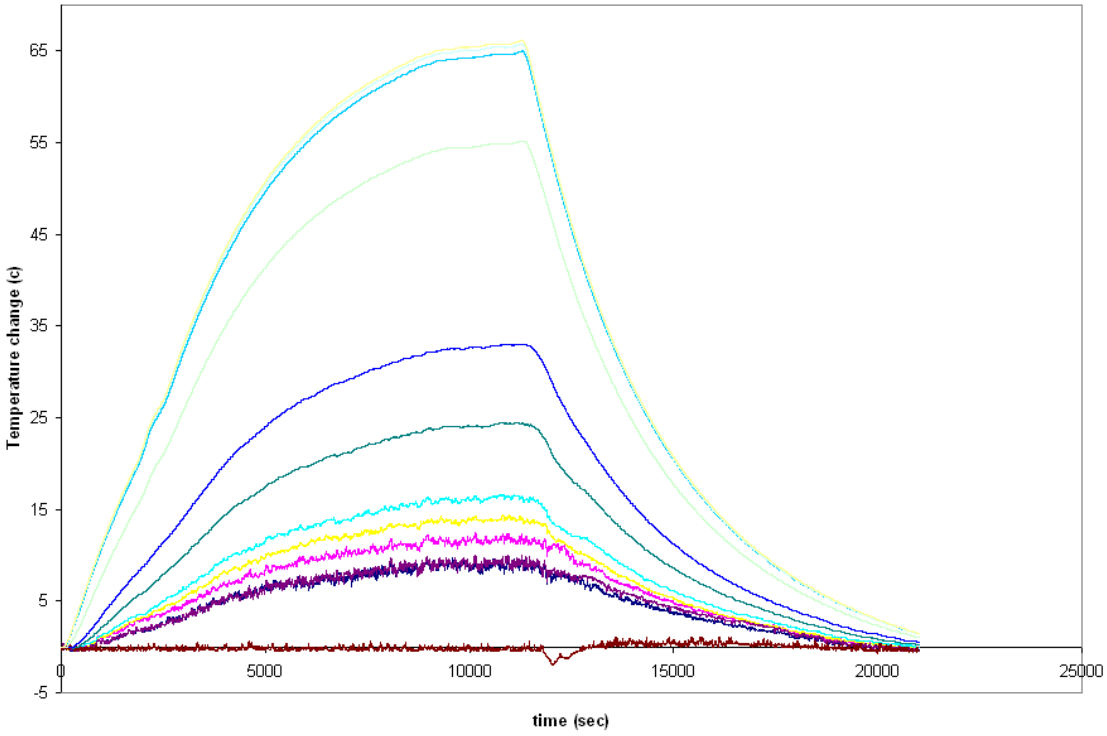

Figure 3.15: Temperature variation along the thickness of 25 mm H100 Foam.

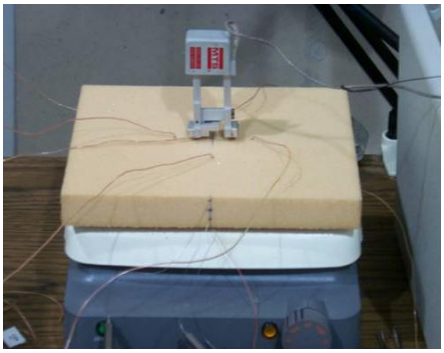

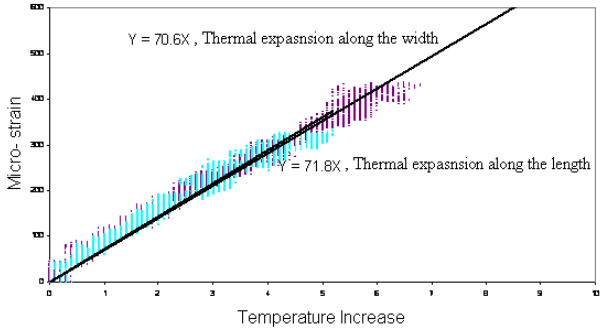

Figure 3.16: Experimental setup for determining H100 foam thermal expansion. (Left)

Figure 3.17: Linear expansion coefficient for H 100 foam for data. (Right)

3.7 Effects of freezing and thermal cycling on mechanical properties

Previous data indicated that the stiffness of 25.4 mm H100 foam panels varies across their thickness. Since these variations may mask the effects of freezing and thermal cycling it was decided that the researchers would test the response of each specific sample under the aforementioned thermal exposure. For this purpose H100 PVC foam specimens were systematically prepared from four 25.4 mm thick foam panels as shown in Figure 3.18. Samples were identified by two letters to represent location followed by a number to account for the across-the-thickness position. Test coupons for both tensile and torsion tests were prepared using the same shape and dimensions as mentioned in section 3.4 and load was introduced through friction over the circular top and bottom faces.

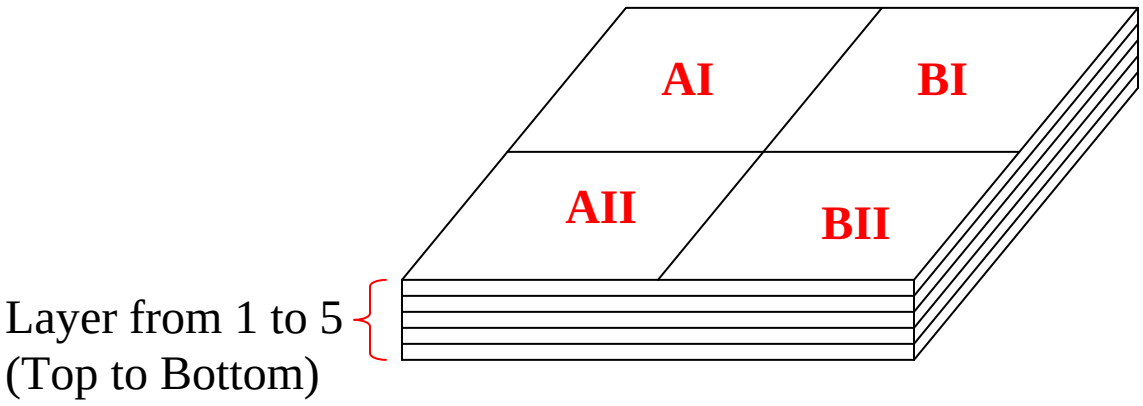

Figure 3.18: Foam panel used for specimen employed in the tensile tests.

3.7.1 Dry, wet, and freezing effects on tensile test

All tensile tests were performed at strain rate of a 0.5 mm/min and up to a peak stress of 0.6 MPa, which is very small compared to ultimate strength. In view of previous experience, each specimen was subjected to preliminary three load/unload cycles to establish a repeatable value of the elastic modulus, E (MPa). Subsequently, each specimen was frozen down to a target temperature in a freezer for a specific period. Detailed stiffness results at ambient temperature are listed in Table 3.1.

Note that stiffness increases consistently towards the middle of the foam panel and varies between 63 and 74 MPa at ambient temperature.

Table 3.1: Values of the tensile E in (in MPa) at the dry state for each layer cut from four panels at room temperature.

Sample layer	AI	AII	BI	BII
1	67.33	67.74	67.55	65.35
2	71.51	72.24	72.86	69.54
3	72.15	73.55	72.39	72.21
4	69.25	70.21	69.57	69.98
5	68.69	69.39	62.83	68.89

Dry AI and BII foam specimens were selected to investigate the effects of cryogenic temperature after freezing down to -5 ˚C for 5 weeks. Figure 3.19 presents the comparative values of the stiffness *E* (MPa), at room and -5 ˚C. It can be seen that exposure to low temperature over period of time does not significantly affect the value of *E*. The minute degradation of *E* falls well within the data scatter caused by foam inhomogeneity.

Foam specimens from the BI location were immersed in seawater for 10 weeks and tested at room temperature to obtain comparative values of $E_{average}$. It was noted that due to data scatter, the sea water seems to cause around **2-3%** degradation in stiffness. Subsequently, those saturated specimens were frozen for 4 weeks and tested in tension to obtain the comparative values of *E*. The data yielded nearly identical values before and after freezing. The overall results are shown in Figure 3.20.

The variability in the values of *E* was even less pronounced between samples tested "dry", "wet" (10 weeks immersion in sea water), and "saturated/frozen" (10 weeks immersion in sea water followed by a 5 week exposure to -5 ˚C). All cases results in 65.4 MPa $\leq E \leq$ 73.6 MPa.

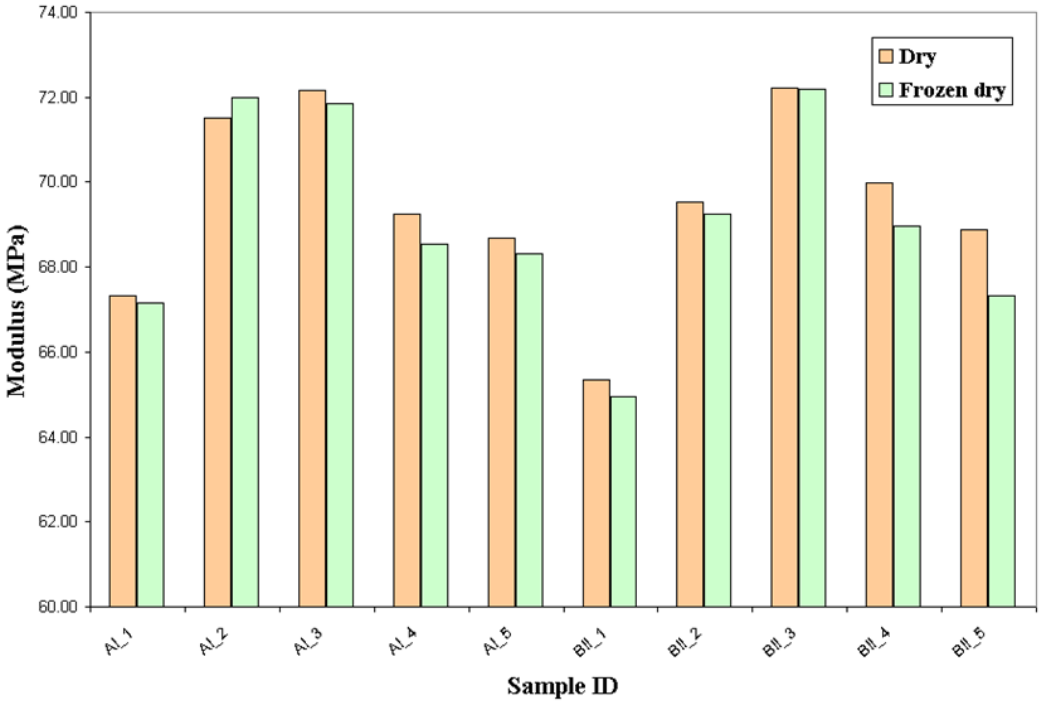

Figure 3.19: Comparative results for foam's modulus degradation (MPa) after 5 week exposure to -5 ˚C.

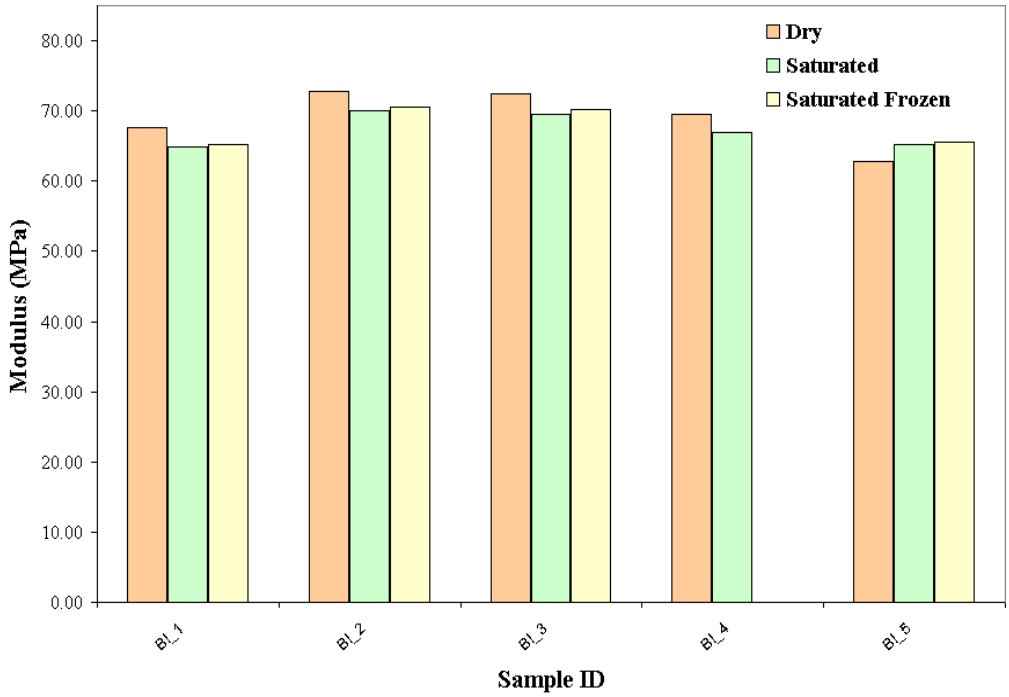

Figure 3.20: Comparison of foam's modulus between dry, saturated, and saturated frozen at -5 ˚C after 5 weeks.

3.7.2 Dry, wet, and freezing effects torsional response

The shear modulus *G* was recorded by means of torsional tests, twisting the sample over the angular range of $-5^{\circ} \leq \theta \leq 5^{\circ}$. The base-line variability ranged between 23.3 MPa $\leq G \leq$ 28.9 MPa tested under torsion at room temperature and, for the same reason noted earlier in section 3.7, it was necessary to establish their reference values. These are listed in Table 3.2. Note again that the highest values of *G* occur at the middle of the foam slab.

Table 3.2: Dry shear modulus from torsional test (MPa) at room temperature for 20 samples cut from adjacent locations.

Sample layer	AIII	AIV	BIII	BIV
1	25.73	24.99	23.15	23.86
2	27.88	27.49	27.74	26.33
3	28.81	28.92	28.41	27.94
4	27.20	27.56	27.69	28.40
5	27.06	27.71	26.55	24.61

Prior to investigating the effects of low temperature and sea water, repeatability was examined on two specimens by conducting 4 sequential tests at 3 load/unload cycles within each sequence[+]. Results shown in Figure 3.21 demonstrate an extraordinary repeatability of torque vs. rotation data. Moreover, the effect of strain rate was also examined on two randomly selected specimens. Rates of 5 deg/min and 10 deg/min were used, again resulting in an excellent repeatability of test data, as exhibited in Figure 3.22.

[+] Note that, unlike the current circumstance, the data shown in Figure 3.7b concerns only one load/unload cycle up to a large rotation of about 200 degree. This fact may account for the discrepancy in the reported differences between the dry and saturated values.

Therefore, the range of $-5^{\circ} \leq \theta \leq 5^{\circ}$ at a rate of 10 degree/min was selected for studying the effects of sea water and low temperature on the shear modulus *G* of H100 foam. Shear modulus values for 10 specimens taken from regions AIII and BIV are shown in Figure 3.23 for dry state. This figure exhibits comparative results for room temperature and subsequent to freezing for 4 and 7 weeks. The testing data fell into a scatter range. Reductions of shear modulus 3-6 **%** were noted after 4 weeks of freezing with no further decrease at 7 weeks.

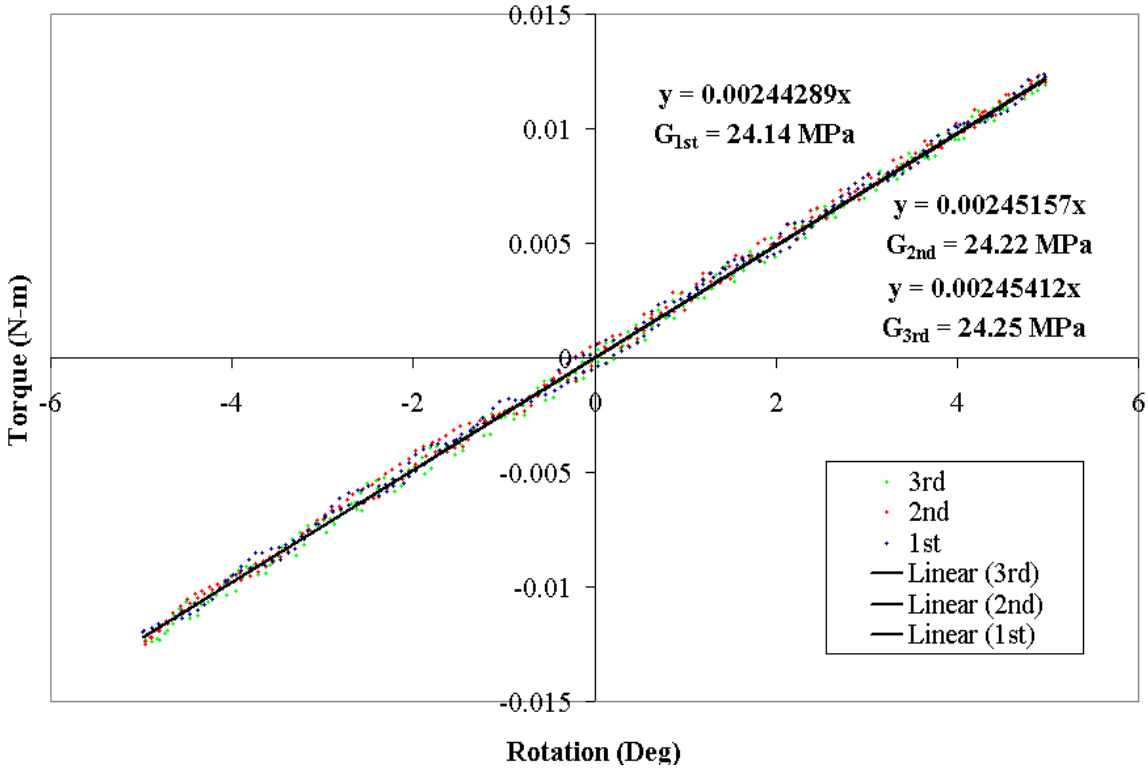

Figure 3.21: Repeatability of typical three cycles of torque vs. rotation test data.

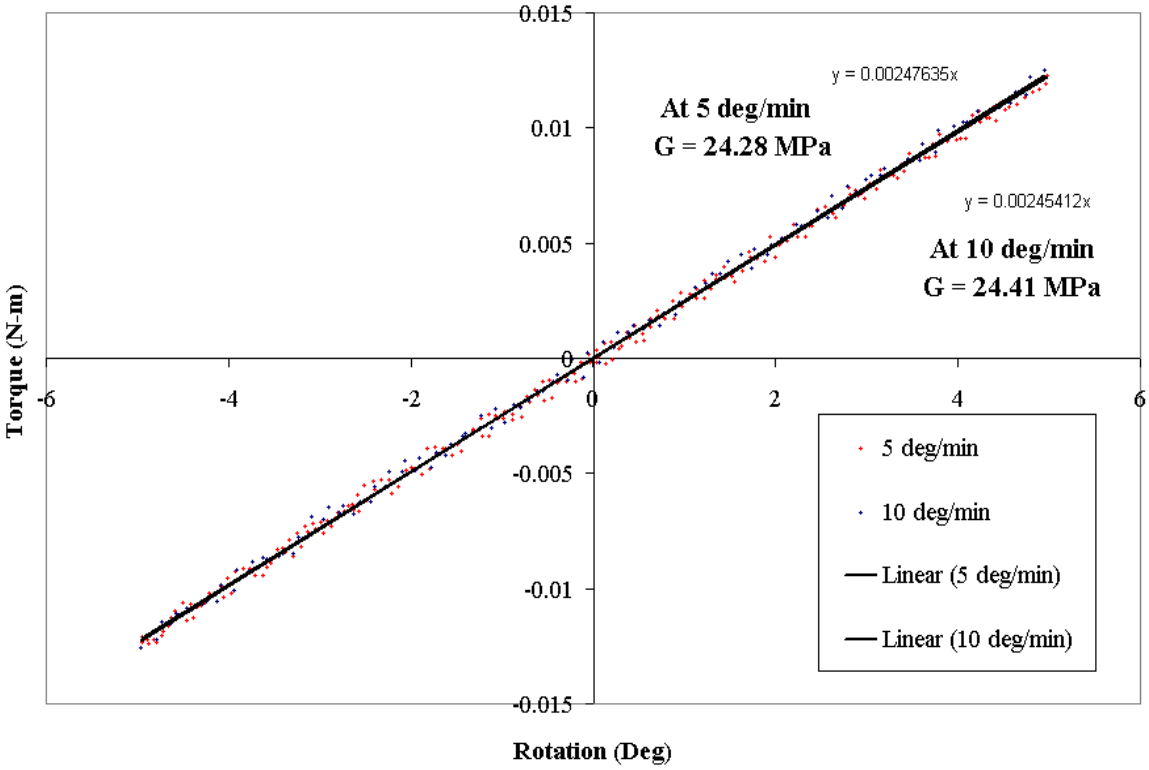

Figure 3.22: Torque vs rotation data at strain rates at 5 and 10 deg/min.

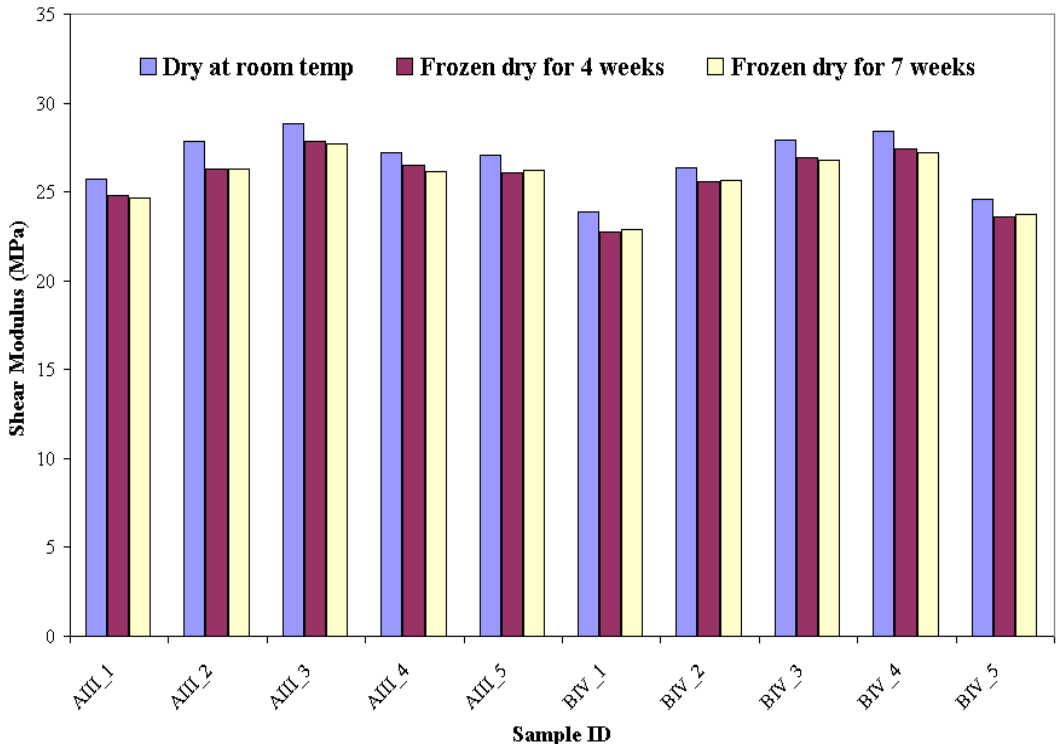

Figure 3.23: The degradation of shear modulus of AIII and BIV

after exposure to low temperature.

Immersion in sea water resulted in an overall reduction of 5% in *G*, though it should be borne in mind that, as noted in section 3.5 this reduction is affected by the presence of sea water that is confined to a region that is approximately 0.2 mm deep along the outer boundary of the specimen in section 3.5 (Li and Weitsman, 2004). Ten specimens from regions AIV and BIII were used to study the combined effects of sea water and low temperature. The overall results, shown in Fig. 3.24, indicate that the 5% decrease in *G* due to immersion is followed by an additional slight decease averaging about 2% after freezing for up to 5 weeks.

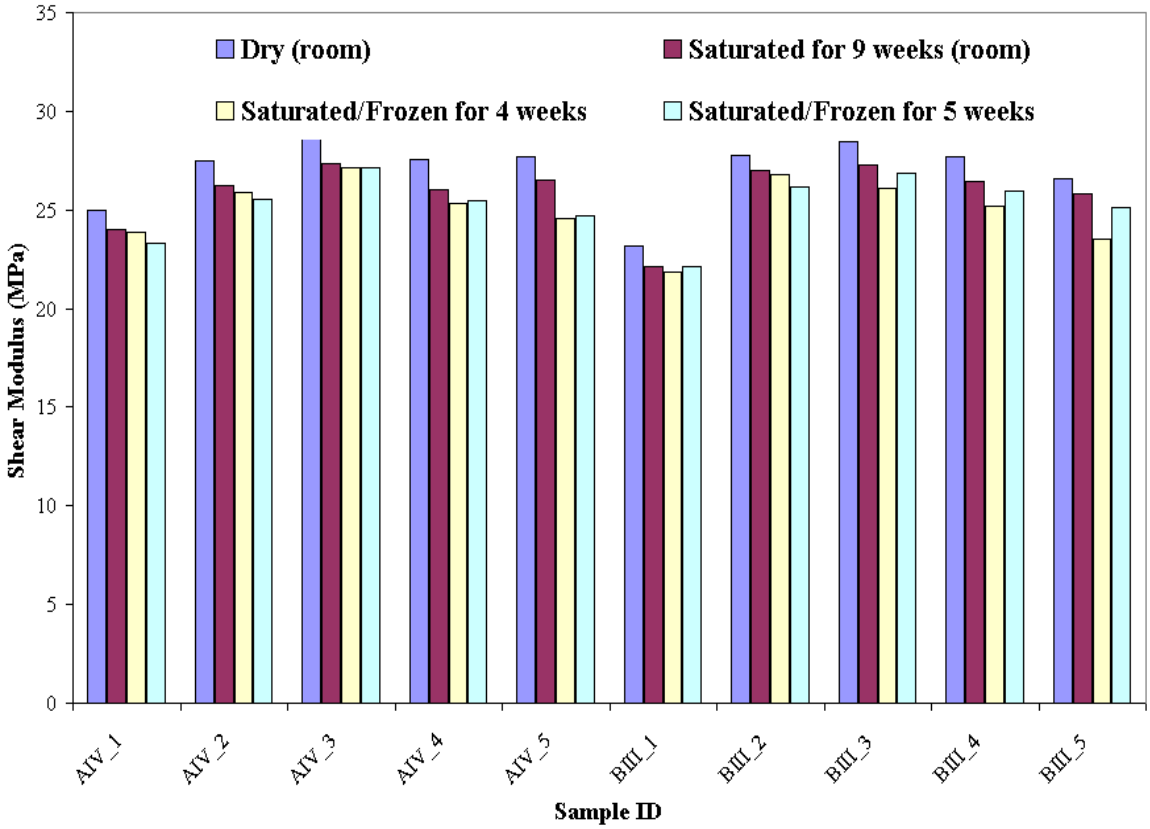

Figure 3.24: Comparison of saturated shear modulus (MPa) degradation before/after exposure to the low temperature and sea water.

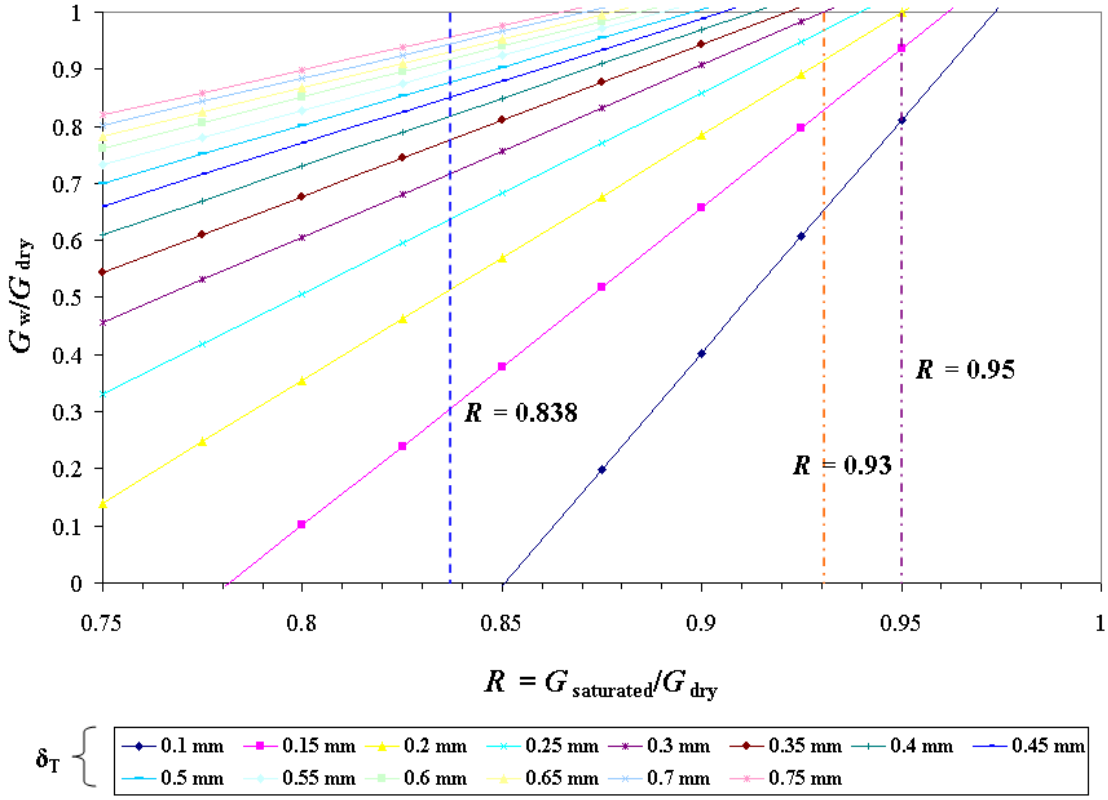

Figure 3.25: A parametric study of G_w/G_{dry} vs. R for various values of δ_T (in mm) according to Eqn. (3.11).

In view of the specimen to specimen variability in G values, as well as observation that the depth of penetration δ_T varies along the exposed boundary, it is advisable to employ Eqn. (3.11) over a range of , varying between -say- 0.15 and 0.25 mm. The values of G_w/G_{dry} vs. R are plotted in Figure 3.25 for various parametric values of δ_T. Thus, for

$R = G_w / G_{dry} = 0.838$ the value of G_w / G_{dry} ranges between 0.31 and 0.64 with an average value of 0.50, while for R = 0.95 0.93 < G_w / G_{dry} < 1 with an average value of 0.98.

3.8 Concluding remarks

Due to the inherent softness of polymeric foam, it cannot be tested by means of standard mechanical grips, and loads must be introduced by means of shear and friction into the specially designed test specimens shown in Figure 3.3 of this article. It is preferable to perform shear tests by means of the custom-made shear device depicted in Figure 3.4, rather than employing the tilted and friction prone ASTM mechanism. Nevertheless, a conclusion was reached based on shear lag analyses that dead weights do not affect the stress-strain data in any significant manner in either of the above devices. The effect of sea water on foam moduli was estimated by means of torsional tests, where response is more sensitive to the ingress of fluid.

It was shown that sea water, whose absorption is essentially confined to the outermost cells of the foam, degrade the shear modulus of the saturated region by up to 70%, though the average value of that reduction is about 50%, while reducing Young's modulus by up to 60%, with an average reduction of 33%. These results are useful in the computational evaluation of fracture toughness in exposed versus dry foam materials.

In view of the established analogy between one-sided exposure of sandwich composites to expansional strain and their subjection to one sided mechanical load, it is much easier

to perform tests under the latter settings and draw conclusions about the prior case. Note that one-sided expansional strains are anticipated to occur in sandwich layups due to the extremely slow ingress of moisture and sea water across their thickness, as well as the non-uniform distribution of temperature caused by the low thermal conductivity of the foam.

The good agreement between the predictions of the shear-lag model and strain data for one sided mechanical loading attests to the advantage of employing that relatively simple model for preliminary designs of sandwich structures with facings of varying thickness and out-of-plane curvatures.

Tensile and torsional stiffnesses at room and cryogenic temperature were recorded for various preconditioning regimens with sea water. It was shown that low temperature and sea water do not significantly reduce tensile properties but that the overall shear modulus had slightly decreased by 7% at sub-zero temperature. This result corresponds to a slight degradation of the shear modulus within the saturated region. This degradation can no longer be predicted by the simplified model that is based on the geometry depicted in Figure 3.10.

CHAPTER 4

EFFECT OF SEA ENVIRONMENT ON INTERFACIAL DELAMINATION BEHAVIOR OF POLYMERIC SANDWICH STRUCTURES

This chapter is a version of a paper with the same title accepted for the Journal of Composites Science and Technology in 2008 by Akawut Siriruk, Dayakar Penumadu, and Y. Jack Weitsman:

Siriruk, A., Penumadu, D., and Weitsman, Y.J. "Effect of sea environment on interfacial delamination behavior of polymeric sandwich structures." *Composites Science and Technology* In Press, Corrected Proof. doi:10.1016/j.compscitech.2008.02.033.

Abstract

Sandwich structures are utilized in naval craft and thereby are exposed to a sea water environment and temperature fluctuations over extended periods. The sandwich layup consists of a closed cell polymeric foam layer placed between thin carbon or glass fiber reinforced polymeric composite facings. Attention in this paper is focused on sea water effects on the interfacial mechanical response between foam and facing due to sustained sea water exposure using carefully controlled laboratory conditions. Pre-cracked sandwich composite samples are soaked in sea water for extended periods and interfacial

fracture behavior compared against dry specimens. Results indicate that the delamination crack propagates close to the interface in the wet case, while it stays within the foam in the dry case. The effect of sea water on values of energy release rate are determined experimentally and predicted using the J-integral concept. A good agreement between data and predictions is achieved, indicating a reduction in fracture toughness by thirty percent due to sustained exposure to sea water. This reduction needs to be considered in the design of ship structures.

***Keywords**:* Sea water effect, fracture toughness, delamination, sandwich structures, J-integral

4.1 Introduction

This article is part of a research effort aiming at the evaluation of the effects of sea water on the deformation, damage, and materials properties of sandwich structures and closed cell polymeric foams. The effects of a sea water environment on the mechanical properties of H100 foam and carbon fiber composite facings, as well as the sandwich structure itself, are being evaluated as a part of ongoing research sponsored by the United States Office of Naval Research (ONR). The experiments to date involved generation of sea water sorption and permeability data, determination of expansional and diffusion coefficients, as well as the measurement of wet and dry interfacial debond fracture energies and sea water induced property degradations. This paper reports the results associated with the effect of sea water on the delamination behavior of sandwich structures.

It has been established in previous works (Li and Weitsman, 2004; Ionita and Weitsman, 2007; Siriruk, Weitsman, and Penumadu, 2008) that most of the sorbed water in closed cell polymeric foams remains confined to a boundary layer adjacent to the exposed surfaces. This water causes volumetric expansion in the foam and enhances the growth of delaminations at the foam/carbon-fiber-facing interface, reducing the resistance to that form of fracture. It was also noted that a secondary mechanism of water ingress is provided by the foam's permeability, adding about 4% to the relative weight gain throughout the interior region of the immersed foam. Both components of the absorbed sea water were accounted for in the sequel.

It is well known that, in the absence of special provisions, cracks in foam cored sandwich specimens do not propagate in a self-similar manner, but often kink up or down. The direction of kinking was determined in the past from the mode mixity associated with the mechanism at hand. Crack kinking analysis has been reported in past research (Prasad and Carlsson, 1994a & 1994b).

The critical values of wet and dry interfacial fracture toughness were evaluated by the same method employed by earlier investigators for glass fiber reinforced facings (Li and Weitsman, 2004), except that some novel refinements were incorporated herein to detect crack length and its morphology, and present computations are based on recently recorded material data (Siriruk, Weitsman, and Penumadu, 2008). The current fracture data were calibrated by means of laminate analysis to enable the performance of comparative computational evaluations. These computations employed the finite element

method (FEM) to determine the levels of fracture toughness by means of the J-integral (Rice, 1968).

Both scatter and average values of the experimental data agreed remarkably well with the computational predictions.

4.2 Materials and experimental setup

4.2.1 Sandwich panel and its constituent materials

The composite sandwich panels of size 60 x 90 cm (2 x 3 ft) and 2.54 cm (1.0 in) thickness were fabricated using the VARTM process (Shivakumar, Swaminathan, and Sharpe, 2006; Swaminathan, Shivakumar, and Sharpe, 2006). The facing material was made of carbon stitch bonded fabric designated by LT650- C10-R2VE supplied by the Devold AMT AS, Sweden. This was an equibiaxial fabric produced using Toray's Torayca T700 12k carbon fiber tow with a vinyl ester compatible sizing. The weight of the fabric was 634 g/m^2 with 315 g/m^2 of fiber in the 0° direction and 305 g/m^2 in the 90° direction. Both the directional fibers were stitched with a 14 g/m^2 polyester knitting thread. Toray's Torayca T700 carbon fiber was chosen because of its lower cost and higher strength. The T700 fiber had a tensile strength of 4.9 GPa (711 ksi), a tensile modulus of 230 GPa (33.4 Msi), and an elongation of 2.1 percent. The matrix used was Dow Chemical's DERAKANE 510A-40, a brominated vinyl ester, formulated for the VARTM process (DERAKANE, 2004). The bromination imparts a fire-resistant property to the composite. The fiber volume was found to be 58 percent by the area density method and includes 2.2 percent weight of polyester stitch fiber. The core material was

H100 Divynicel PVC foam having an average density of 100 kg/m^3 and average cell size of 0.15 mm.

4.2.2 Specimen preparation and conditioning

The above mentioned panels were cut and machined to form 254 mm long, 25.4 mm wide, and approximately 29 mm high sandwich specimens. In addition to the foam and facings, the height dimension included also the thickness of top and bottom adhesive layers. Fifty millimeter long pre-cracks were cut with a sharp edge along the top facing/core interface in order to stimulate the growth of the interfacial delamination (Wood and Walter, 1997).

Load application was facilitated by using hinges glued to the facings in a Tilted Sandwich Debond (TSD) configuration (Li and Carlsson, 1999; Li, 2000). The hinges were mounted 38 mm away from the edge of the loaded, top, facing and the sandwich specimens were centered about the sides of the steel plates. The effect of exposure to sea water on fracture toughness was investigated by pre-soaking the specimens for three months in simulated sea water using natural coarse sea salt at a controlled temperature of 40 °C in a water bath prior to the initial delamination testing. Subsequently the specimens were soaked for interim periods of two weeks during intermittent crack growth between unloading and reloading cycles.

4.2.3 Delamination testing

The samples were loaded according to the set-up shown in Figure 4.1. Loading was introduced by means of an MTS servo-hydraulic 22 kN capacity testing machine under displacement control at a crosshead rate of 2 mm/min. A very precise smaller load cell with a full-scale capacity of 0.44 kN was used to perform the carefully controlled delamination testing. Specimens were tested in either dry or "wet" states. The latter state was obtained under immersion for the aforementioned intermittent durations. Loads were monotonically increased under displacement control until noting an abrupt drop in their amplitudes, at which stage crack extensions were observed. At that point, the crosshead displacement was programmed to stop and the machine to unload to zero displacement. The above loading-unloading procedure was repeated at each new crack length until total separation of the upper facing. The system affords most accurate observations of crack tip positions on both sides of the delaminating specimen and a nearly definitive determination of load levels at the onset of intermittent crack growth. As noted earlier, it was necessary to re-soak each "wet" specimen for at least two to three weeks, in order to maintain a fully saturated crack tip region after each unloading and prior to each reloading. The digital images of the interfacial cracks were obtained during testing as shown in Figure 4.2, using digital image analysis software (ImagePro®). Crack morphology was also determined for possible use in calculating values of energy release rate. This was done by transferring the gray scale image to binary form using thresholding technique and by focusing on the region of crack-tip. The exact length of crack was obtained by tracking the number of pixels and conversion to length units using the known optical magnification at which digital images were obtained. In addition to observing crack propagation along the front of the specimen, the advancing cracks were

also captured digitally along the back of the specimen with the aid of a highly polished mirror. Overall, the testing program involved 6 specimens in the dry state and 4 in the wet state.

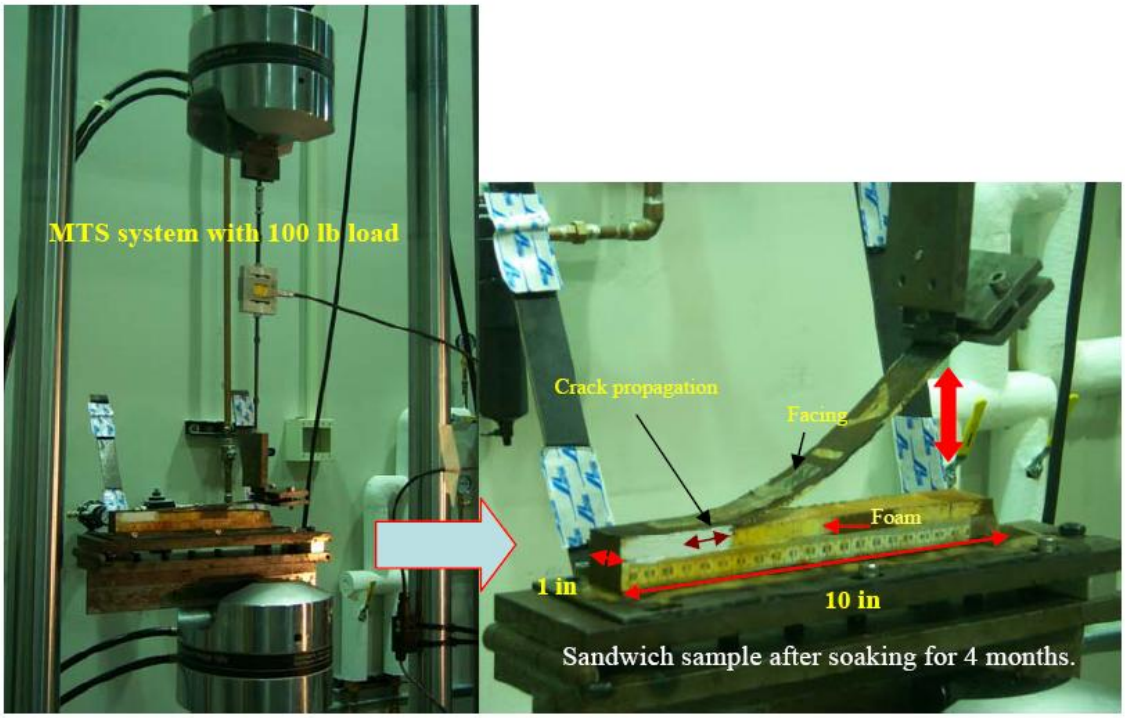

Figure 4.1: Delamination testing setup using 0.44 kN load cell, and a delaminated wet sandwich specimen.

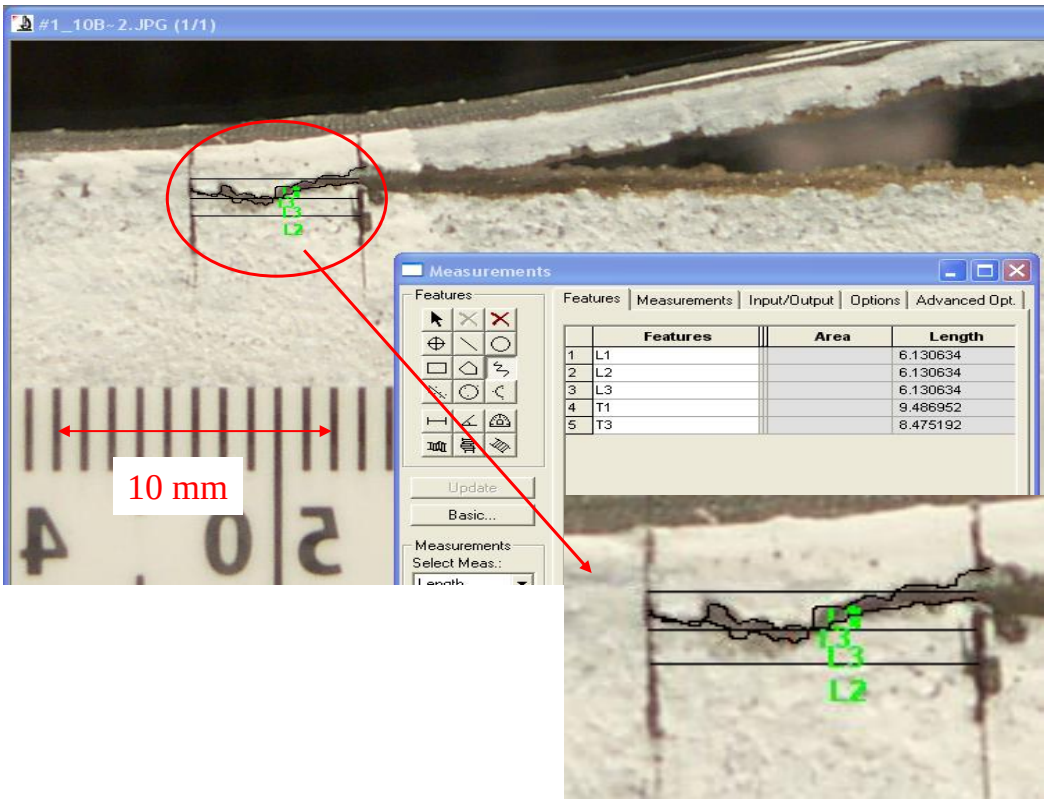

Figure 4.2: Digital image analysis of a delaminated crack morphology for dry case.

4.3 Evaluation of fracture toughness

The resistance to delamination growth can be characterized by the strain energy release rate (G), where the critical energy release rate (G_c) is used as a measure of the interminar fracture toughness.

Assuming a linear elastic response, it was chosen to determine the critical strain energy release rates by means of the "area method" (Broek, 1982). The area under each load/unload cycle was calculated numerically using the trapezoidal rule. Critical energy release rate, which defines the fracture toughness, was obtained using the expression:

$$G_c = \frac{1}{b} \cdot \frac{\Delta U}{\Delta a} \tag{4.1}$$

Where ΔU is the area under the load-displacement trace as the crack grows; Δa is the extended crack length noted during the test, and b is the width of specimen. The value calculated is the average energy consumed during the crack extension Δa.

4.4 Experimental results

Typical experimental results are shown in Figure 4.3, in which the data associated with the first two load/unload cycles were discarded in the evaluation of the critical energy release rate G_c due to the fact that these cycles originated at an artificially pre-cut crack which may not be representative of a natural crack and does not possess a sufficiently sharp crack-tip to satisfy theoretical assumptions. Typical delamination configurations are shown in Figure 4.4. It can be observed that in the dry case cracks exhibited more asperities and stayed comparatively farther from the interface than in the wet circumstance. This supports an earlier suggestion (Li and Weitsman, 2004) that the fracture mode mixity in the interfacial region differs for the dry and wet conditions. The fact that, in the wet case, cracks stayed closer to the interface is consistent with the observation that sea-water remained confined to the exposed surfaces of the specimens. Employment of equation (4.1) gave the values of G_c that are listed in Table 4.1. That table gives values that correspond to crack lengths observed on both sides of the specimens. Accordingly, exposure to sea water causes an approximate 30% reduction in G_c.

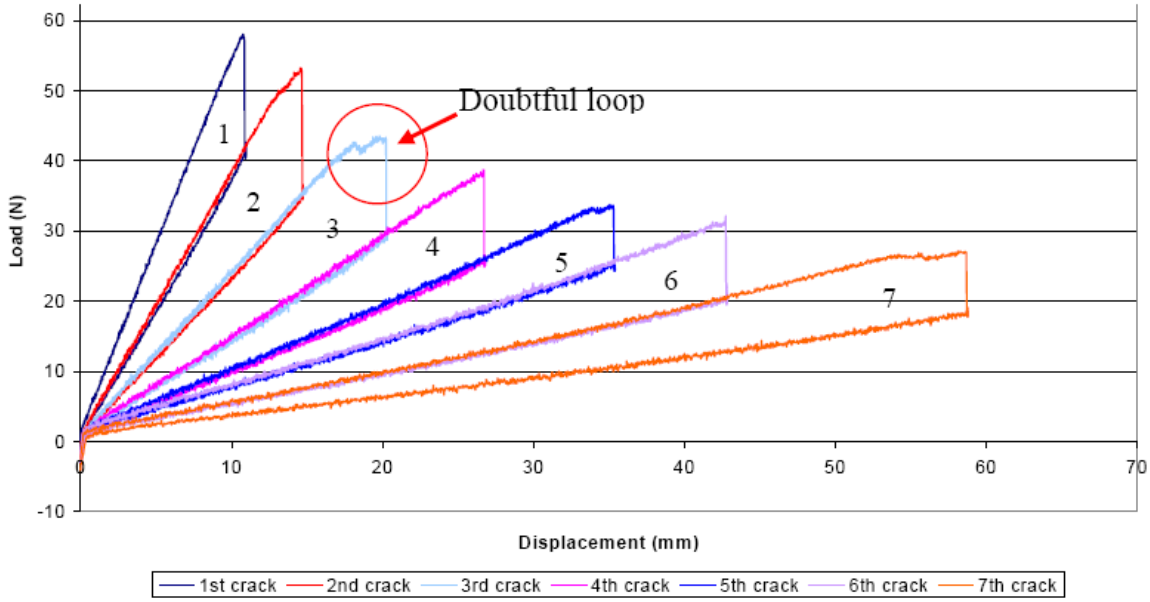

Figure 4.3: Typical experimental data for an intermittent growth of a delamination crack. Load plotted vs. displacement under the loading point.

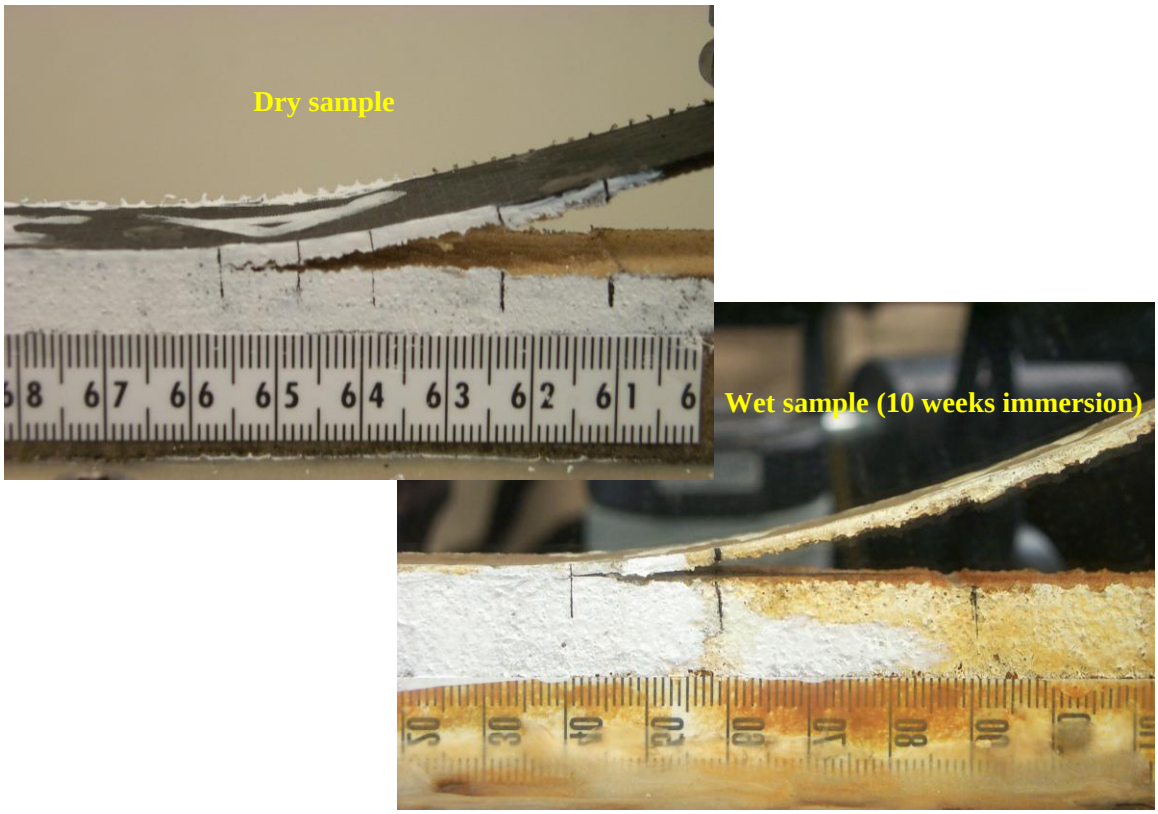

Figure 4.4: Typical morphologies of dry (top) and wet (bottom) delamination cracks.

The wide range of values reported in Table 4.1 reflects the sample to sample variability in the thickness of the facings (to which G_c is extremely sensitive), the random nature of the foam as well as the observation that interfacial cracks are not planar and do not maintain straight fronts.

Table 4.1: Experimental values of wet and dry interlaminar fracture toughness G_c, including data scatter and percent reduction caused by exposure to sea water.

	G_C (Front) Lower & Upper limit (N/m^2)	G_C (Back) Lower & Upper limit (N/m^2)	Representative Range (>50%) (N/m^2)
Dry	580-952	541-963	780-890
Wet	432-619	451-632	522-588
% Reduction	*25-35%*	*17%-34%*	*33-34%*

4.5 Finite element analysis of fractured specimens

4.5.1 Material properties, and data calibration

Elementary beam theory relates the deflection δ of a cantilever beam subjected to a concentrated load P acting at a distance a from the built-in support by

$$\delta = \frac{Pa^3}{3D} \tag{4.2}$$

where D denotes bending stiffness. Since the experimental data at hand provide values of P, a, and δ, it would be a simple matter to compute D.

Nevertheless, such computations lead to values of D that exhibit a variability of up to 30 percent. Since D varies like h^3, where h is the facing's thickness, any variability in h, or any misinterpretation of its value in a computational scheme, may result in serious discrepancies.

Though not entirely essential for employment in the numerical scheme, it was deemed useful to estimate D and derive a reasonable value for h on the basis of some elementary reconsideration.

As noted in section 4.2, the facings consist of $[0/90]_s$ layup of a equibiaxial fabric, for which $E \approx 80$ GPa. Let E_L and E_T denote the individually unknown longitudinal and transverse moduli of each "fabric layer". It follows that $(E_L + E_T)/2 = 80$ GPa.

Straight forward employment of laminate theory yields that for the lay up at hand

$$D = \frac{h^3}{12}\left(\frac{7}{8}E_L + \frac{1}{8}E_T\right) \tag{4.3}$$

In view of a multitude of material data (Daniel and Ishai, 2005) it is reasonable to assume that $0.05 < E_T/E_L < 0.15$. Considering $E_T/E_L \approx 0.1$ (i.e., E_L = 145 GPa and E_T = 15 GPa), one obtains that $D = 130\ h^3/12$ (GN-m^2).

Substitution into equation 2 yields that the value of h, which best matches the average values of the entire data set, is h = 1.25 mm. The aforementioned values E_T, E_L, and h were incorporated into the finite element program.

In addition, the program contained the following material and dimensional values: wet and dry foam moduli of 60 and 22 MPa, respectively, and a Poisson's ratio $\nu = 0.13$ for both. The thickness of the wet layer was taken to be 0.15 mm (Siriruk, Weitsman, and Penumadu, 2008). Properties of the adhesive between foam and facings were E = 3.4 GPa, ν = 0.35 (DERAKANE, 2004) and thickness 0.1 mm. The overall length of the sample was taken to be 250 mm and the thickness of the foam core to be 25 mm.

4.5.2 Finite Element Modeling

To compare J-integral computational predictions with test results, two data sets were chosen from among those tested. This established twelve computational models, with different initial and subsequent crack lengths, as well as the corresponding levels of applied loads. All computations assumed a rigid boundary condition (u_x, u_y =0) at the bottom facing as shown in Figure 4.5.

Eight-node biquadratic quadrilateral elements with reduced integration (CPEG8R) were used in the FEM model to calculate the J-intergral. A free meshing technique from ABAQUS (ABAQUS/CAE, 2007) with quadrilateral elements using a medial axis algorithm was used for the meshing of the two-dimensional region. To reduce mesh distortion, and thus improve mesh quality, "the minimum mesh transition" option was also used, resulting altogether in the mesh as shown in Figure 4.6. The J-integral values were obtained from ABAQUS using contour integral analysis surrounding the crack tip. The crack was modeled as a straight line, representing a traction free boundary that allows free nodal displacements. In this regard, ABAQUS places overlapping duplicate nodes along the above line when the mesh is generated. As expected, the results predict that very high stress concentrations arise in the vicinity of the crack tip. Although accuracy is expected to increase with diminishing mesh size, the J-integral procedure was not sensitive to this matter, since it provides an overall measure of energy. In fact, for the circumstances considered herein it was shown by a careful study that complete convergence of J-integral values was obtained for a mesh size 0.5 mm. However, it should be noted that the mesh size is also delimited by the dimensions of the foam cells.

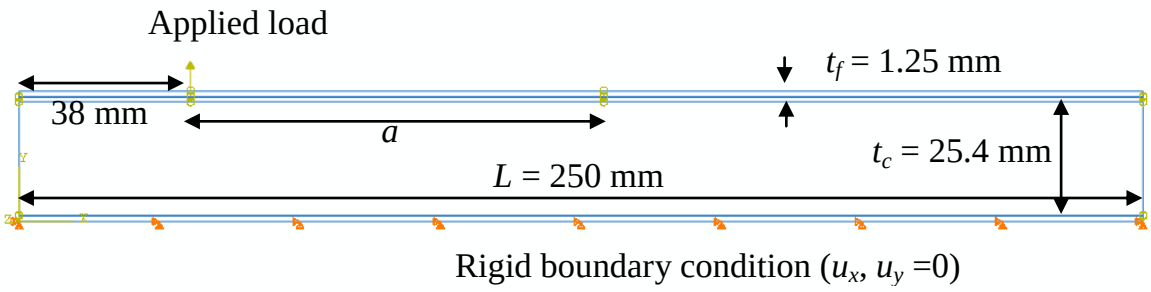

Figure 4.5: Dimensional configuration of specimens utilized in the finite element model.

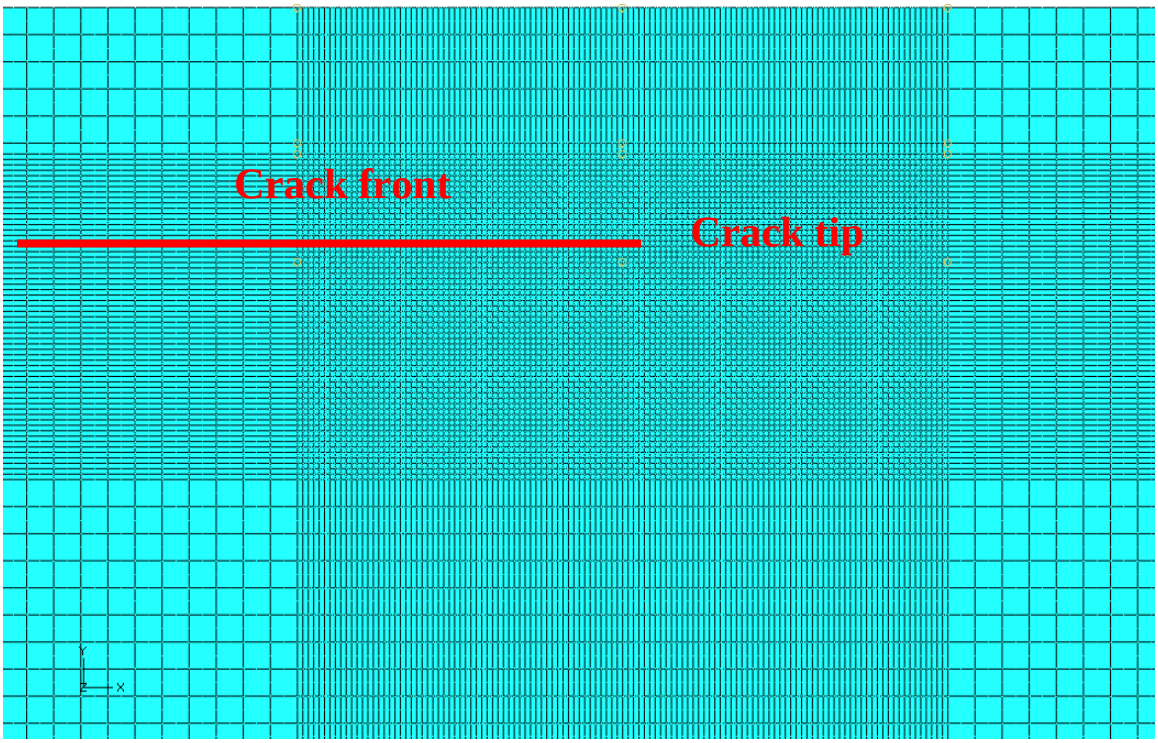

Figure 4.6: Finite element mesh configuration.

Figure 4.7a and 4.7b show typical predicted stress distributions in the vicinity of wet and dry crack tips. Figures 4.8 and 4.9 provide comparisons between predicted and experimental values G_c, and displacements at the location of the applied load, respectively. Both are plotted versus crack length a. Results, similar to those shown in Figure 4.8, are displayed in Figure 4.10 for the wet case. An additional comparison is provided in Figure 4.11 between the predicted values of the wet and dry delamination fracture toughness, plotted versus crack length a.

Note that the predicted average value of the toughness of the dry, as obtained from 12 different computational simulations was 823 N/m^2, which compares very well with the range of 780 to 890 N/m^2 listed in Table 4.1. It is to be noted that the evaluation of the J-integral in the presence of water involved the embedding of a 0.15 mm thick zone of elements along the crack front with reduced material properties. For the four crack lengths employed in the computations, a reduction of approximately 30% was predicted below the dry levels was predicted. This agrees very well with the experimental results.

It should be recalled that all computations employed a common values for the facing's thickness, namely h = 1.25 mm, which matched the data only in the average sense.

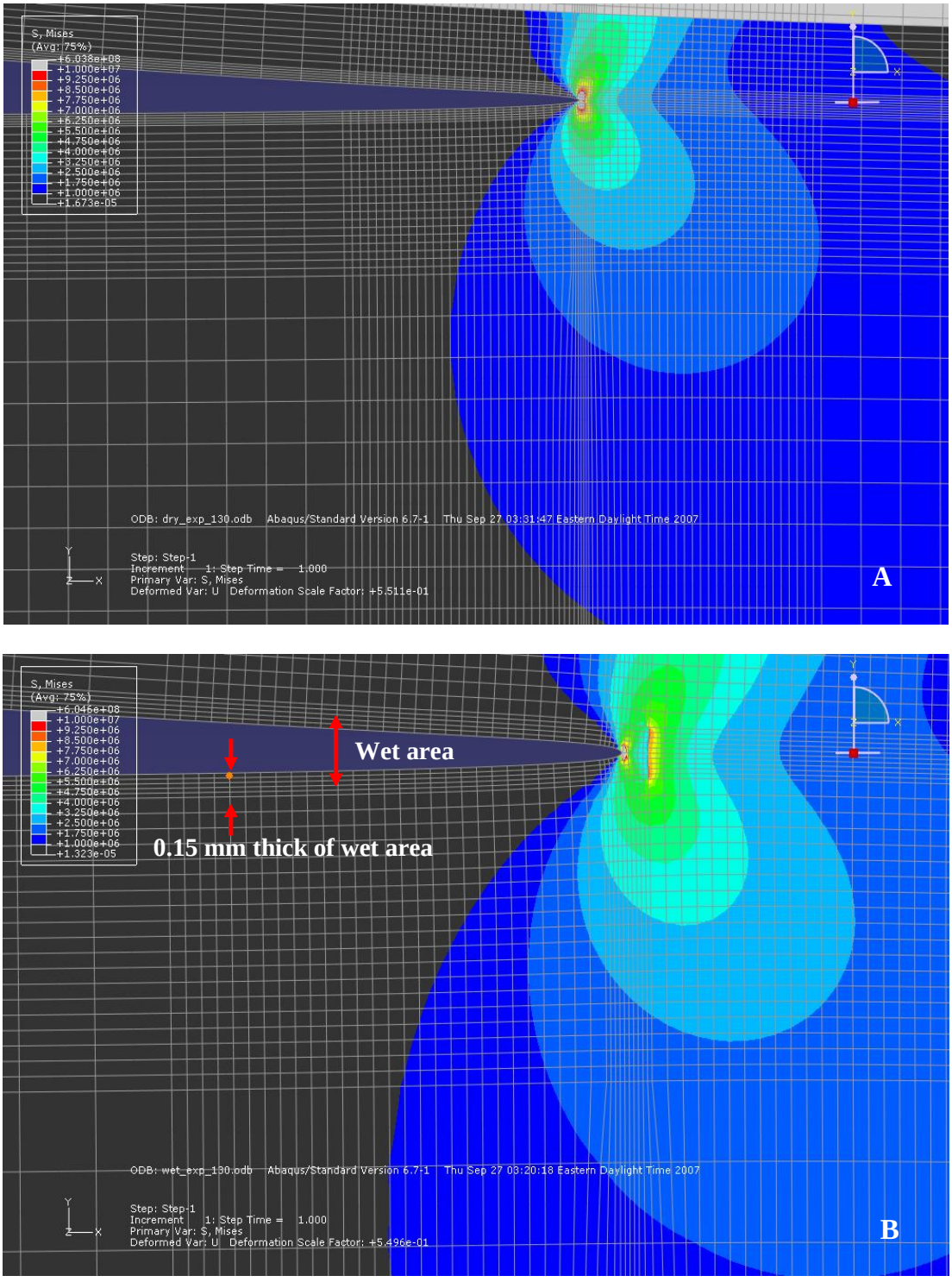

Figure 4.7: Stress distributions in the vicinity of, (a) dry and (b) wet, crack tips. Note the disparity in the spread of the highly stressed zones.

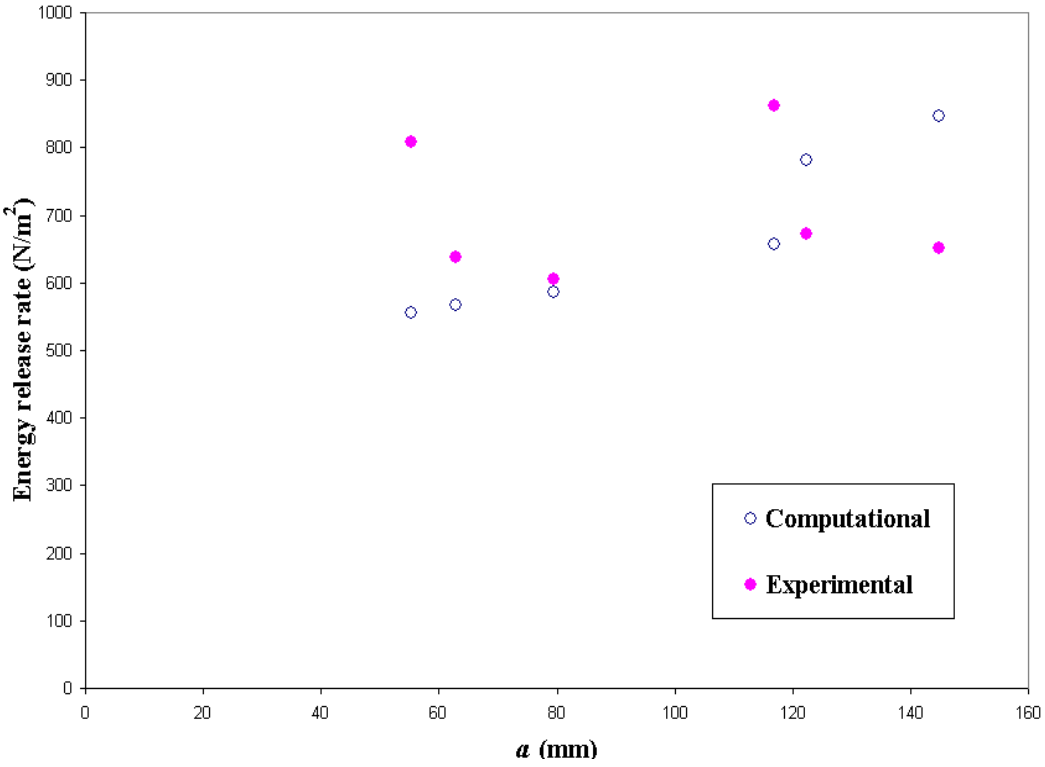

Figure 4.8: Comparative values of predicted and experimental of interfacial fracture toughness vs. crack length, a .Results shown for dry case.

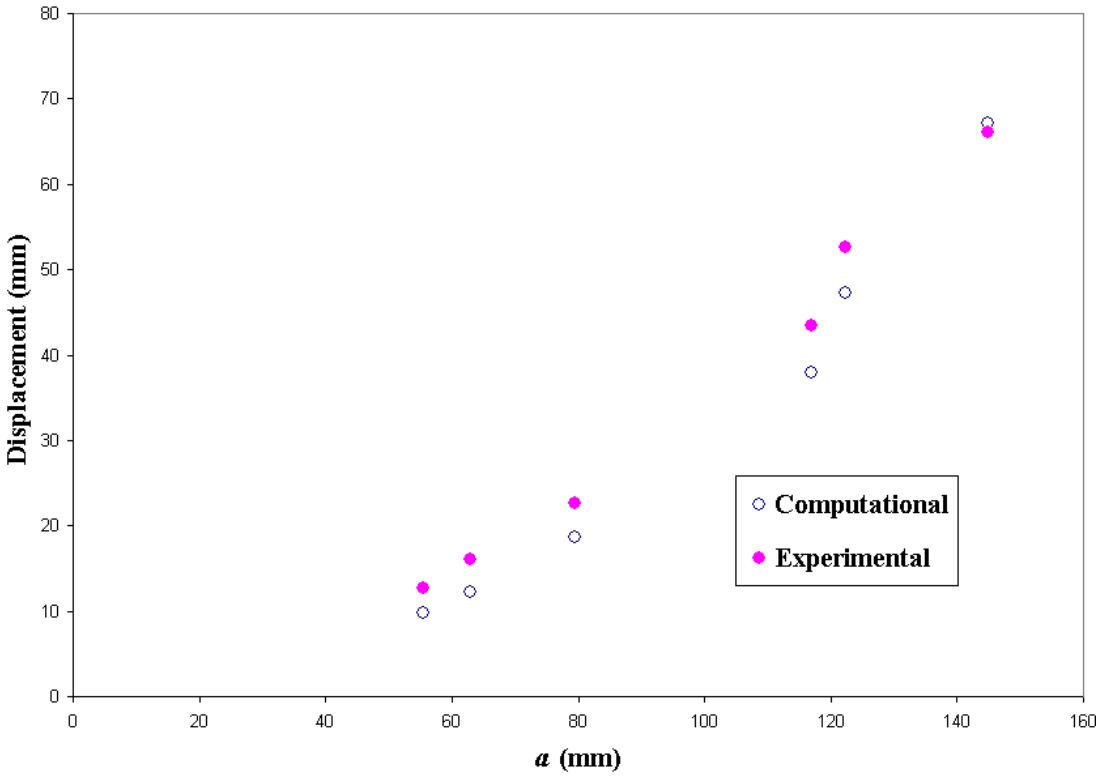

Figure 4.9: Comparative values of predicted and recorded values of displacements at the location of the applied load vs. crack length, *a*.

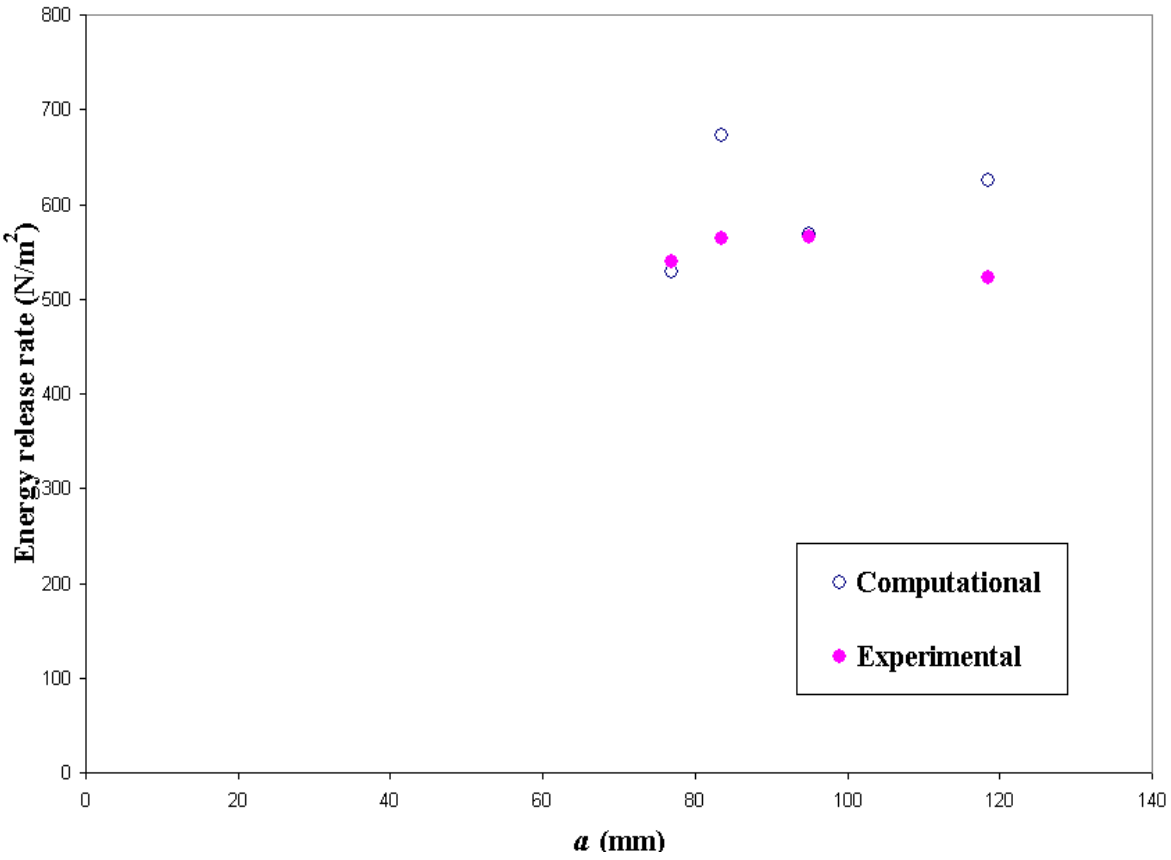

Figure 4.10: Comparative values of predicted and experimental of interfacial fracture toughness vs. crack length, *a*. Results shown for wet case.

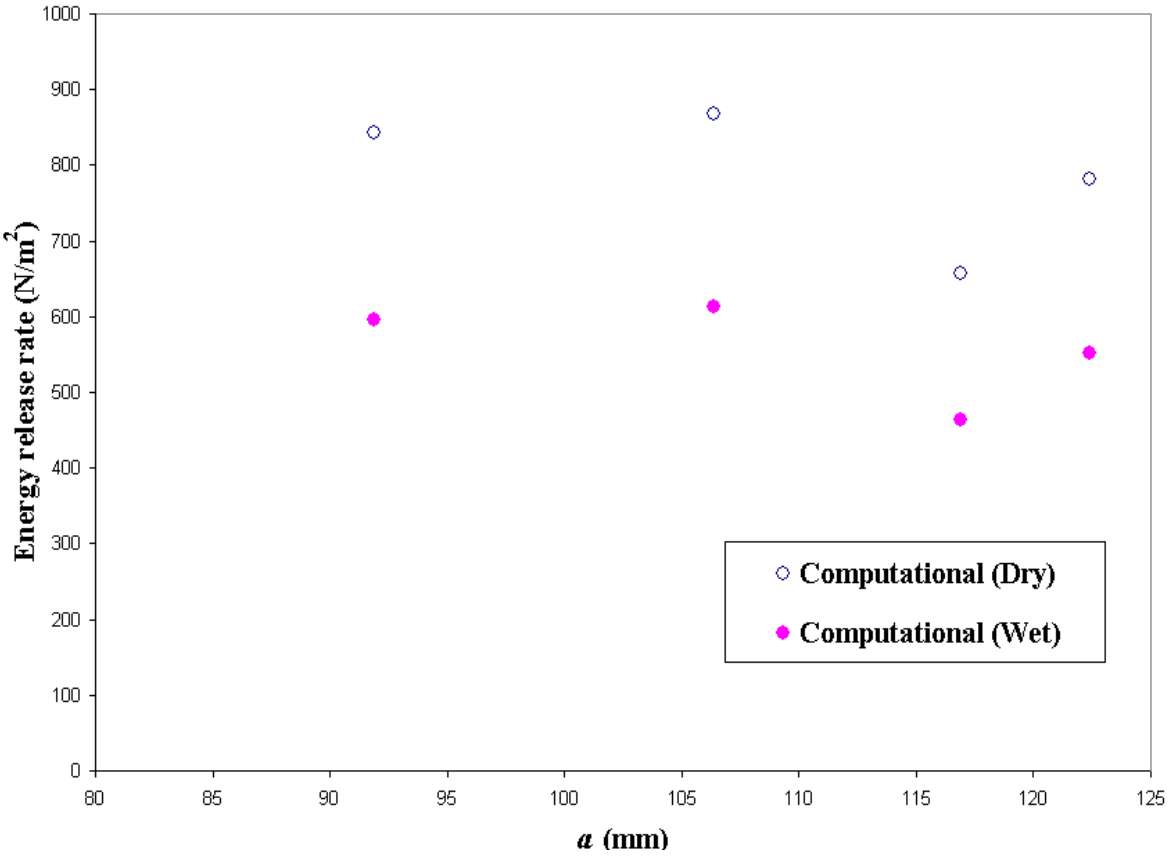

Figure 4.11: Comparisons between computed values of a J-integral (with $J = G_C$) for the dry and wet states. Results plotted vs. crack length, *a*.

4.6 Summary and conclusions

A careful experimental procedure was devised to evaluate the both dry and wet values of delamination toughness at the facing/foam interface of a sandwich structure. The results exhibited a noticeable degree of scatter, which can be traced to a sample-to-sample variability in facing thickness as well as to the inherent randomness of the foam structure. Nevertheless, it was demonstrated beyond doubt that sustained exposure to sea water resulted in 30% reduction in delamination fracture toughness. Results indicate that the delamination crack propagates close to the interface in the wet case, while it stays within the foam in the dry case.

A rational, mechanics-based analysis, derived from the J-integral and employing the finite element method yielded predictions that agreed very closely with the aforementioned experimental observations, both in regards to scatter and average values.

CHAPTER 5

CARBON COMPOSITE FACINGS

This chapter is a combined version of a conference paper accepted for 16th International Conference on Composite Materials (ICCM-16): July 8-13, 2007, KICH, Kyoto, JAPAN and 2007 and 2008 ONR annual report by Akawut Siriruk, Y. Jack Weitsman, and Dayakar Penumadu:

Weitsman, Y.J., Siriruk, A., and Penumadu, D. "Sea Water Effects on Polymeric Composites- A Comparative Study."

Abstract

This article concerns the ingress of water into $[0/90]_{2s}$ and $[\pm 45]_{2s}$ carbon reinforced vinyl ester facing layups and the ensuing mechanisms of property degradation. Experimental results are presented for water weight gains and their effect on Young's modulus. Expansional strain data are provided and some effects of cryogenic temperatures are investigated.

5.1 Introduction

This study was motivated by the increasing interest in applying polymeric composites and sandwich layups to naval craft. All polymers and polymeric composites absorb noticeable amount of water when exposed to ambient atmosphere or under immersed conditions. The process of water absorption in polymeric composites is a rather complex

issue, which was investigated by many researchers in past decades (Shen and Springer, 1977; Tucker and Brown, 1989; Grant and Bradley, 1995; Weitsman and Guo, 2002; Weitsman, 2006). The most common method for evaluating water ingress is the recording of weight gain data versus time. It was noted that water ingress tends to degrade the fiber matrix interface and induce internal swellings within the composite, resulting in reduction of material properties such as shear modulus and ultimate strength.

Carbon fiber composites are often used as facings in sandwich structures that are currently employed in naval applications. Exposure to sea water and the ambient environment would instigate the onset of the aforementioned degradations within the outer composite facing layer. In view of earlier observations that the inner polymeric foams, which form the core of the sandwich lay-ups, are essentially impervious to water ingress and possess high thermal insulation properties, it follows that one-sided environmental exposure would cause both shape distortions and unbalanced failure in sandwich lay-ups.

5.2 Material and specimen preparation

The facing material consisted of stitch-bonded fabric of carbon fiber tows embedded in vinyl ester resins. Each carbon tow consisted of 12k Toray's Torayca T700 individual fibers and the facing was laid up into an equibiaxial fabric. The vinyl ester compatible sizing, designated by LT650- C10-R2VE, was supplied by the Devold AMT AS, Sweden. The weight of the fabric was 634 g/sq.m with 315 g/sq.m of fiber in the 0° direction and 305 g/sq.m in the 90° direction. The fibers were stitched together with a 14 g/sqm

polyester knitting thread. Toray's Torayca T700 carbon fiber was chosen because of its lower cost and higher strength. From manufacture's data, the T700 fiber had a tensile strength of 4.9 GPa (711 ksi), a tensile modulus of 230 GPa (33.4 Msi), and an elongation of 2.1%. The matrix material was Dow Chemical's Derakane 510A-40, a brominated vinyl ester, formulated for the VARTM process. The bromination imparts a fire-resistant property to the composite. Vinyl ester has a higher fracture strain than the typical polyesters, and hence produces composites with superior mechanical properties and impact resistance.The fiber volume was found to be 58% by the areal density method and includes 2.2% weight of polyester stitch fiber (Penumuadu, Weitsman, and Siriruk, 2007).

The aforementioned VARTM process was used to fabricate composite panels by combining individual carbon fiber and vinyl ester based face sheets so as to form a symmetrical lay-up of woven cross-ply pairs of 0˚ (warp) direction with the warp face down and pairs of 0˚ with the warp face up as shown in Figure 5.1. Figure 5.2 demonstrates the orientation of the facing. The VARTM process, including set up and cure time-temperature profile, was described by Shivakumar (Shivakumar, Swaminathan, and Sharpe, 2006). The total thickness of the facing averaged at 2.7 mm, varying by less than ±5%. Material was delivered in the form of plate measureing 60 × 60 cm.

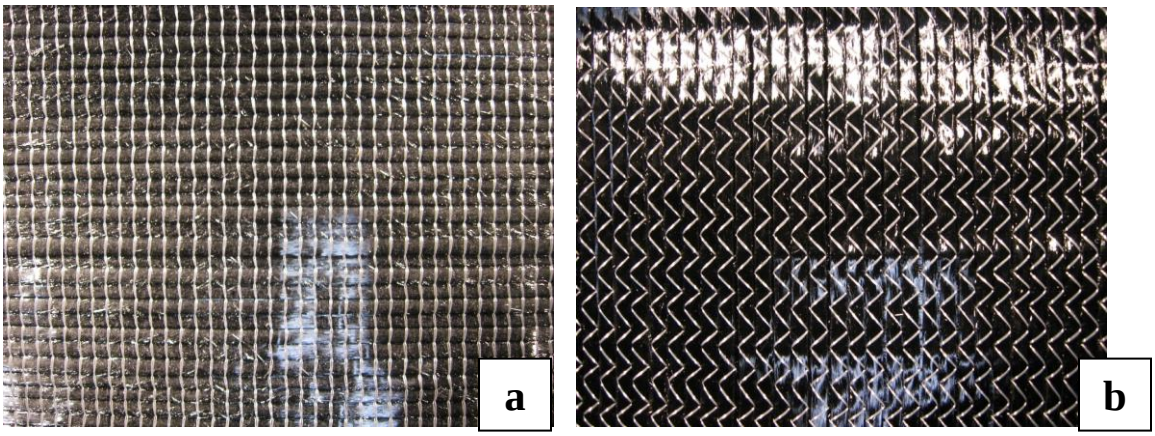

Figure 5.1: Devold LT650 T700 carbon fiber: (a) fill (horizontal) and (b) wrap (vertical).

At first, specimens were roughly cut from the panel using a band saw, which was then followed by surface grinding with a diamond saw. For standard mechanical testing, all speicmens were machined to be 200 mm long and 25 mm wide as specified in ASTM D 3039 “Standard Test Method for Tensile Properties of Polymer Matrix Composite Materials” and shown in Figure 5.3. This type of specimens with four double plies was used to perform four experimental tasks, namely: 1) Tensile tests of $[0/90]_{2s}$ and $[\pm 45]_{2s}$ coupons, 2) Uptake and effects of sea water, 3) Comparison of sea, tap, and distilled water effects and 4) Evaluation of cryogenic effects.

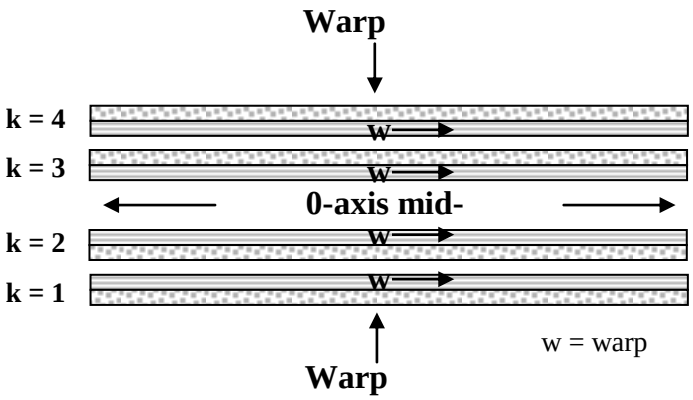

Figure 5.2: Facing orientation configuration.

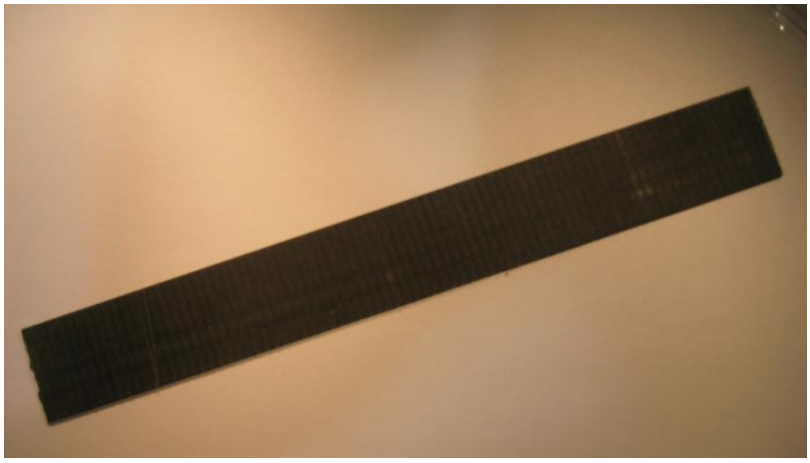

Figure 5.3: A carbon fiber facing sample (200 mm × 25 mm).

5.3 Mechanical properties

The tensile modulus was determined from the slope of the stress-strain curve prior to yield using four double plies T700. An MTS 600 test system was used for that purpose at a strain rate of 300 με/min. Load, displacement, and strain data were recorded continuously by the computer-aided system. A 25 mm gage length extensometer was used to acquire strain data at the center of the specimens. Tabs were mounted at the ends of the specimens, in order to direct failure away from the stress concentrations at the gripped portions. Prior to the tensile tests, all the specimens were completely dried at ambient temperature in a desiccator. In the dry state, the $[0/90]_{2s}$ and $[\pm 45]_{2s}$ facing composites were found to have an approximate average moduli of elasticity of 80 GPa and 15 GPa, respectively. Figure 5.4 shows the set up of a tensile test and a typical result used to calculate an initial stiffness.

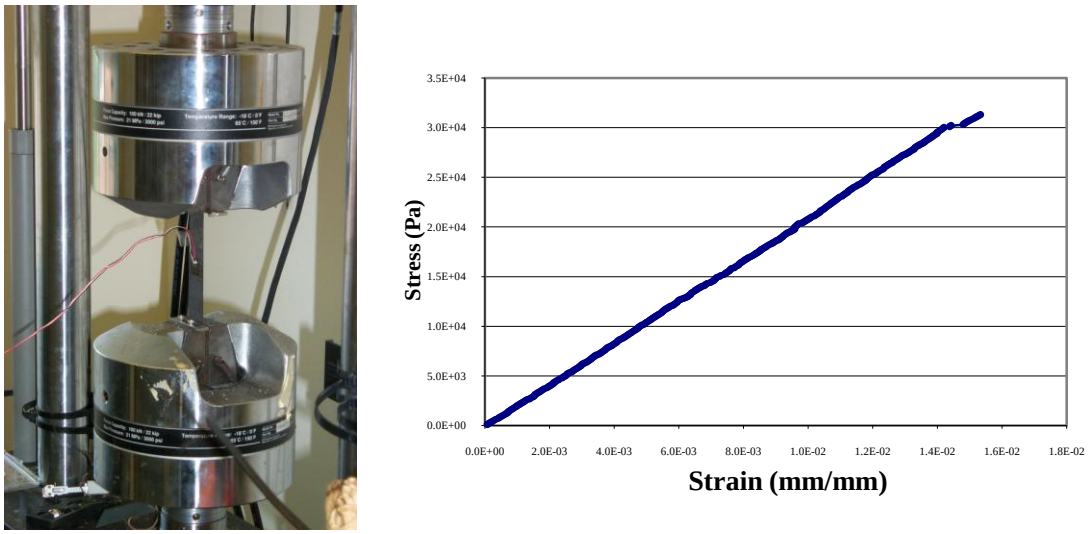

Figure 5.4: Tension test set up (left), Tensile testing data on facing (right).

5.4 Effects of sea water

The effects of long-term immersion in sea water on carbon fiber polymeric composites have been reported in the past (Tucker and Brown, 1989; Grant and Bradley, 1995; Mouritz et al., 2004). The subsequent water induced damage has been summarized in several review articles (Weitsman, 2000; Weitsman and Elahi, 2000). It has long been known that the polymeric phases of these composites absorb moisture when soaked in simulated sea water at ambient temperature. This study focuses on the effect of the sea environment on the facing materials at hand by the preconditioning of the aforementioned coupons in simulated sea water up to saturation, by recording changes in mechanical properties such as strength and modulus.

Moisture absorption was monitored by the periodic weighing of pre-dried coupons after immersion in simulated sea water baths at 40°C. Saturation was achieved within approximately three months, with an equilibrium weight gain of about 0.5 %. The specimens were subsequently removed from the baths and tested for tensile properties using the same procedure in section 5.3. The moisture content during testing was not controlled but since the duration of each test was about 4 minutes, only a negligible amount of drying took place. It was noted that immersion caused only small differences in properties of the facings.

5.5 Expansional strain for facing immersed in sea water

It was rather difficult to record experimentally the expansional strains associated with seawater-induced moisture sorption. Attempts to evaluate those strains by marking

reference lines on dry facing specimens prior to soaking and measuring their increasing distances by means of microscopy resulted in unreasonable data scatter. In addition, more accurate and consistent results were derived by recording the shrinkage associated with the drying of pre-soaked specimens. These data were obtained by using a high precision strain sensor attached to the soaked specimen encased in a desiccated chamber, where strain was recorded as a function of drying time. Assuming reversibility, this method gave a close approximation for the seawater-induced expansional strain. This technique was used to evaluate strain on facings soaked in any types of water and for specimens with different fiber orientation (Figure 5.5). Figure 5.6 shows the typical strain response with time.

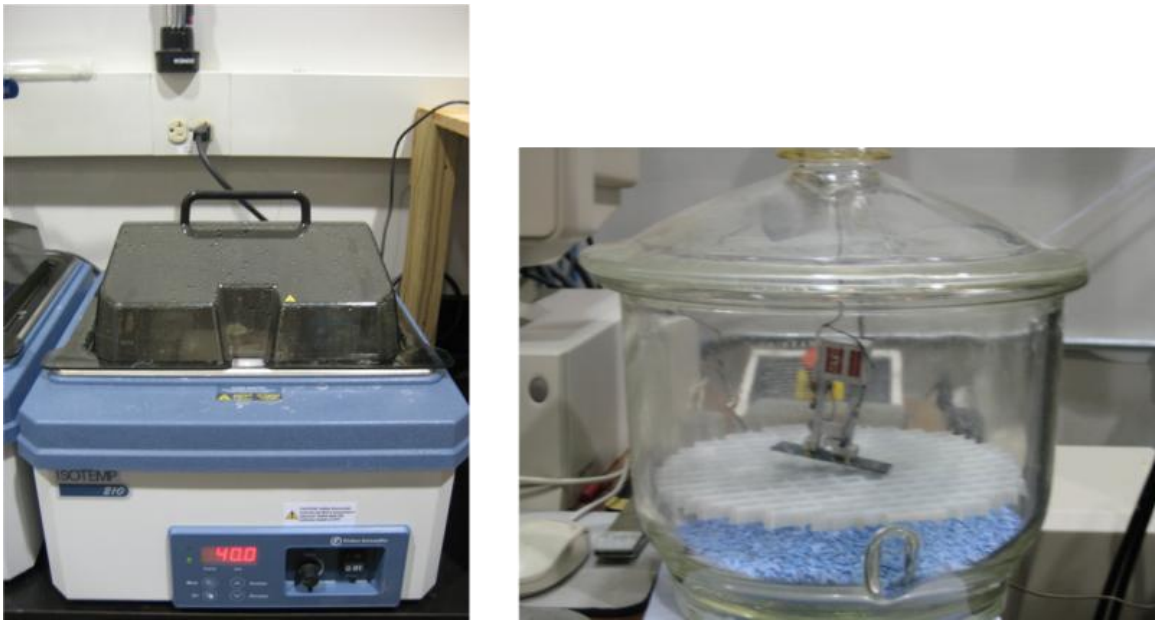

Figure 5.5: Water bath and desiccated chamber.

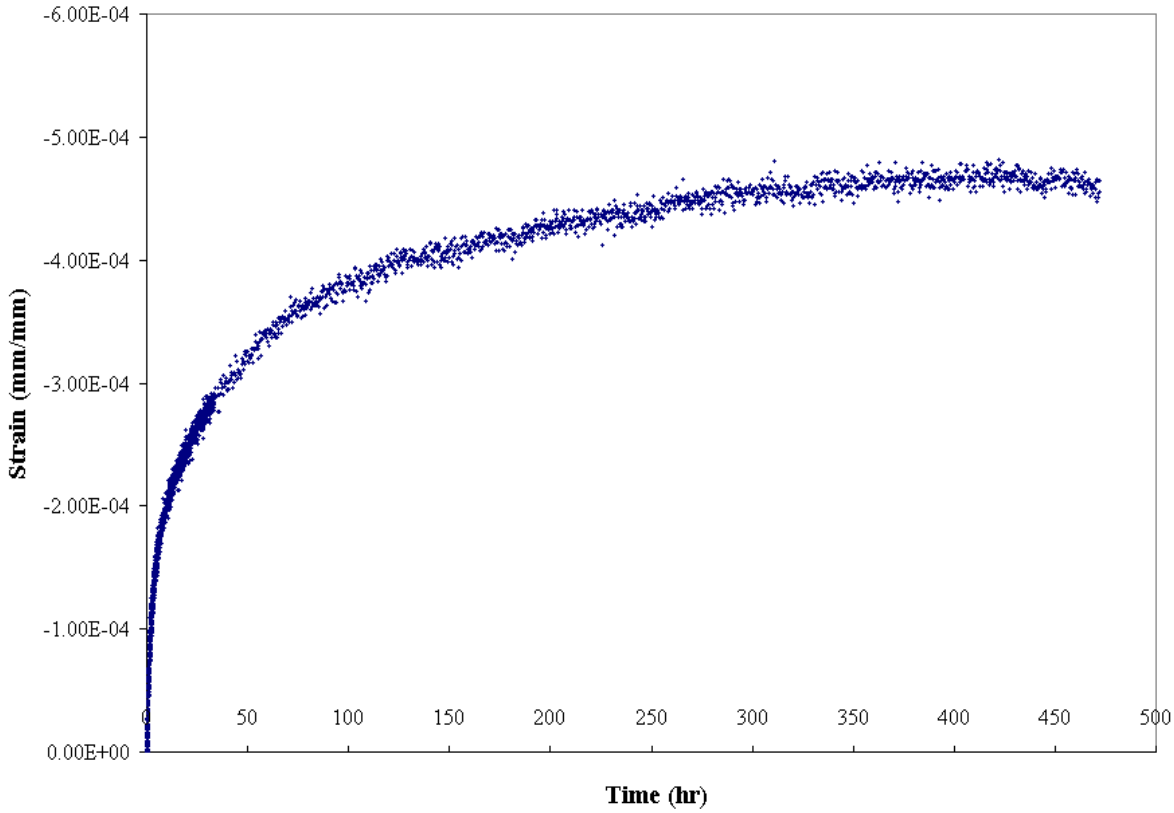

Figure 5.6: Sea water induced strain of carbon fiber and vinyl ester facing.

Tests on three samples with dimensions 25 mm × 67 mm attached to an extensometer were repeated using the above mentioned technique, and sea water induced expansions were recorded in the manner discussed above, resulting in ε_H = 450 με per 0.5 % saturation weight gain for $[0/90]_{2s}$ orientation.

5.6 A comparative study of sea, tap and distilled water

The purpose of this experimental study is to evaluate on the comparative effects of sea water, distilled water, and tap water on the weight gain and elastic stiffness of the aforementioned carbon fiber reinforced polymeric composite facings (Weitsman, Siriruk, and Penumadu, 2007). Coupon specimens having a length of 8 inches and a width of 1

inch were immersed in three water baths containing distilled, tap, and sea water at a controlled temperature of 40 °C for 5 months before conducting mechanical property assessment tests. Weight gain data were recorded for all three types of water using the ASTM D 5229 standard "Standard test method for moisture absorption properties and equilibrium condition of polymer matrix composite materials". Measurements were taken after 1, 4, 9, 16, and 24 hours of soaking time, followed by weekly intervals. Water absorption data for $[\pm 45]_s$ specimens suggest that they absorb sea water the most, followed by distilled and tap water, respectively, as shown in Figure 5.7.

As shown in Figure 5.8, the mechanical properties after five months of soaking are essentially the same for all types of water. A comparative study of the effect on modulus of elasticity was recorded by subjecting the specimens to three load/unload/reload uniaxial tensile cycle. During the second and third cycle, tensile coupons were loaded only to 90% of the stress level that was applied at first cycle. The average values of the moduli were E_{sea} = 14 GPa, E_{tap} = 14.2 GPa, and $E_{distilled}$ = 14.5 GPa. The aforementioned values vary insignificantly from that of the dry modulus as shown in Figure 5.8. The comparison of permanent deformation upon unloading caused by sea, distilled and tap water in term of inelastic stress-strain behaviors for $[\pm 45]_{2s}$ composite facings was also obtained; however, those results indicated only a minimal difference in the mechanical property degradation.

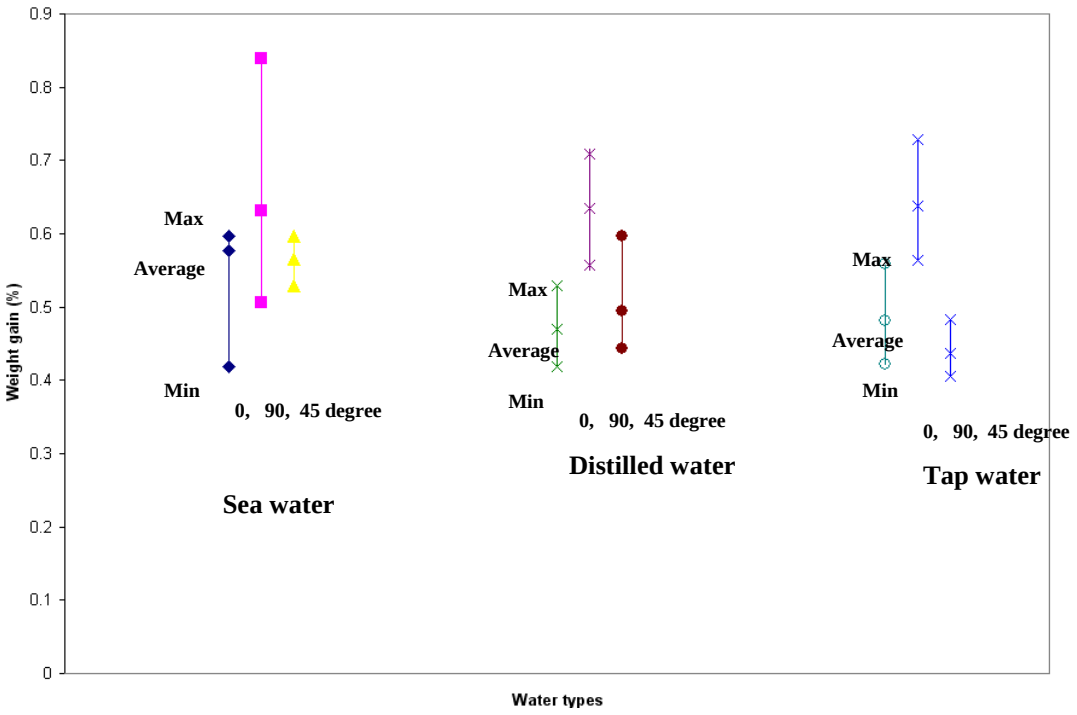

Figure 5.7: Weight gain data for specimens immersed in sea, distilled, and tap water.

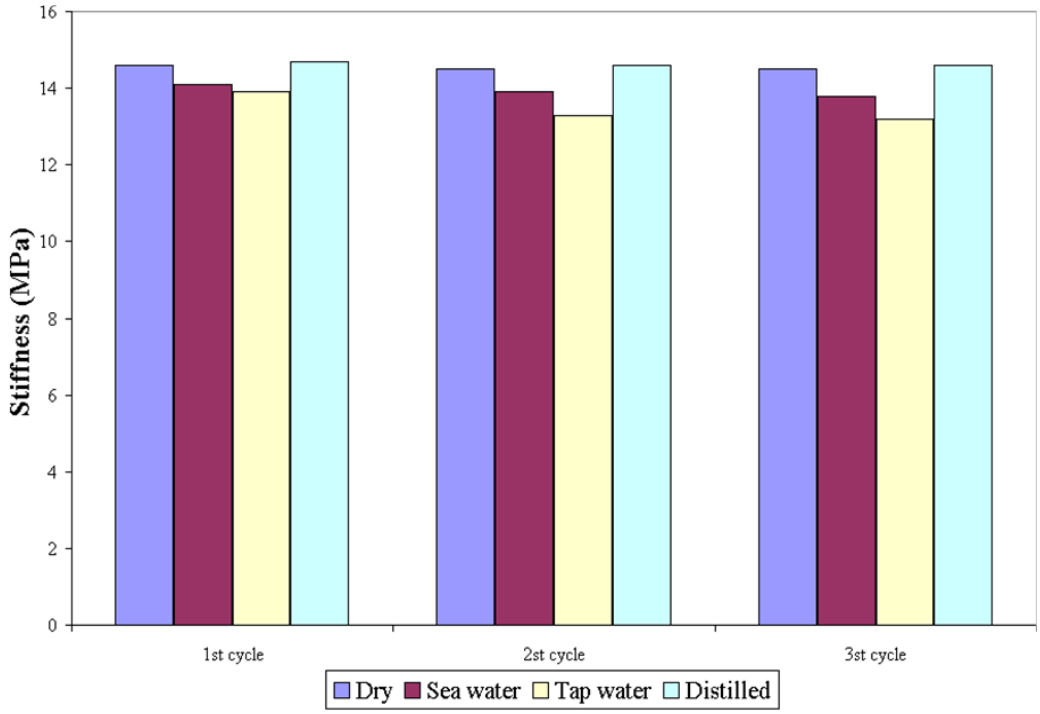

Figure 5.8: Comparison of modulus (GPa) due to immersion of $[\pm 45]_{2s}$ facing layups in sea water, distilled water and tap water at different cycles.

5.7 The effects of freezing and thermal cycling on mechanical properties

The effects of low temperature on the tensile modulus of $[\pm 45]_{2s}$ specimens were investigated in a manner similar to that described above under strain control at a rate of 300 με/min and up to 750 με. Strain levels were recorded with an extensometer and stayed within the linear elastic range. To study the effects of low temperature, the specimens were enclosed within an environmental chamber connected to a liquid nitrogen (LN2) and cryogenic solenoid as shown in Figure 5.9a. Figure 5.9b demonstrates the attainment of a considerably uniform temperature profile along the gage length of the specimen inside the environmental chamber at both 0 °C, and -15 °C. At each temperature level, the condition was maintained for at least two hours prior to testing, in order to allow for free thermal shrinkage.

At least eight $[\pm 45]_{2s}$ replicate facing specimens were used to ascertain the experimental results. For each specimen, three cycles of load-unload were employed to obtain consistent stiffness records as shown in Fig. 5.10. Figure 5.11 shows the set up of the tensile test of a facing specimen with an attached extensometer in a controlled environmental chamber at target temperature. The repeatability of experiments resulted in $15 \text{ GPa} \leq E \leq 16.5 \text{ GPa}$ at room temperature as shown in Figure 5.10.

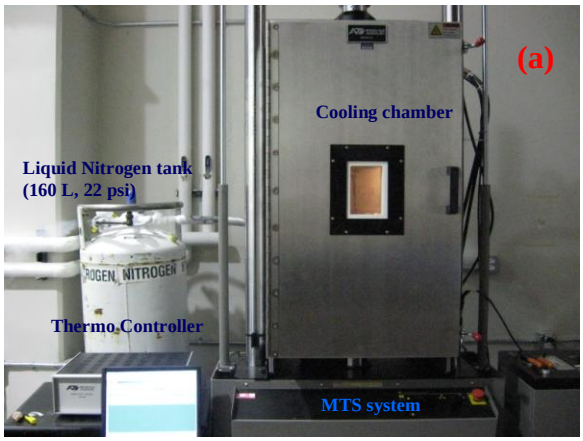

(b)

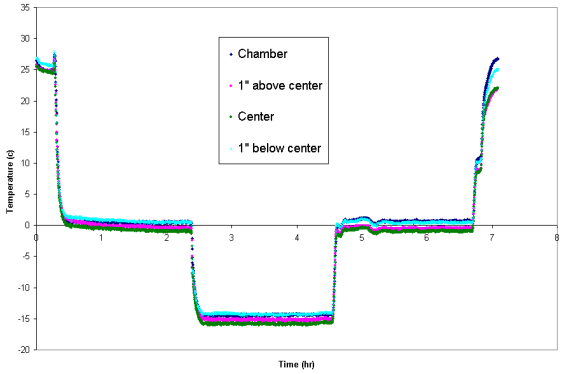

Figure 5.9a: Experimental setup. (Left)

Figure 5.9b: Temperature profile along specimen gage length. (Right)

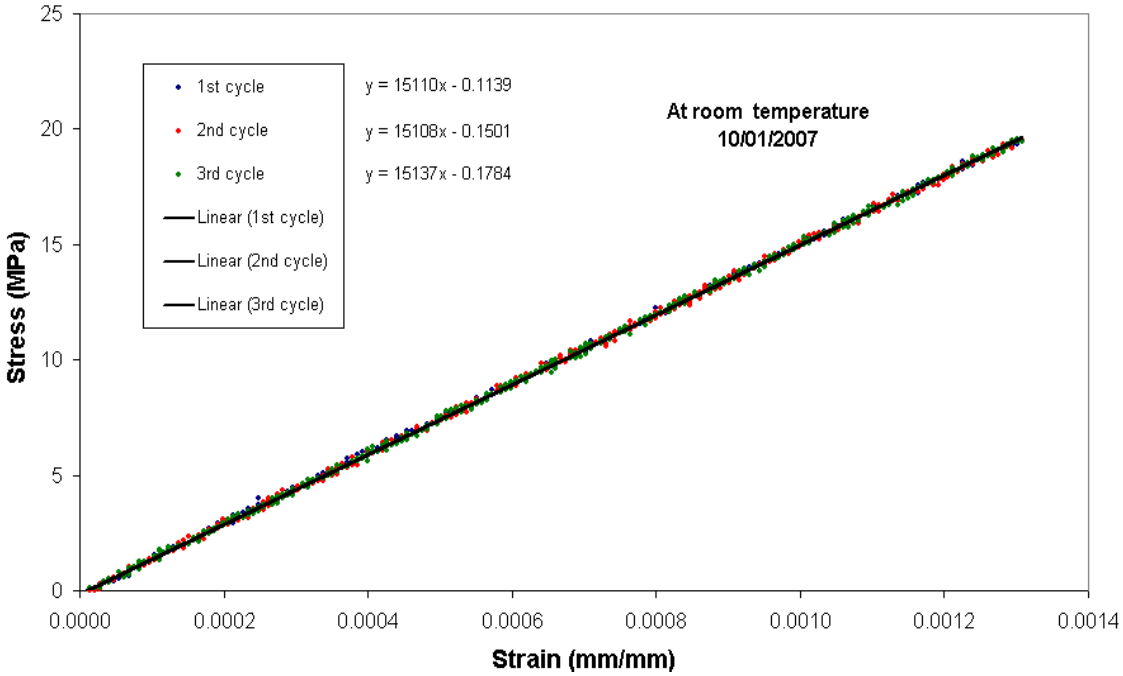

Figure 5.10: Typical data of E (3 cycles) for a $[\pm 45]_{2s}$ facing layup.

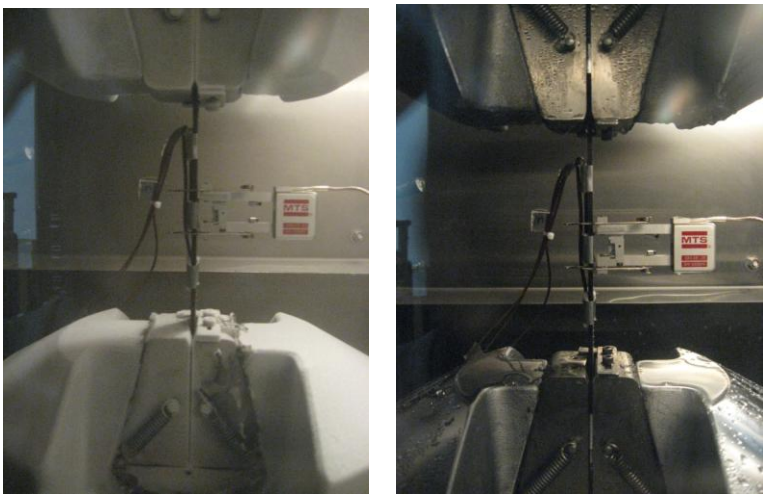

Figure 5.11: Facing specimen being tested at -15 °C and upon returning to room temperature.

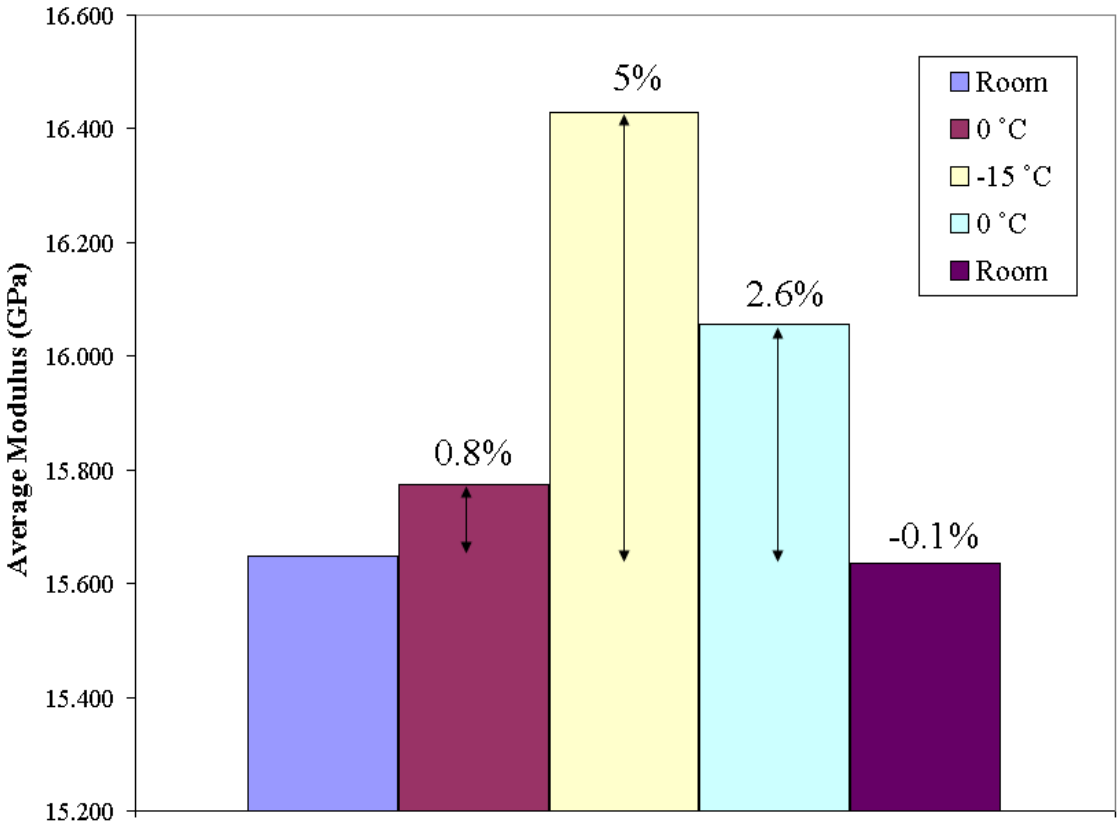

Figure 5.12: Average values of dry elastic modulus at low temperatures.

The value of the elastic modulus of dry eight $[\pm 45]_{2s}$ specimens ranged between 15 and 16.5 GPa. Comparative values of average of stiffnesses and percent changes at various temperatures are shown in Figure 5.12. Note the slight irreversibility that occurs upon the raising of temperature up from -15 °C.

A similar procedure was employed to record values of *E* after exposure to cyclic temperature. The combined effect of sea water and freezing was tested by pre-immersing the sample up to saturation at 40 °C for 3 months and measuring stiffness *E* immediately upon their removal from the bath. These wet specimens were then kept in a freezer at a target temperature of -10 ˚C for approximately 2 weeks and tested in tension. Then, the

same specimens were kept in the freezer for four additional weeks. To simulate a cold environment, the target temperature in the chamber was held roughly 1 hour before testing. The overall results were close to those of dry facing where the average stiffnesses at low temperature increased by ***3-5 %*** at -10 ˚C beyond those of the dry specimens as shown in Figure 5.13.

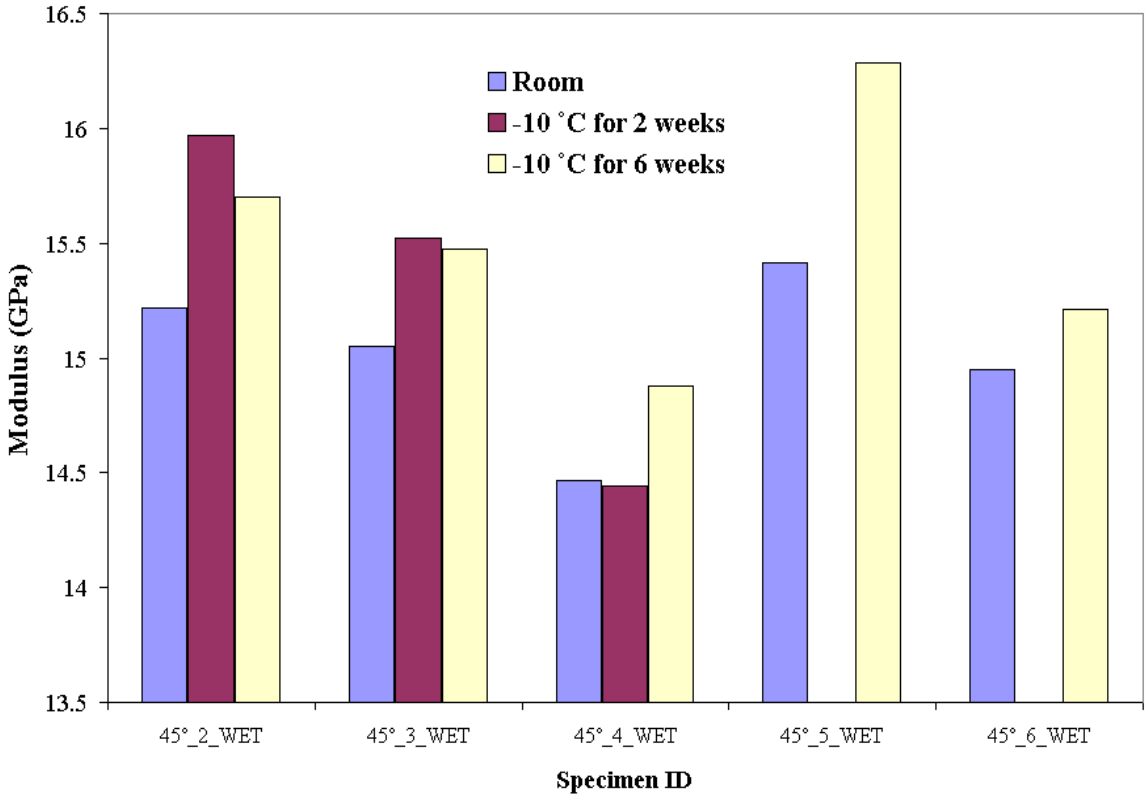

Figure 5.13: Comparison of stiffness values at ambient temperature and -10 ˚C over 6 weeks.

5.8 Thermal expansion of facing

The $[0/90]_{2s}$ facing specimens of planar dimension (200 mm × 25 mm) were dried in a desiccant chamber until the removal of all residual moisture. Subsequently, the

specimens were placed within a thermally insulated chamber subjected to controlled temperature variation with an extensometer attached to their centers to record strain. Three thermocouples were placed at different locations along the length of the specimen, namely at its center and 1" away in either direction to read temperature levels. Typical results for variation of strain with temperature are shown in Figure 5.14.

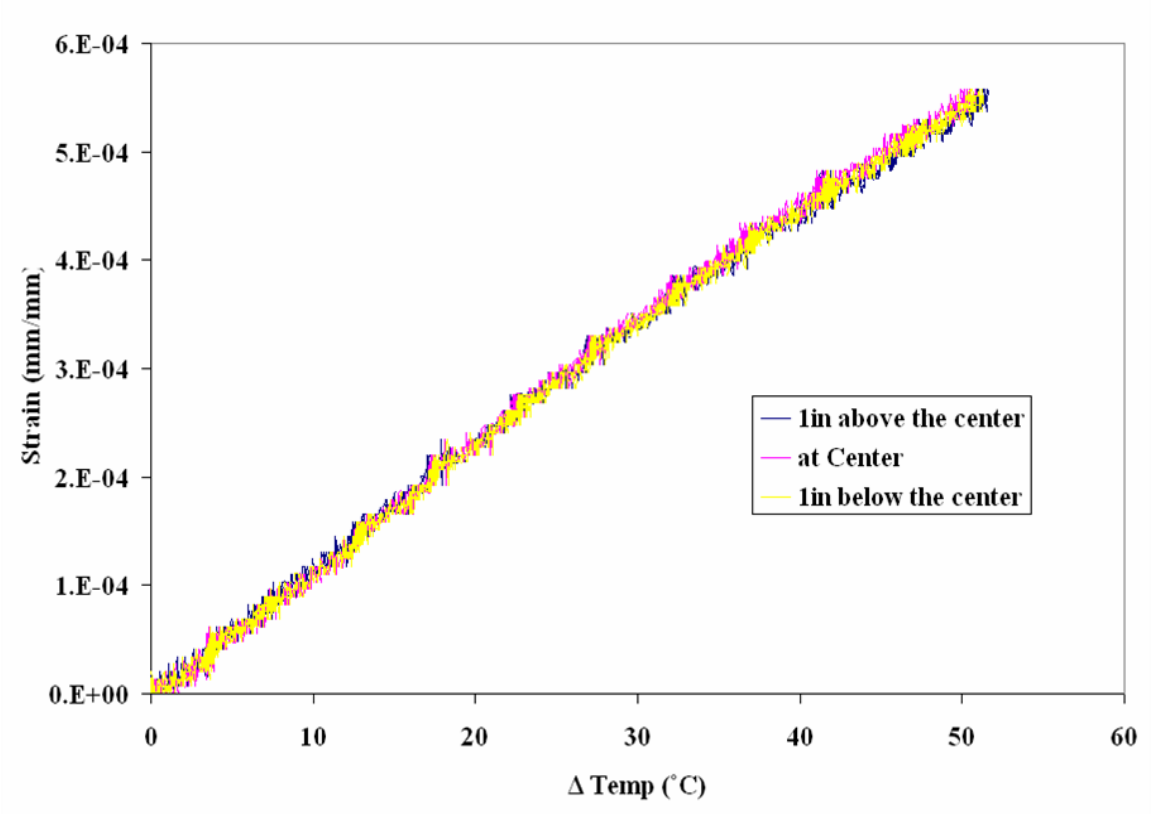

Figure 5.14: Typical thermal expansion data of $[0/90]_{2s}$.

The test temperature increased from 25 ˚C to approximately 75 ˚C, resulting in a temperature difference ΔT of about ~ 50 ˚C. Based on the results, an average thermal expansion coefficient of 11.5 με/˚C was obtained from the three specimens. It should be noted that in view of the thermal insulation provided by the foam core material a one-

sided exposure to ambient temperature would affect the deformation of the outer facings for a considerable duration prior to the onset of thermal equilibrium across the thickness of the sandwich structure

5.9 Summary

The tensile moduli of the $[0/90]_{2s}$ and $[\pm 45]_{2s}$ configurations of facing composites were found to average at about an elasticity of 80 GPa and 15 GPa, respectively. Immersion to saturation in simulated sea water had little effect on the above moduli. Moreover, a comparative study of exposure to sea, tap, and distilled water showed no significant differences in the ensuing values of strength and stiffness.

For tensile loading, cryogenic temperature was shown to have a very slight influence on the $[0/90]_{2s}$ layup while a 3-5% increase in the stiffness of the $[\pm 45]_{2s}$ layup was noted as temperature decreased. The latter increase disappeared upon returning to ambient temperature. The modulus of the $[\pm 45]_{2s}$ layup was also stiffer by 3-5% due to exposure to low temperature over 6 weeks.

Finally, it was found that for the $[0/90]_{2s}$ layup seawater induced an expansion of ε_H = 450 με per 0.5 % weight gain at saturation and the thermal expansion coefficient was 11.5 με/°C.

CHAPTER 6

A MODEL OF MOISTURE DIFFUSION IN POLYMERIC COMPOSITES AND ITS EFFECTS ON LAMINATE DEFORMATION

Abstract

A mathematical model is presented to describe the one-sided water ingress into a $[90/0]_s$ graphite/epoxy laminate using realistic values for moisture concentration and the diffusion coefficient. It is considered that moisture induces swelling strains and subsequent stresses in the laminate. Moisture profiles are obtained using one-dimensional diffusion with appropriate boundary conditions. The resulting stresses cause both extension and bending in the laminate.

6.1 Introduction

It has already been noted that polymers and polymeric composites absorb fluid when exposed to moist ambient environments or upon immersion in liquids. Consequently, this phenomenon occurs when these materials are utilized in an ocean environment. For sufficiently thin layers this absorption can be viewed as spatially one-dimensional

proceeding along the thickness dimension. The sorption of fluid is accompanied by expansion transversely to the fiber direction with little or no strain parallel to the fibers (Daniel and Ishai, 2005). For the cross ply lay-up of the composite laminates, the expansional mismatch between adjacent layers with different fiber orientations induces internal stresses, which deform and distort the laminate (Harper, 1987; Chung, 1994; Sala, 2000; Wan et al., 2002). These dimensional changes are analyzed in the sequel by means of laminate theory that accounts for both bending and stretching effects. The process of moisture diffusion is assumed to follow the classical Fickian model, which serves to predict water distribution across the laminate's thickness that accords with various boundary and initial conditions (Weitsman, 1976; Lee and Peppas, 1993; Roy et al., 2001).

6.2 Classical one-dimensional diffusion

Considering both material isotropy and homogeneity, the diffusion process is assumed to follow the classical form of Fick's law, as mentioned in Chapter 2. For the one dimensional case of moisture absorption that proceeds across the thickness of both the 0^{o} and 90^{o} laminate of a cross-ply laminate, this phenomenon is not affected by fiber orientations. The assumption of isotropy resulted in weight gain data that agreed rather well with Fick's law predictions (Shen and Springer, 1977; Gopalan et al., 1986).

Consider the one-dimensional circumstance of diffusion shown in Figure 6.1.

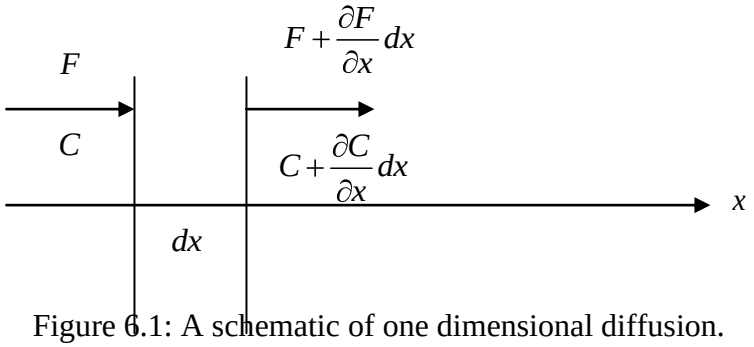

Figure 6.1: A schematic of one dimensional diffusion.

Where: F -Fluid flux, or rate of transfer

D -Diffusivity

C -Content of the diffusing substance in medium

t -Time

x -Spatial coordinate for one dimensional

The basic requirement of mass conservation, in the absence of sources or sinks reads

$$\frac{\partial C}{\partial t} = -\frac{\partial F}{\partial x} \tag{6.1}$$

while the assumption that flux is directed from higher concentrations to lower ones results in the constitutive expression

$$F = -D\frac{\partial C}{\partial x} \tag{6.2}$$

Combining Eqn. (6.1) and (6.2) one obtains

$$\frac{\partial C}{\partial t} = -\frac{\partial}{\partial x} F = \frac{\partial}{\partial x}\left(D\frac{\partial C}{\partial x} \right)$$

The further assumption that D is a constant results in the classical form of Fick's law

$$\frac{\partial C}{\partial t} = D\frac{\partial^2 C}{\partial x^2} \tag{6.3}$$

Equations 6.1 and 6.2 are usually referred to Fick's first and second laws of diffusion.

6.3 A specific boundary value problem of diffusion

The purpose of the following analysis is to evaluate the variation over time of the moisture distribution in a thin plate of thickness *h* under a one-sided exposure to the ambient environment. The plate consists of a $[90/0]_s$ fiber-reinforced lay-up with diffusion transverse to the fiber direction, as shown in Figure 6.2.

Water ingress is considered to occur only in the direction normal to the surface, i.e. across $0 \le x \le h$, and the plate is assumed to be initially dry (Chang, Wang, and Tsai, 2008).

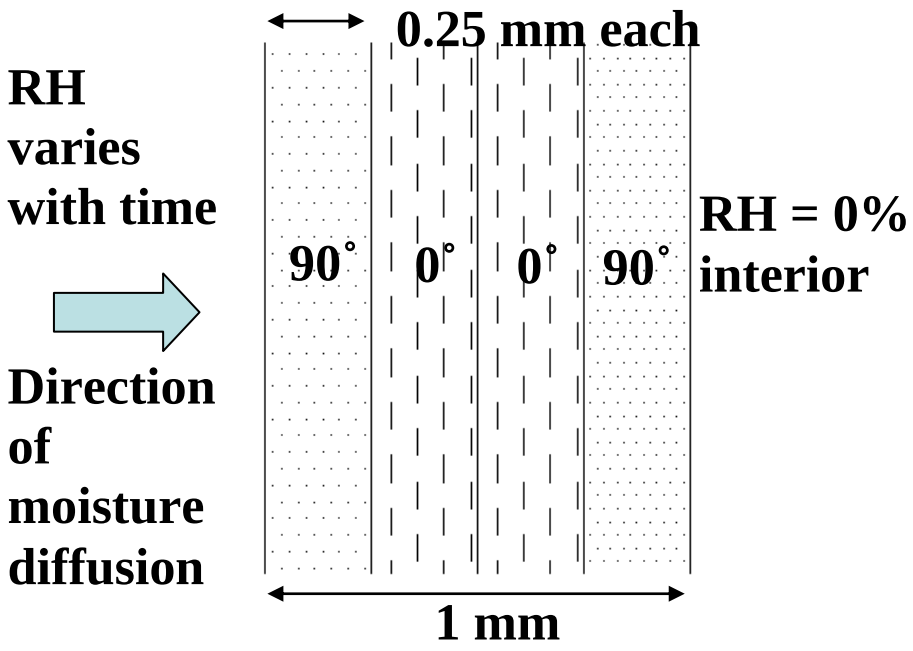

Figure 6.2: Schematic of fiber orientation of graphite/epoxy lay-up.

The boundary conditions are applied and initial conditions for this case read

$C = C_o$, $x = 0$, $t \geq 0$,

$C = 0$, $x = h$, $t \geq 0$,

$C = 0$, $0 \leq x \leq h$ $t = 0$,

The solution to the above problem is given by Crank (Crank, 1980) to read

$$C(x,t) = C_1 + C_1(1 - \frac{x}{h}) + \frac{-C_1}{\pi} \sum_{n=1}^{\infty} \frac{1}{n} \sin \frac{n\pi x}{h} \exp(\frac{-Dn^2\pi^2 t}{h^2}) \qquad (6.4)$$

where the first term corresponds to the equilibrium state as $t \to \infty$ and the series portion converges extremely slowly as $t \to 0$. For typical graphite/epoxy composites the diffusivity D is D = 2 $\times 10^{7}$mm^2/sec. Therefore, for h = 1 mm the diffusion process at early times can be approximated to within 0 (10^{-6}) by assuming the plate to be of infinite thickness. It follows that

For $t < 10^4$ sec

$$C(x,t) = C_1 erfc \frac{x}{2\sqrt{Dt}} \text{②} \tag{6.5}$$

Namely, for $t < 10^4$ sec the interior boundary remains essentially dry when the outer boundary is exposed to moisture.

Assuming the laminate to be exposed to moisture concentration C_1 = 1% on one side of a $[90/0]_s$ lay-up, Figure 6.3 shows moisture distribution $C(t,x)$ calculated from Eqn. (6.4) for $10^4 < t < \infty$ (sec) until attaining equilibrium. For the earlier time spans it was necessary to employ up to 30 terms in the series expressed therein. The distributions for $0 < t < 10^4$ sec obtained from Eqn. (6.5) are shown in Figure 6.4. These distributions will cause time-dependent expansional extension and curvatures of the $[90/0]_s$ laminate. In

② The complementary error function $erfc(z)$ is defined as $erfc(z) = \frac{2}{\sqrt{\pi}} \int_z^\infty e^{-t^2} dt$ and for sufficiently large values of z (i.e. short time t). It is given by $erfc(z) \sim \frac{e^{-z^2}}{z\sqrt{\pi}} \sum_{n=0}^{\infty} \frac{(-1)^n (2n!)}{(n!)(2z^2)^n}$.

view of h = 1 mm, it follows that each ply has 0.25 mm thick. It can be seen that fluid stays mostly within the first ply ($0 < x < 0.25$ mm) for very long time.

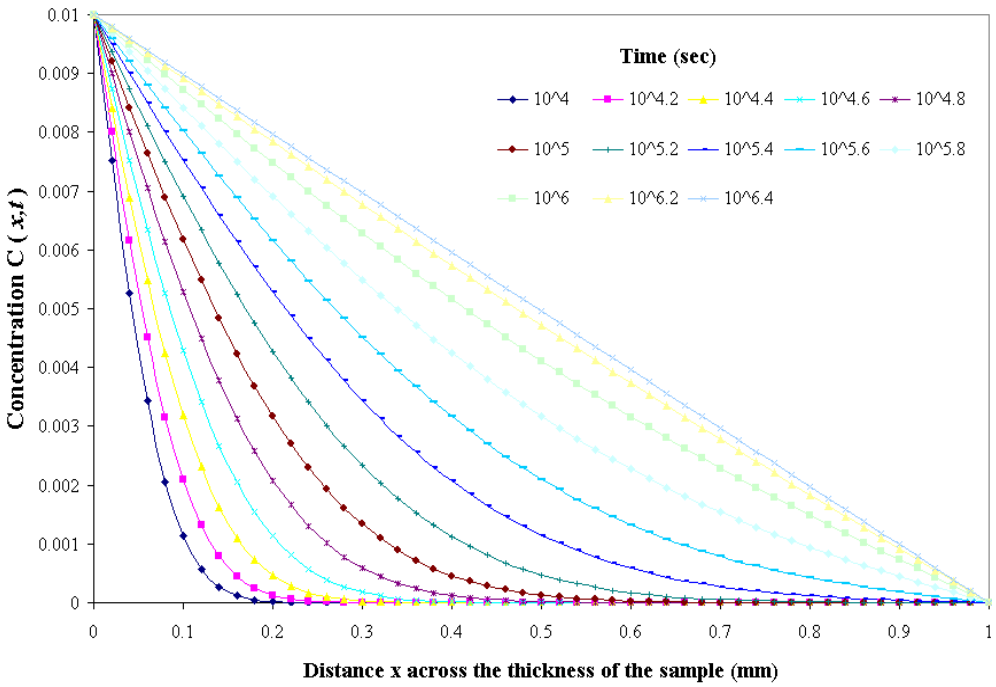

Figure 6.3: Moisture distribution at interested period of $10^4 < t < 3.6\times10^6$ sec

(Approximate 3 hours < t < 4 weeks).

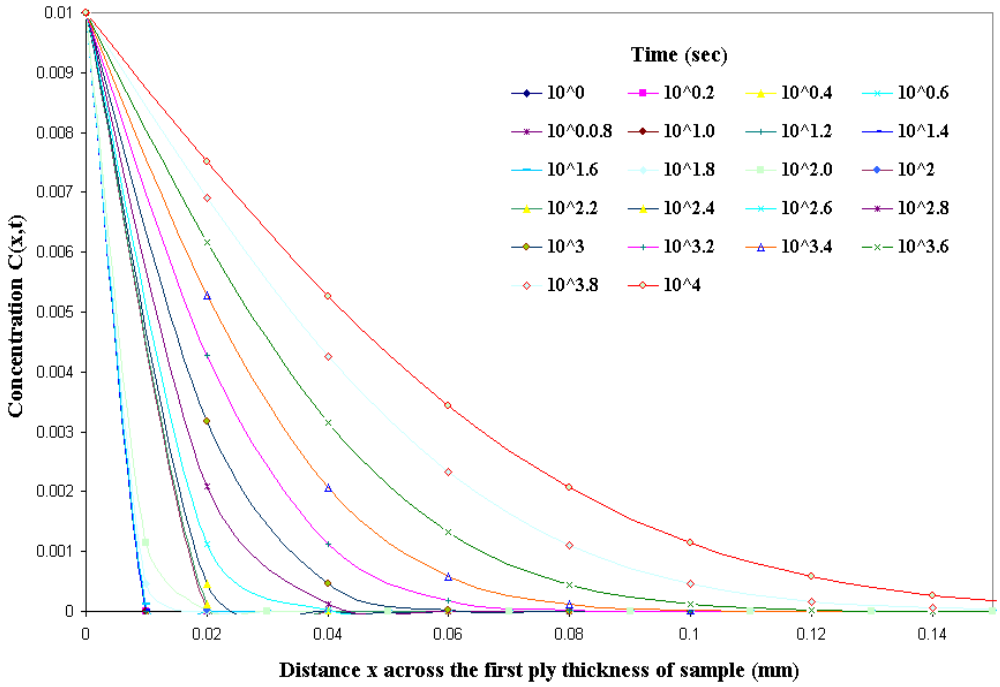

Figure 6.4: Moisture distribution at interested period of $0 < t < 10^4$ sec.

6.4 Expansional strain as related to moisture uptake

Laminate theory combines the individual response of each ply within the context of plate theory. The simplest formulation follows the Love-Kirchhoff assumption that planes normal to the mid-surface of the plate remain so in the deformed state as well. Furthermore, both plies and plate are assumed to be in a plane stress state (Daniel and Ishai, 2005). Since it was recorded that expansional strains develop in the 90˚ plies alone, their tendency to expand freely- sketched in Figure 6.5- is constrained by the joint laminate action.

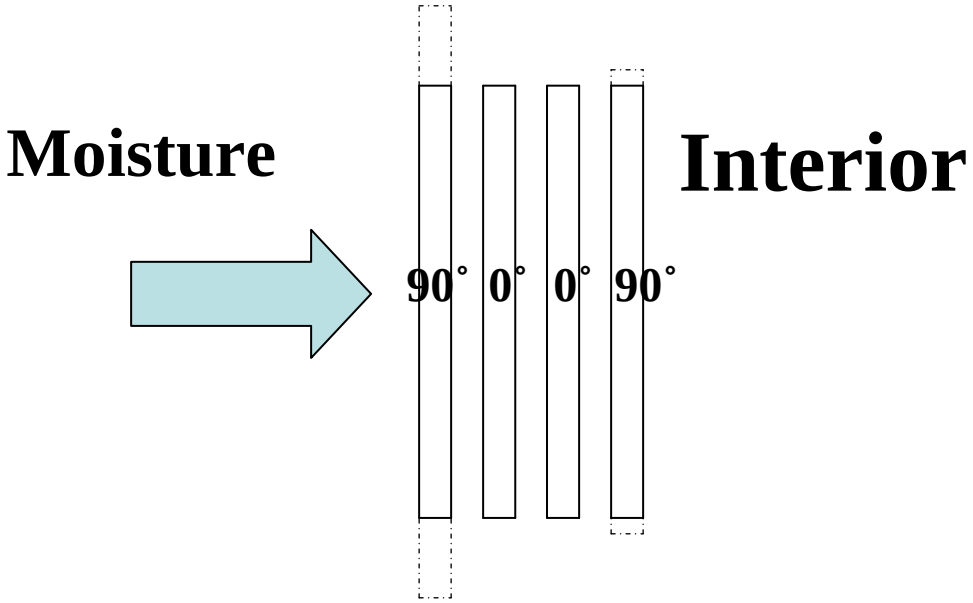

Figure 6.5: Free expansional strains if each ply could swell independently.

To account for the laminate action, consider first that the 90˚ plies are constrained against expansion by the application of compressive stresses $\sigma_{90} = -E_T \beta_T \cdot C(x,t)$, where E_T and β_T denote the transverse modulus and the transverse coefficient of moisture expansion, respectively. These stresses eliminate any moisture-induced expansion and thus allow the laminate to maintain a perfect bond between all its plies. The next and final step is to apply the above stresses in the opposite direction and consider them to act on the laminate employing laminated plate theory. In that final step the following external stresses are equivalent to the effect of the moisture induced swelling:

$$\sigma = \begin{cases} 0 & \frac{h}{4} < x < \frac{3}{4}h \\ E_T \beta_T \cdot C(x,t) & 0 < x < \frac{h}{4} \text{ and } \frac{3}{4}h < x < h \end{cases} \tag{6.6}$$

The resultant force and its location are

$$N(t) = \int_0^h \sigma(x,t)dx \tag{6.7}$$

$$e(t) = \frac{M(t)}{N(t)} \tag{6.8}$$

Where

$$M(t) = \int_0^h x \cdot \sigma(x,t)dx \tag{6.9}$$

As shown in Figure 6.6, laminated plate theory is used to account for the effects of *N* and *M* on the extension and bending caused by moisture ingress.

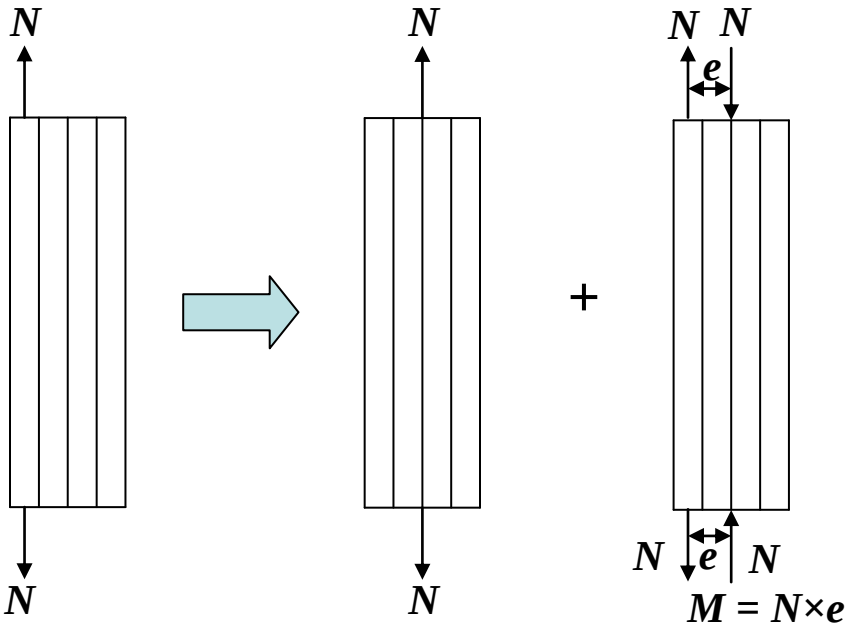

Figure 6.6: Interior moisture distribution induces strains from both normal stresses and bending.

6.5 Laminate deformation vs. time

From laminate theory, the deformation corresponding to moisture ingress is derived on the basis of the Love-Kirchhoff assumption that $\varepsilon = \varepsilon_o + kz$ **.** Where z is the thickness coordinate, perpendicular to *x*, and *k* and ε_o are the common laminate curvature and in-plane strain, respectively.

Upon denoting the longitudinal and transverse moduli of the individual piles by E_L and E_T, respectively, it follows that for the laminate at hand, one has

$$\varepsilon_o = \frac{N}{\frac{h}{2}(E_T + E_L)} \tag{6.10}$$

$$k = \frac{96M}{h^3(E_L + 7E_T)} \tag{6.11}$$

Employment of the material values listed in Table 6.1 together with the time dependent moisture distributions shown in Figure 6.3, and the corresponding integrated values for *N(t)* and *M(t)*, yielded the temporal results for k and ε_o shown in Figure 6.7a and b. Note that ε_o and *k* have reached the values of 100 $\mu\varepsilon$ and 1 m^{-1} after 4 weeks.

Table 6.1: Typical material properties of uni-directionally reinforced graphite/epoxy material

Property		Dimension
Longitudinal modulus	142	GPa
Transverse in-plane modulus	10.3	GPa
Transverse moisture expansion coefficient, β_T	0	
Transverse moisture expansion coefficient, β_T	0.3%	Per 1% wt gain
Diffusion coefficient $D = D_T$	2×10^7	mm^2/sec

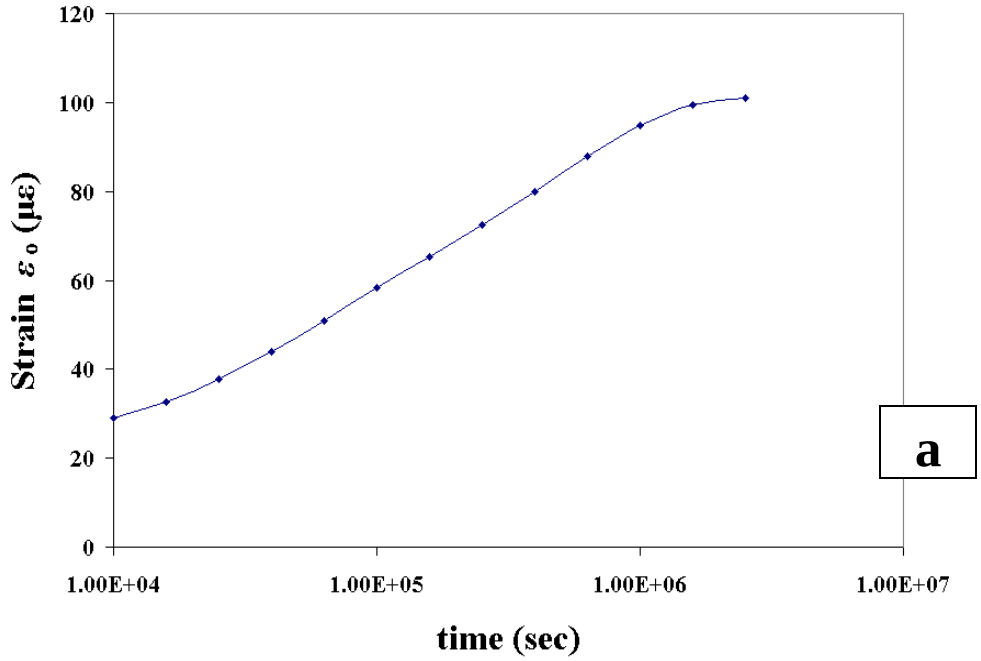

Figure 6.7a: The mid-plane strain ε_o caused by moisture concentration 1% during 3 hr < t < 4 weeks.

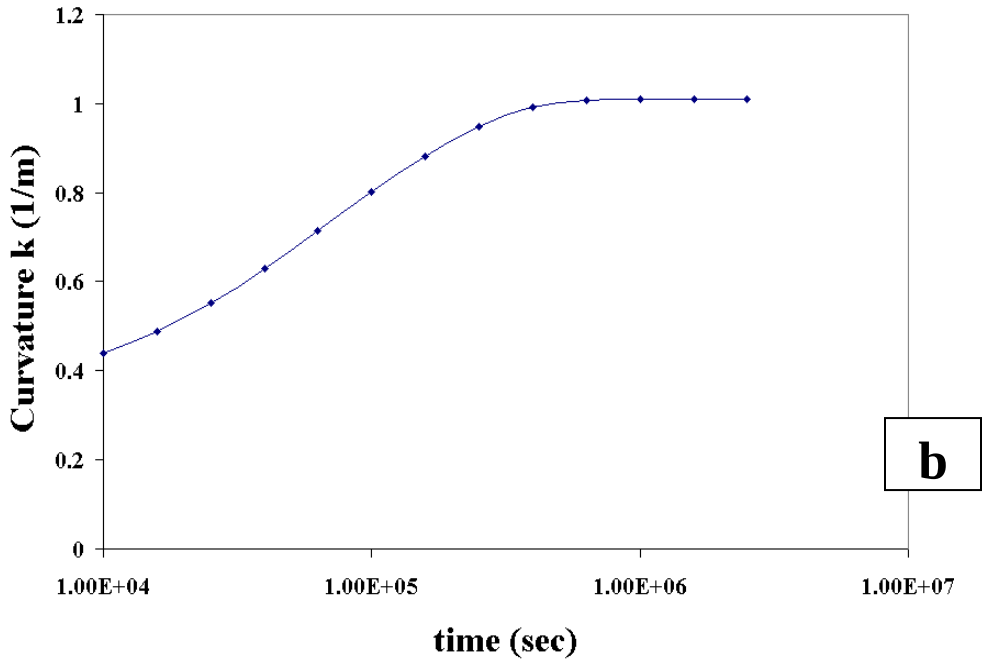

Figure 6.7b: The mid-plane curvature k caused by moisture concentration 1% during 3 hr < t < 4 weeks.

Consider now that the one sided moisture concentration of 1% was maintained for 4 weeks and suddenly withdrawn at that time due to abrupt external drying. Figure 6.8 shows moisture distribution over a time period of 2 hr < t < 4 weeks during water egress.

There were two different ways to obtain the same solution for the moisture distribution shown in Figure 6.8. The first was a superposition method whereby the results of the early one sided exposure at time t = 0 were employed up to $t \to \infty$, from which were subtracted the very same values, shifted by a time lag of 10^4 sec, up to $t \to \infty$. This is formally expressed by $C(x,t) = C(x,t=0) - C(x,t-10^4)$.

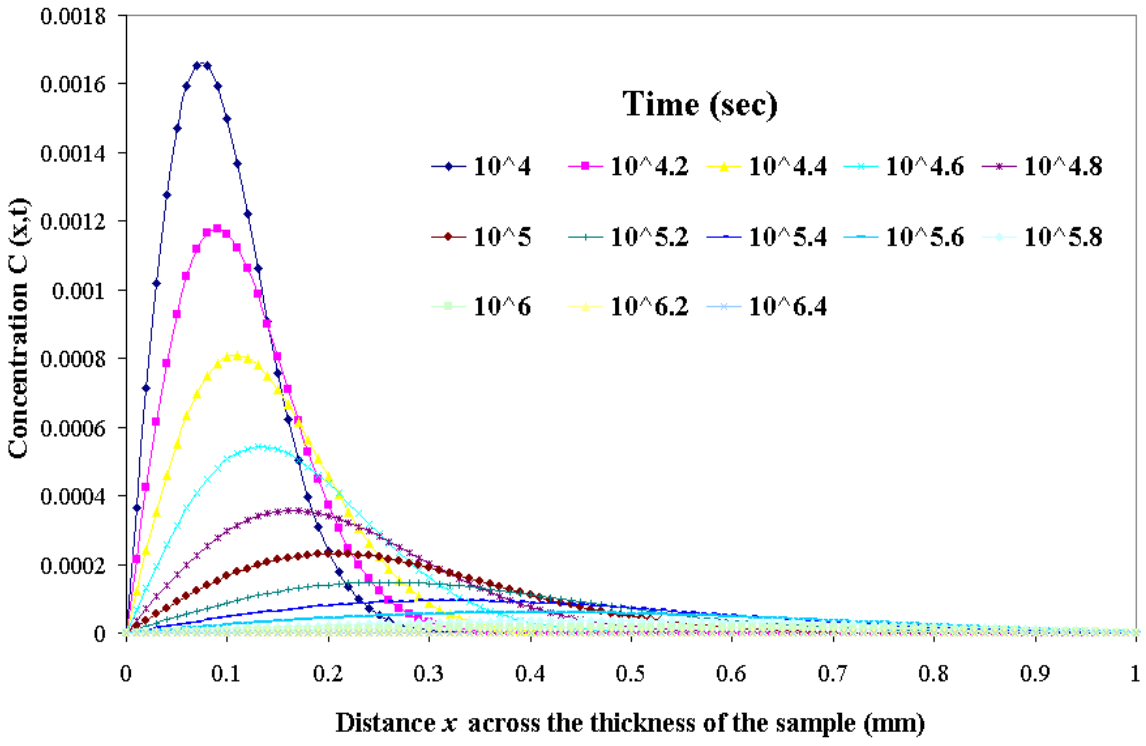

Figure 6.8: Moisture distribution after facing starts desorbing over 3 hr < t < 4 weeks.

The second approach employed the Green's function method and is based on the Fourier series solution expressed in Eqn. (6.3). This, more general, approach applies to circumstances when an initial moisture distribution cannot be described in known analytical forms. Accordingly, moisture is considered to be concentrated over a very short portion about an arbitrary location within the interior region, say

$$C(x,0)=\begin{cases} C_o & x_o < x < x_o + \Delta x \\ 0 & \textit{elsewhere} \end{cases} \tag{6.12}$$

The general solution with an initial distribution $C(x,0) = f(x)$, $C(0,t) = C_1$, and $C(0,h) = C_2$ is given by (Crank, 1980)

$$\begin{aligned} C(x,t) = C_1 + (C_2 - C_1)\frac{x}{h} + \frac{2}{\pi}\sum_{n=1}^{\infty}\frac{C_2\cos n\pi - C_1}{n}\sin\frac{n\pi x}{h}\exp\left(\frac{-Dn^2\pi^2 t}{h^2}\right) \\ + \frac{2}{h}\sum_{n=1}^{\infty}\sin\frac{n\pi x}{h}\exp\left(\frac{-Dn^2\pi^2 t}{h^2}\right)\int_0^h f(x')\sin\frac{n\pi x'}{h}dx' \end{aligned} \tag{6.13}$$

when $C_1 = C_2 = 0$ in Eqn. (6.13) reduces to

$$C(x,t) = \frac{2}{h}\sum_{n=1}^{\infty}\sin\frac{n\pi x}{h}\exp\left(\frac{-Dn^2\pi^2 t}{h^2}\right)\int_0^h f(x')\sin\frac{n\pi x'}{h}dx' \tag{6.14}$$

And with $f(x)$ given in Eqn. (6.12) the integral in Eqn. (6.14) reduces to

$$\begin{aligned} \int_0^h f(x')\sin\frac{n\pi x'}{h}dx' &= \int_{x_o}^{x_o+\Delta x} C(x_o,0)\sin\frac{n\pi x'}{h}dx' \\ &= -C(x_o,0)\frac{h}{n\pi}\cos\frac{n\pi x'}{h}\Big|_{x_o}^{x_o+\Delta x} \\ &= -\frac{C(x_o,0)h}{n\pi}\left(\cos\frac{n\pi(x_o+\Delta x)}{h} - \cos\frac{n\pi x_o}{h}\right) \end{aligned} \tag{6.15}$$

Upon setting $x_o = i\Delta x$ $(i = 1, 2, ..., \frac{h}{\Delta x})$, expression Eqn. (6.15) reads

$$-C(i\Delta x, 0)\frac{h}{n\pi}(\cos\frac{n\pi(i+1)\Delta x}{h} - \cos\frac{n\pi i\Delta x}{h}) \quad ③ \tag{6.16}$$

Upon employment of Eqn. (6.16), for the entire initial distribution $C(x,0)$, Eqn. (6.14) reads

$$C(x,t) = -\frac{2}{\pi}\sum_{n=1}^{\infty}\frac{1}{n}\sin\frac{n\pi x}{h}\exp(\frac{-Dn^2\pi^2 t}{h^2})\cdot \left\{\sum_{i=0}^{h/\Delta x - 1} C(i\Delta x, 0)[\cos\frac{n\pi(i+1)\Delta x}{h} - \cos\frac{n\pi i\Delta x}{h}]\right\} \tag{6.17}$$

With the distribution $C(x_o,0)$ prescribed by the values shown in Figure 6.3 and 6.4, the utilization of the Green's function method resulted in the plots drawn in Figure 6.8.

Note that the moisture distributions shown in Figure 6.3 and 6.4 match at time $t = 10^4$sec, though they were computed by Eqn. (6.4) and (6.5), respectively. Similarly, both the superposition method and Green's function approach yielded the same plots for the residual moisture distribution shown in Figure 6.8. Note that agreement was achieved for $\Delta x = h/100$.

The incorporation of the results shown in Figure 6.8 within the laminate theory expressions (6.6)-(6.11) result in the plots drawn in Figure 6.9(a) and (b).

---

③ Taylor's series expansion about $i\Delta x$ of Eqn. (6.16) reduces it further to

$$C(i\Delta x, 0) \sim \sin\frac{n\pi i\Delta x}{h}\cdot i\Delta x + 0(i\Delta x)^2.$$

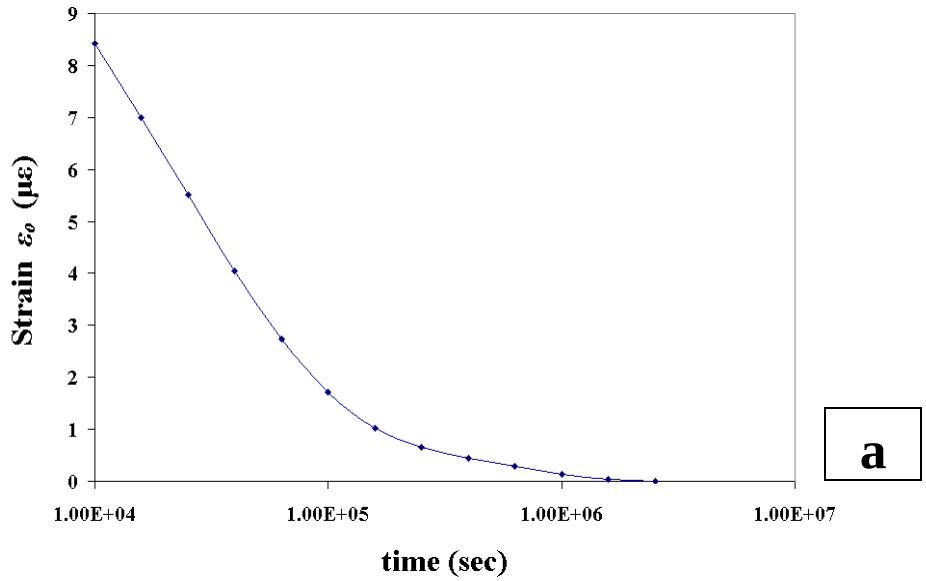

Figure 6.9a: The mid-plane strain ε_o profile vs. time corresponding to residual moisture induced stress, following desorption after absorbing water for 4 weeks.

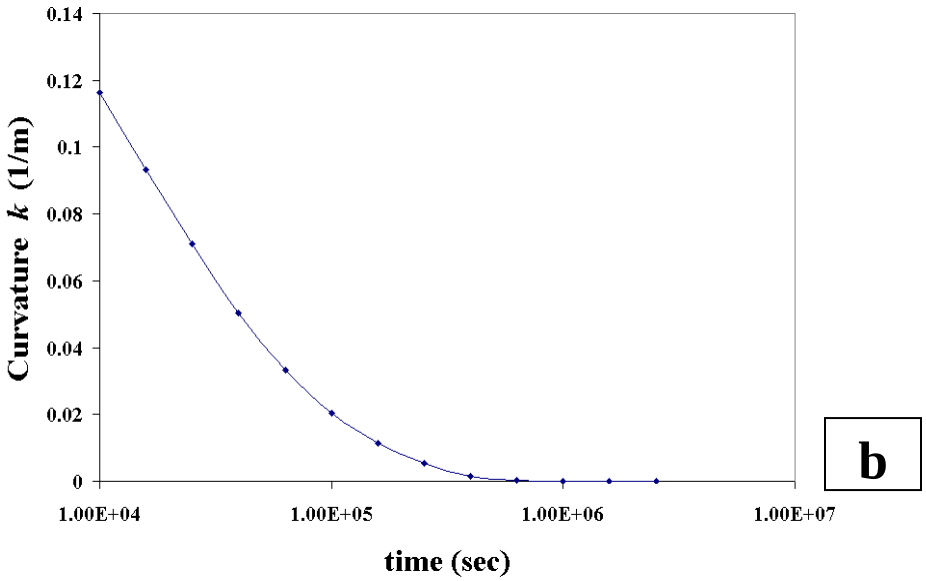

Figure 6.9b: The mid-plane curvature *k* vs. time corresponding to residual moisture induced stress, following desorption after absorbing water for 4 weeks.

6.6 Summary

Following a large body of data, it has been assumed that the primary mechanism of moisture uptake in polymeric composites was by diffusion, whereby the usage of composites in sea environment gives rise to stresses induced by sea water. Due to the small thickness of the composite laminate, the mathematical prediction used herein was based upon the one dimensional Fickian diffusion model. It was shown that exposure to one sided moisture concentration that corresponds to an equilibrium weight gain of 1% can distort a 1 mm thick cross-ply laminate by strain and curvature of 100 $\mu\varepsilon$ and 1 m^{-1}, respectively. This amount of deformation may lead to the failure of laminate by creating internal cracks, especially under cyclic exposure.

CHAPTER 7

FRACTURE BEHAVIOR AND MOISTURE UPTAKE OF H100 PVC FOAM

This chapter is the combination of a portion of a conference paper submitted to the 17th International Conference on Composite Materials (ICCM-17): 27-31 July 2009 Edinburgh, UK and quarterly reports under a sub-contract from Florida Atlantic University (FAU).

D. Penumadu, Y. J. Weitsman, A. Siriruk, K. G. Thomas "Novel Experimental Techniques to Determine Fracture Toughness of Cellular Foam and Sea Water Effects"

Abstract

Polymeric sandwich composite structures are routinely used in a variety of naval and aerospace applications and are inevitably exposed to humidity, sea water, hydrostatic pressure, and large temperature variations over extended periods of time. Foam core materials are often used for sandwich panels, and H100 foam is used in this study for evaluating the influence of temperature variation and moisture content on foam core materials. In a previous study, a minimal effect of 5% reduction in stiffness was observed when foam core specimens were soaked in simulated sea water for an extended duration. Previous studies have also shown a degradation loss of 30% in the energy release rate for the facing-foam interface due to long-term exposure to a sea environment.

The present study is focused on the H100 foam core material in order to isolate its role within the overall seawater-induced degradation observed in the fracture behavior of sandwich structures. For this purpose, a specific experimental set-up was developed that uses side-notched specimens of rectangular cross section in order to channel Mode I cracks in a self-similar manner. Using this technique, the effects of sea water on the fracture behavior of PVC foam was quantified. In addition, to simulate the effect of the hydrostatic pressure present in an ocean environment, specimens were immersed in a pressurized chamber to study the water uptake of H100 foam over time and its subsequent mechanical behavior. It is concluded that PVC foam core material does not show any significant degradation in its mechanical properties due to sustained exposure to sea water.

***Keywords**:* Sea water effects, fracture toughness, sandwich structures, PVC foam core

7.1 Introduction

The Divinycell H type foam is DIAB's most commonly used core material for sandwich panels. In general Divinycell foam has a high strength-to-weight ratio, good dynamic strength, excellent insulating properties, and a closed-cell structure that has advantages when used in close proximity to water. The Divinycell foam is widely used in the marine, transportation, and aerospace industries, and is often used for applications where strength, stiffness, and low weight are desired.

This study is part of a research effort aimed at evaluating of the effects of sea water on composite materials and sandwich structures for naval use. Delamination at the interface of the facing and foam core is one of the major failure mechanisms in sandwich composites. In this study, H100 foam core material, which is tested in both dry and soaked states, was evaluated using the mid-plane fracture toughness test on sandwich layup using Mode I sandwich beam configurations. The usual definition of Mode I pertains to the opening mode for a crack lying in a plane of symmetry parallel to the material. The energy necessary to initiate and propagate a crack was measured following established procedures (Anderson, 2004). In a previous investigation (Li and Weitsman, 2004) a weight gain of 2.5 mm thick H100 and H200 PVC foam immersed in sea water at ambient temperature for over 400 hours was recorded. The water content saturation was measured at 170% for H100 and 40% for H200 PVC. In the current study, similar experiments were repeated by soaking 4mm thick samples of H100 in sea water baths at 40 ˚C until a state was reached where no further weight gain was recorded over time. To determine the effects of hydrostatic pressure, comparable mechanical properties were obtained for dry samples as well as for samples immersed in water under several levels of hydrostatic pressure. The combined effects of cryogenic temperatures and hydrostatic pressures were also investigated.

7.2 Comparison of Mode I dry and wet foam fracture toughness

7.2.1 Material and specimen preparation

For this study, DIAB Divinycell H100 PVC foam core material was selected. H100 is a semi-rigid foam consisting of a closed-cell structure with a density of 100 kg/m^3. Tensile

and shear strength properties of H100 were measured using test specimens of dog bone geometry as detailed in Chapter 3. A summary of measured tensile and shear moduli values for H100 in both dry and wet states is presented in Table 7.1**.**

Table 7.1: Mechanical properties of H100 PVC foam core.

Property	Foam	Dimension
Coefficient of thermal expansion, α	70	με/˚C
Moisture expansional strain at saturation, ε_H	2200	με at saturation
Longitudinal modulus, *E* (Dry)	60	MPa
Longitudinal modulus, *E* (Wet)	22*	MPa
Shear modulus, *G* (Dry)	25	MPa
Shear modulus, *G* (Wet)	7.3*	MPa
Poisson's ratio, *v* (Dry)	0.13	

* Implied from data by means of analysis of Eqn. (3.11)

Figure 7.1 shows the configuration of modified double cantilever beam (DCB) specimen used to evaluating Mode I fracture toughness (Camps et al., 2000). The DCB specimens were obtained from a larger panel using a band saw with final dimensions of 250 mm in length, 25 mm in width, and 25 mm in thickness. Although channeled to remain in the mid-plane of the sample by means of the 6 mm deep notches cut on both sides (see Figure 7.1), the cracks were nevertheless ragged rather than smooth. This is due to the random cellular structure of foam material. To obtain behavior close to Mode I and prevent the specimen from the excessive bending, aluminum T-bars were adhesively bonded to reinforce the top and the bottom planes of the sample as shown in Figure 7.2. In order to simulate a natural crack, a sharp V-shaped blade was used to precrack the specimen 25.4 mm from its loaded edge.

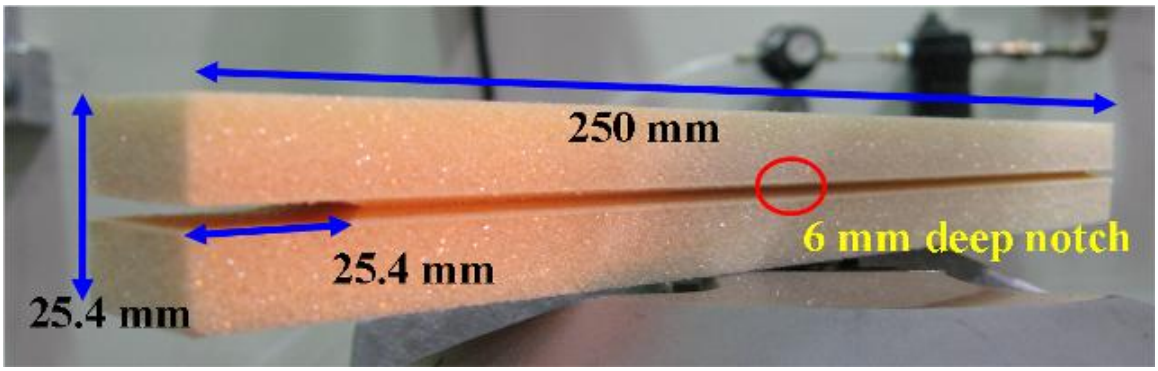

Figure 7.1: H100 PVC foam double cantilever beam configuration.

7.2.2 Experimental testing procedure

Fracture tests were carried out using a 100 kN MTS test system with a 3.5 kN external load cell. During the tests, the T-bars used to reinforce the specimens were attached to hinged connections so that the specimen rotation was unrestrained. A magnifying glass and DC back light were used to pinpoint the crack tip locations whenever intermittent crack growth came to a halt. The crack tip location was recorded immediately using a digital camera and a white out was used to locate the position of the crack tip during its propagation. The test configuration and a typical digital image are shown in Figure 7.2. Using digital image analysis software (ImagePro®), crack morphology was analyzed for use in determining energy release rates (G_{IC}).

Load was applied to the pre-cracked specimen using displacement control at a rate of 1 mm/min in a fashion similar to the delamination tests described in Chapter 4. Load and displacement data were recorded throughout the test. Axial tension was monotonically increased under displacement control until an abrupt drop in load amplitude was noted, at which stage crack extensions were observed, and the machine was unloaded back to zero displacement. This procedure was repeated until approaching the far edge of a specimen. The crack tip location were recorded on both front and back of the foam specimens to obtain information about the nature of the crack front and thereby estimate energy release rates.

In order to study the degradation of PVC foam core material due to sea water exposure, specimens were immersed in simulated sea water at a controlled temperature of 40 ˚C for at least 10 weeks prior to testing during which time they reached the saturation state. After completion of the ten week soaking cycle, the specimens were tested until the first stage of crack growth and arrest. Subsequent unloading established the first loop labeled No. 1 in Figure 7.3. As shown in Figure 7.3, the load immediately drops when the crack is arrested. Each subsequent reloading was done after the immersed specimens were re-soaked for an additional period of 2 weeks to ascertain the presence of a wet crack tip region. Six dry and two wet specimens were studied for eight frature loops (No. "2" through "8" in Figure 7.3) to facilitate interpretation of the G_{IC} results.

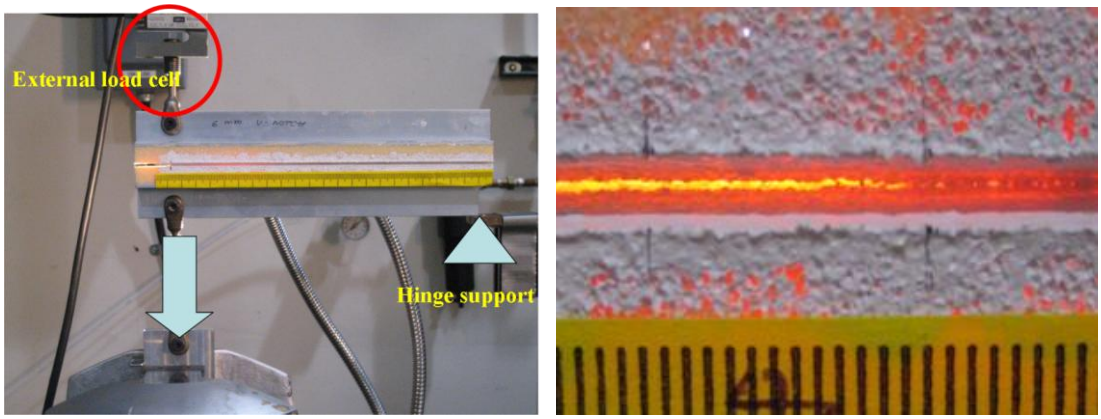

Figure 7.2: Experimental setup (left) and observed crack propagation (right).

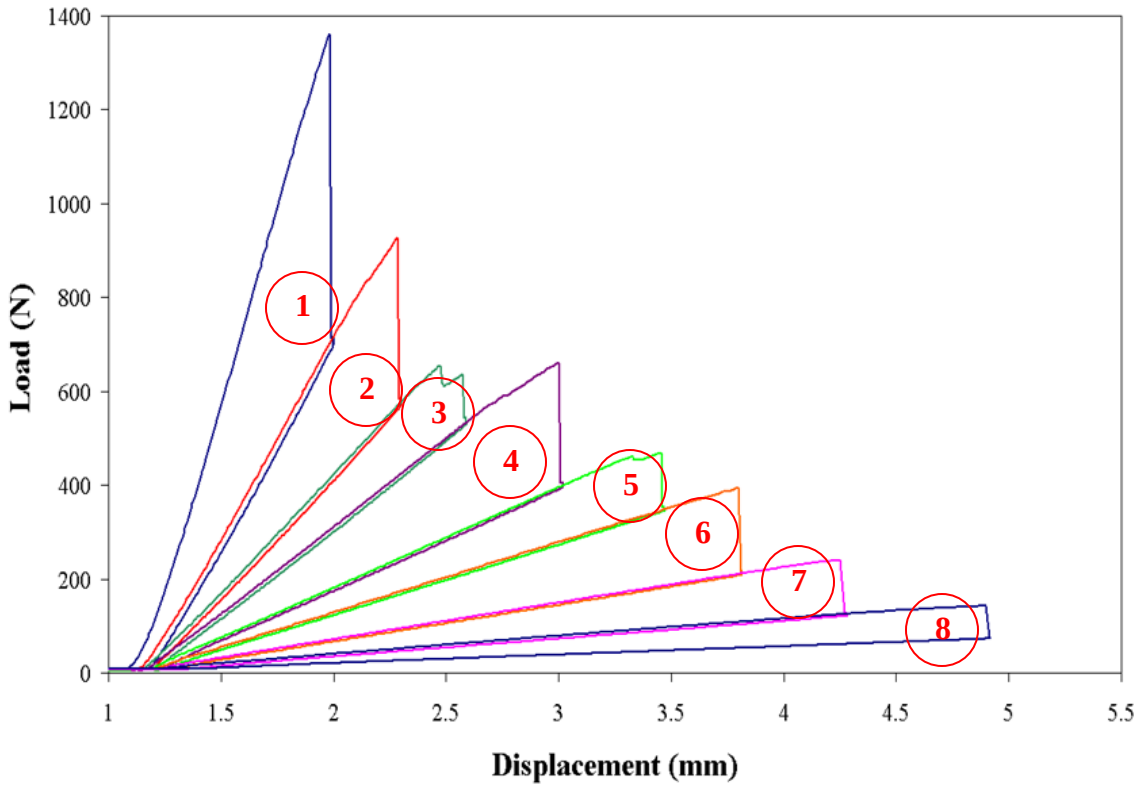

Figure 7.3: Typical crack propagation results.

7.3 Evaluation of wet and dry values of G_{IC} for H100 foam

A specific amount of energy per unit area is required to initiate crack growth in PVC foam core. Accordingly as for all materials, energy-based criteria (such as critical energy release rate G_c for linear elastic response or the more general critical values of the J-integral J_c) provide relevant information about material failure. In particular, linear elastic fracture mechanics (LEFM) is applicable in cases where small scale yielding is localized near the crack tip which is sufficiently far away from the next geometric feature of the material region. In such cases $G_c = J_c$ and both can be related to the critical stress intensity factor K_c.

Similar considerations apply to the resistance to delamination growth at the interface between two materials.

The critical strain energy release rate was obtained using the "area method" (Broek, 1982) assuming linear elastic response. Critical energy release rate, which defines the fracture toughness, was obtained using the expression:

$$G_c = \frac{1}{b} \cdot \frac{\Delta U}{\Delta a} \tag{7.1}$$

where ΔU is the triangular area under the load-unload lines during intermittent crack growth, Δa is the extended crack length observed during the test, and b is the width of specimen. The calculated value of G_c represents the average energy consumed for the crack extension Δa. The area ΔU was computed numerically using the trapezoidal rule of integration.

The average values for G_C calculated using Eqn. (7.1) with ΔU given by the regions under each load/unload cycle No 2-8 in Figure 7.3 are presented in Table 7.2. The wide range of values in Table 7.2 reflects the inherent material variability of the foam due to its random cellular structure. Upon consideration this variability, it appears that sea water environment does not significantly degrade the value of G_{IC}. It may therefore be concluded that the observed reduction in delamination fracture toughness for the sandwich lay-up presented in Chapter 4 may not be due to any foam core material degradation but could be mostly attributed to the seawater-induced degradation of the resin rich region at interface between the facing and foam core.

Table 7.2**:** Dry and wet experimental results of foam fracture toughness G_{IC}.

Condition	**Average G_C (Front) (N/m^2)**	**Average G_C (Back) (N/m^2)**
Dry (6 specimens, 7-9 cycles each)	844	829
Dry (STD)	309	213
Wet (2 specimens, 9cycles each)	890	900
Wet (STD)	118	109

7.4 Effects of hydrostatic pressure on water ingress in PVC foam

7.4.1 Material and testing procedure

Closed cell dry foam specimens (H100) with varying thicknesses were randomly chosen to investigate the effects of hydrostatic pressure on the ingress of sea water into that material. This was achieved by immersing the above samples in sea water contained within a pressure chamber and applying various levels of hydrostatic pressure within it. The system and the confining pressure chamber are shown in Figure 7.4.

The objectives of this study were to relate water weight gain data to hydrostatic pressure, and to observe the depths of water penetration into the cellular structure. Hydrostatic pressures of 70, 140, and 280 kPa were applied within the chamber containing the immersed foam samples and weight gain data were collected at one or two day intervals until saturation was reached. Rectangular specimens 4, 8, and 12 mm thick were used to

study both weight gain and depth of water penetration. In parallel, 4 mm thick dog bone shaped specimens were used to study the effects of weight gain and hydrostatic pressure on mechanical properties.

All specimens were desiccated prior to immersion until their weights stabilized in order to establish their subsequent per-cent weight gain values upon immersion. To study water ingress into foam cells, a colored dye was mixed with the water within the pressure chamber to aid the subsequent microscopic observation of penetration depths. The samples were immersed at various levels of hydrostatic pressure until saturation. The specimen's weights were recorded both in their saturated state and again after their re-drying in an oven for 24 hours.

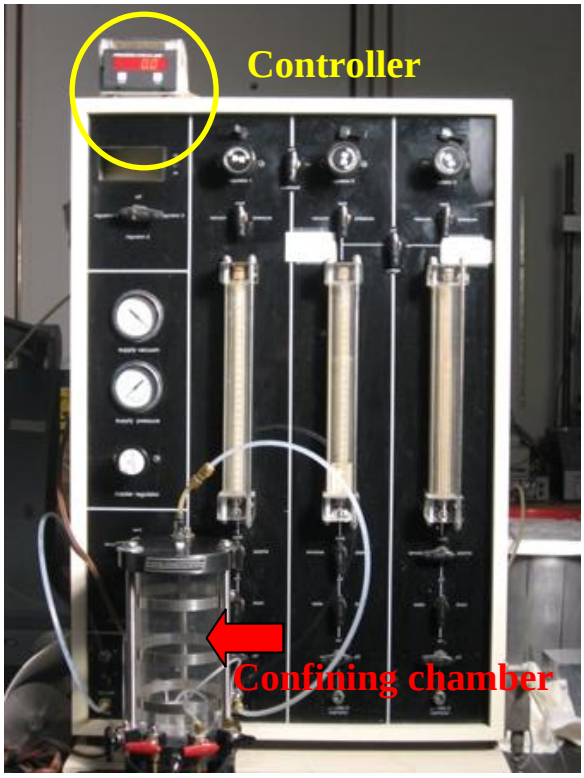

Figure 7.4: Confining pressure system.

7.5 Results and discussion

The samples of varying thicknesses (4, 8, 12 mm) were exposed to different levels of confining pressure. It was noted that only a 3-6 % increase in weight gain resulted from an additional 265 hours exposure under a pressure of 280 kPa. Typical weight gain trends are shown in Figure 7.5

Thus, an increased duration of exposure to high hydrostatic pressure does not enhance the absorption of sea water in H100 foam. However, it should be noted that the increase in confining pressure accelerated the time to saturation, despite the fact that saturation gain levels remained nearly the same for all imposed amplitudes of hydrostatic pressures (i.e, 70, 140, and 280 kPa) as listed in Table 7.3.

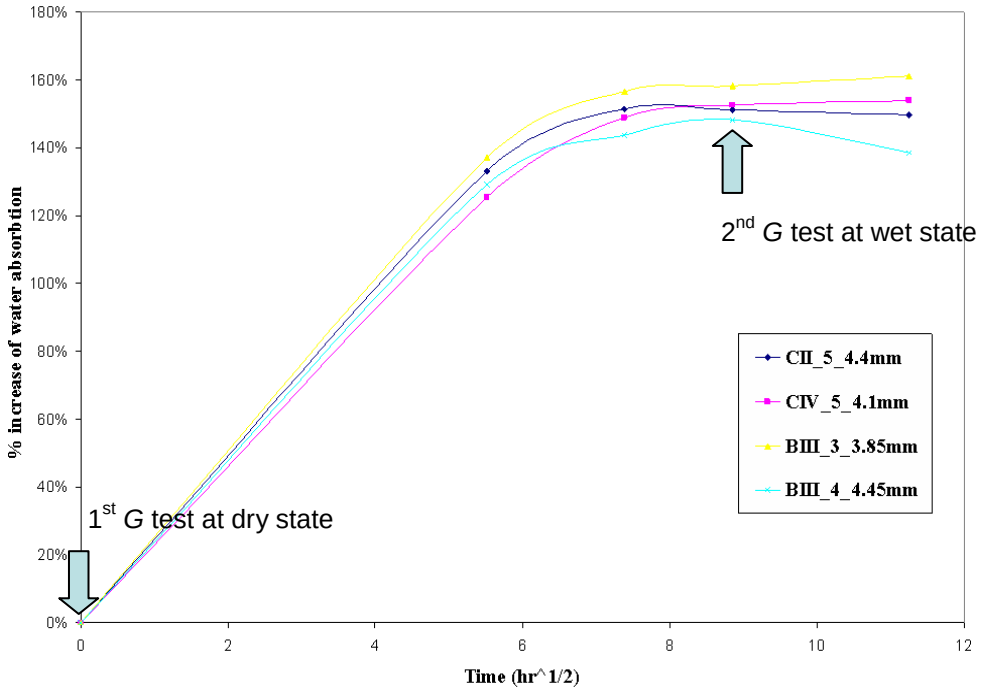

Figure 7.5: Percent weight gain data vs. Time ($hr^{1/2}$) under 140 kPa, and the corresponding stages where shear moduli *G* were obtained.

Table 7.3: The effect of confining pressure on weight gain (%) of H100 PVC foam

Pressure	Time duration to reach saturation (hr)	Max weight gain (%)
0 psi	1400	95 %
70 psi	167.5	151.4 %
140 psi	70	149 %
280 kPa	< 60	147 %

Percent weight gain of the 8 and 12 mm thick specimens was significantly lower, namely about 90% and 60% respectively, compared to the 4 mm thick specimens shown in Figure 7.6. Figure 7.7 shows almost identical results for other foam specimens of various thicknesses (4, 8, and 12 mm) after exposure to fluid for 15 days under a pressure of 280 kPa. When compared to 95% water absorption at atmospheric pressure determined in previous experiments, the weight gain of the foam under 280 kPa is considerably higher.

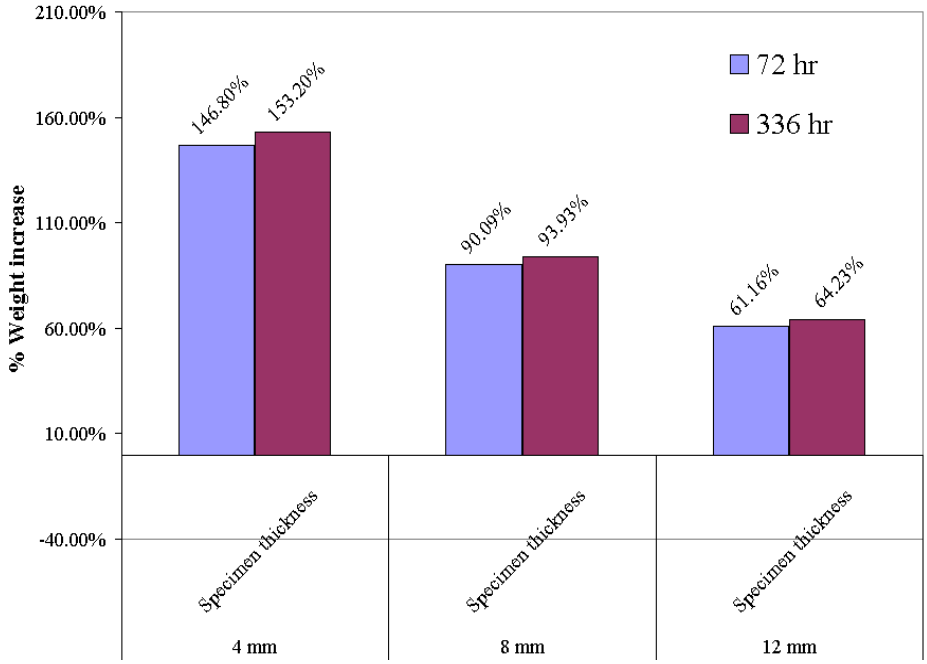

Figure 7.6: Percent increase in weight gain after immersion at pressure p = 280 kPa for 72 and 336 hours of specimens of different thickness.

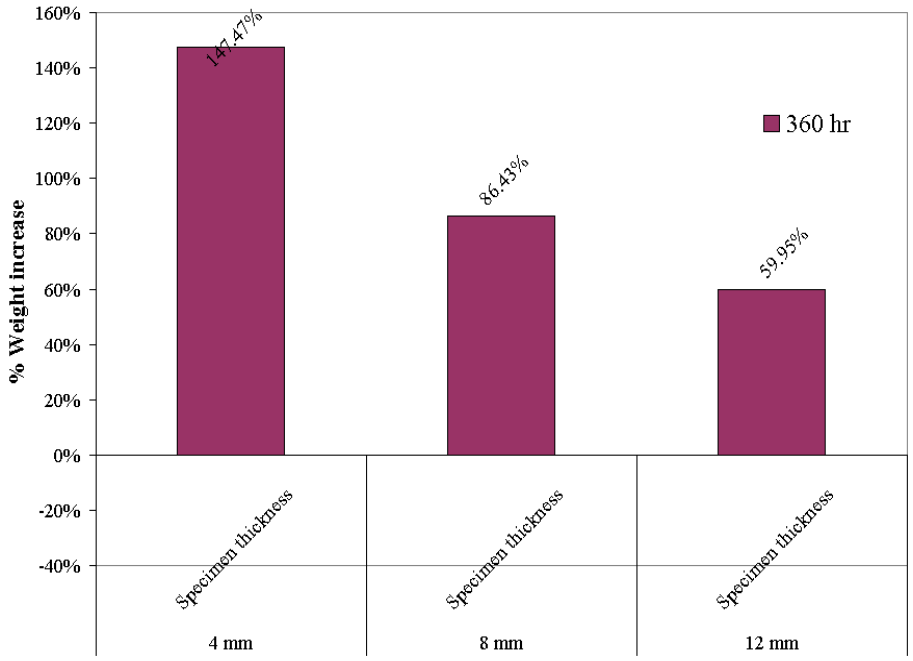

Figure 7.7: Repeated data on percent increase in weight gain after immersion at pressure p = 280 kPa for 360 hours of various thickness specimens.

It is significant to note that the equilibrium weight gain levels for the different samples are nearly linearly proportional to the ratio of their surface area to their volume. This observation is consistent with the study reported in Chapter 3 that all sea water is confined to cells adjacent to the exposed boundary. This fact was supported by microscopic observations. The penetration of sea water into H100 PVC foam was confined to a depth of δ_T between 0.6 and 0.8 mm depending on different thicknesses as shown in Figure 7.8. It appears that the depth of water penetration under a hydrostatic pressure of 280 kPa seems to have increased to 0.7-0.8 mm compared with the previously reported value of 0.2 at 0 kPa proposed in past research (Li and Weitsman, 2004). Figures 7.9 and 7.10 demonstrate repeatable results of water ingress into foam cellular structures.

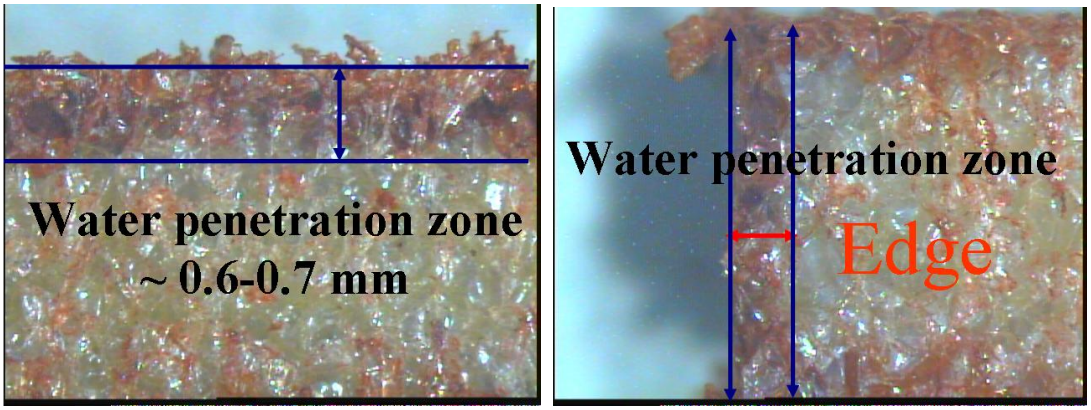

Figure 7.8: Water penetration in H100 foam cell under a microscope.

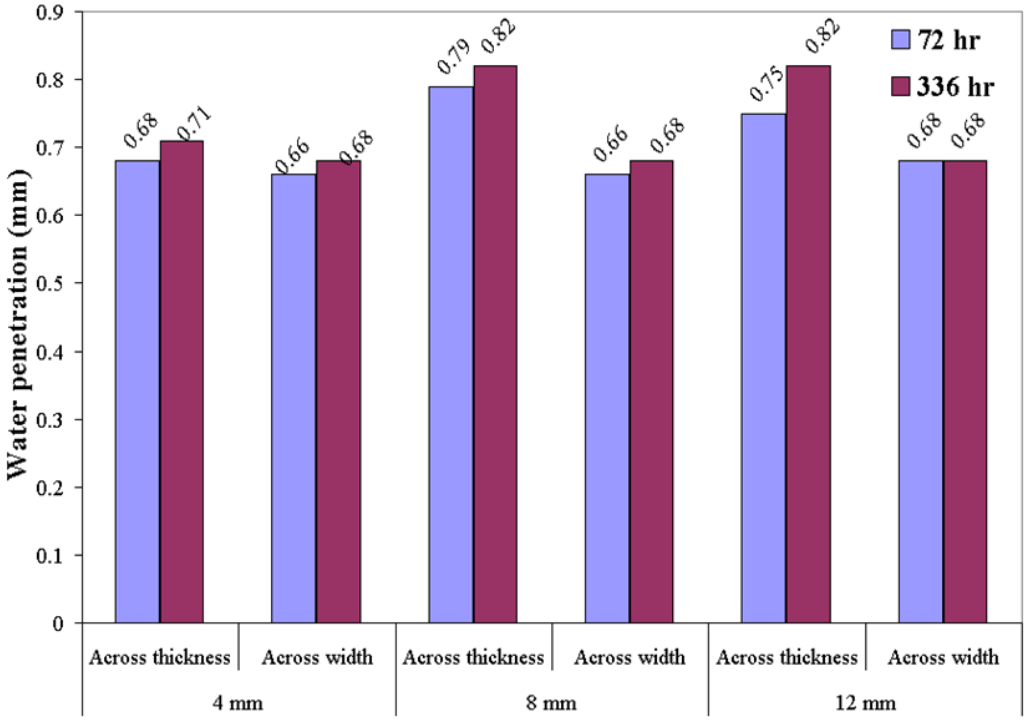

Figure 7.9: Summary of microscopic observations of depths of water penetration (mm) under 280 kPa after 72 and 336 hrs.

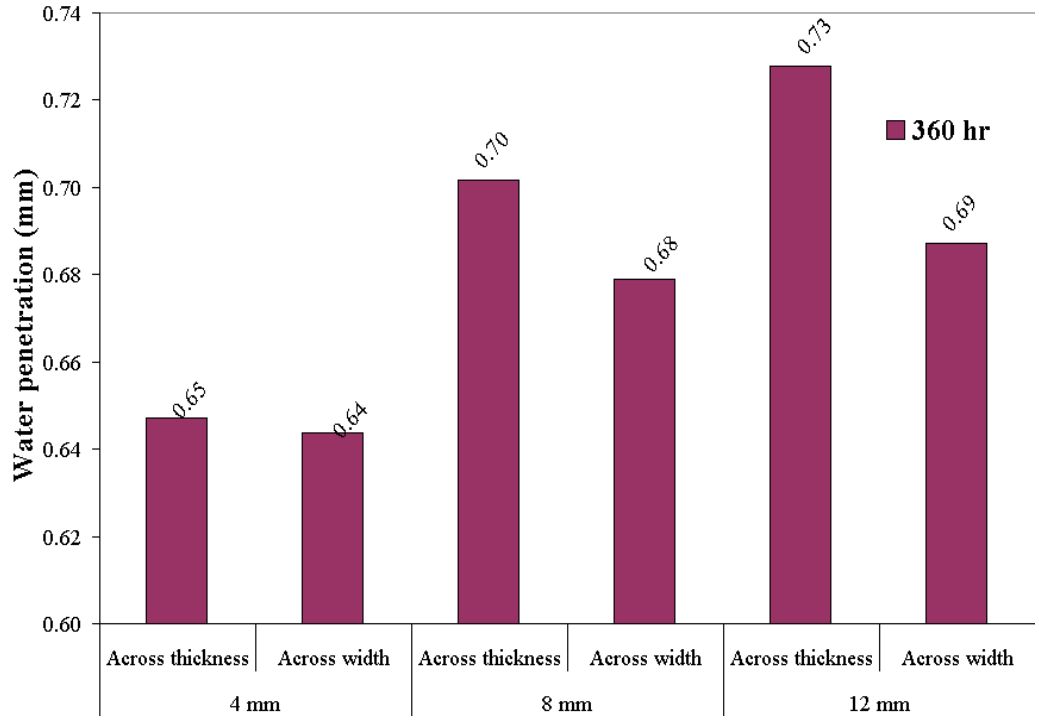

Figure 7.10: Summary of microscopic observations of depths of water penetration (mm) under 280 kPa after 360 hrs.

Shear modulus values of dry and saturated specimens were also obtained showing a reduction in shear modulus (G) of approximately 5% at saturation (Figure 7.11). The saturated specimens were subsequently placed in a freezer for 4 weeks and re-tested in shear resulting in an additional decease of 1-2% in modulus values as shown in Figure 7.11.

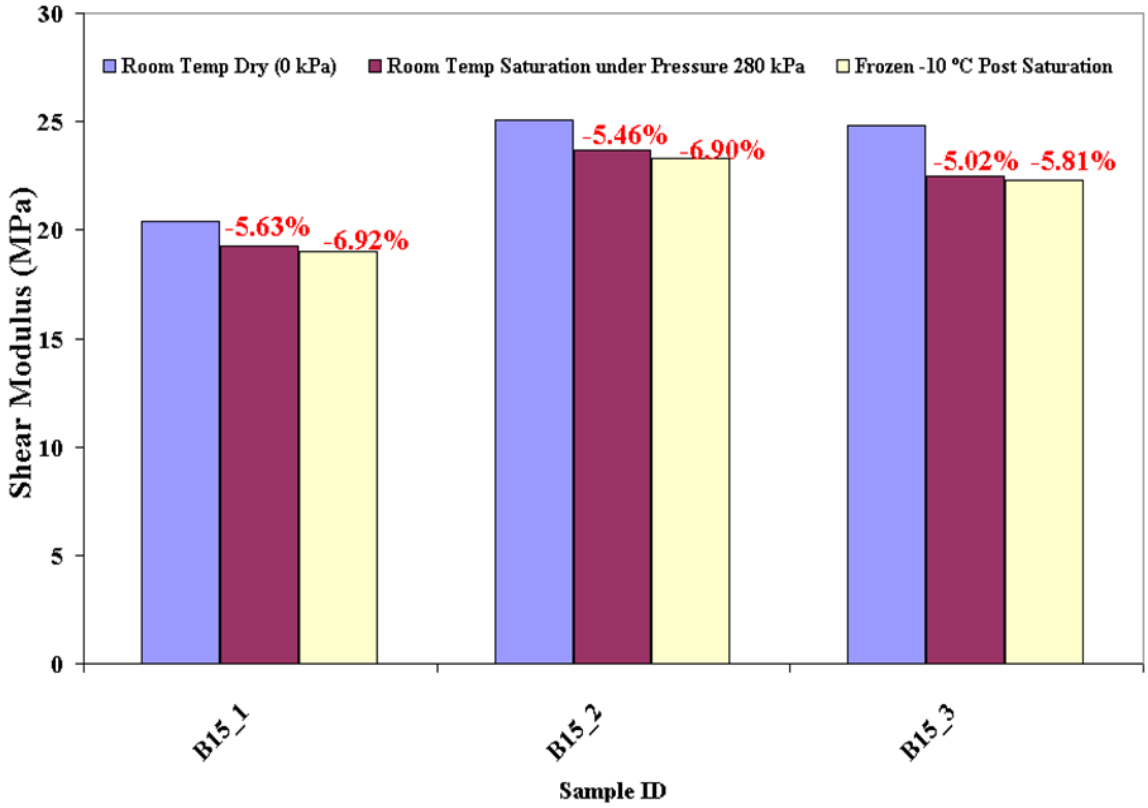

Figure 7.11: Summary G reduction before/after saturation and freezing for 4 weeks.

Recalling the plots shown in Figure 3.25, with $0.6 < \delta_T < 0.7$ mm and $0.93 < R < 0.95$ as suggested by Fig. 7.11, it follows that under a hydrostatic pressure of 280 MPa $G_w / G_{dry} \geq 1$ approximately 1.0 with a further drop to 0.99 of G_w / G_{dry} upon freezing. These results appear to be unreasonable, since in this case, Figure 3.25 shows that Eqn. (3.11) no longer applies predicting (it predicts $G_w \geq 1$ which contradicts $G_{saturated} < G_{dry}$). This is most likely due to the large variations in δ_T along the interface that do not render themselves to the simple depiction shown in Figure 3.10.

7.6 Concluding remarks

In the present study, the effect of sea water on Mode I foam fracture toughness was experimentally investigated using the modified double cantilever beam (DCB) configuration. Exposure to a sea water environment does not appear to have considerable effect on the critical strain energy release rate, G_C. From this point of view, it appears that PVC foam could well be used in sea environment.

The results of the water absorption experiments show that hydrostatic pressure can increase the amount of water uptake by up to 50%. In addition, hydrostatic pressure accelerates water ingress and increases the depth of water penetration into the cellular structure. Microscopic examination of foam cells revealed a consistent water penetration depth up to 0.7 mm along the exposed surfaces. However, in this case the excessive jaggedness of the boundary of the saturated zone does not render itself to the simplified

depiction shown in Figure 3.10 and G_w / G_{dry} can no longer be evaluated by Eqn. (3.11). It is obvious that some reduction does occur because $G_{saturated} < G_{dry}$.

CHAPTER 8

CONCLUSIONS AND FUTURE WORK

Conclusions

A Sandwich structure consists of two thin carbon fiber/vinyl ester face sheets adhesively bonded to both sides of a polymeric foam (PVC foam) core. The face sheets carry the tensile and compressive loads, while the foam core transmits shear loads and serves to hold the face sheets in positions far away from the neutral axis so as to maximize the flexural stiffness of the structure. Temperature and moisture are major environmental factors affecting the use of sandwich composites. Double cantilever beam (DCB) specimens from a sandwich panel were prepared and exposed to long-term hygrothermal conditions, and tested for delamination resistance. Extended sea water exposure was found to degrade the bond between facing and foam core, facilitating crack advance along the interface. It has been shown that the interfacial fracture toughness G_c of sandwich structure decreased by 30%. J-integral calculations employing the finite element method showed the good predictions that agree well with the aforementioned experimental results.

The shear and Young's moduli of PVC polymeric foam were tested by means of novel techniques and found to be G = 25 MPa and E = 60 MPa, respectively. Exposure to sea environment resulted in a 20% degradation under torsion but no significant reduction could be detected under tensile tests. It was noted the ingress of sea water into PVC foam was confined to the near vicinity of the exposed boundary. Therefore, the inner portions

of the materials remained dry. Consequently, shear data were much more sensitive to the presence of water since the highest shear stresses in torsion occur at the outer regions of the foam as well. An elastic analysis predicted that the shear modulus of the saturated region was reduced by up to 70%. The lesser sensitivity of the Young's modulus to the presence of water is due to the uniform distribution of tensile strain under tensile load.

Additional tests to evaluate the sensitivity of Mode I fracture toughness, G_{IC}, to the presence of water, did not show any significant effect.

Under hydrostatic pressure up to 280 kPa, it was observed that the weight gain of 4 mm thick PVC foam increased by 50 %, and the depth of water penetration increased from 0.5-0.6 to 0.7-0.8 mm when compared to ambient pressure. Moreover, the increase in confining pressure also accelerated the time to saturation, but resulted in only a slight decease in shear modulus.

Hygrothermal behavior of PVC foam at cryogenic temperature was investigated under both tension and torsion. It was found that while the tensile stiffness did not change significantly, cryogenic temperatures caused a 4-6% reduction in the shear modulus. In addition, a combination of sea water and low temperature effect showed nearly identical tensile results and a 7% degradation of shear modulus after exposure for extended periods of time.

The tensile strength and stiffness of two different laminate orientations, $[0/90]_{2s}$ and $[\pm 45]_{2s}$ of carbon composite skin facing, were evaluated at room and cryogenic temperature, as well as under a sea environment. The $[0/90]_{2s}$ and $[\pm 45]_{2s}$ facings were recorded to have approximate moduli of 80 GPa and 15 GPa, respectively, and no significant degradation due to exposure to the ocean environment. As the temperature decreased to -10 ˚C, the tensile stiffnesses of $[\pm 45]_{2s}$ tended to increase slightly (by 3-5%), but then reduced back upon returning to ambient temperature.

The effects of one-sided cyclic exposure to cross ply laminates were investigated analytically. This analysis showed that such exposure results in a cyclic variation in the curvature of the laminate, which may finally lead to failure.

The following recommendations for future work on the response of sandwich panels in sea environments may lead to the achievement of improved long-term durable marine designs.

Future work

- The effects of moisture and immersion on the fatigue life of facing materials should be investigated, especially as it was noted in some earlier studies that such effects may be quite significant.
- The combined effects of low temperatures and sea water on the fatigue life of sandwich structure still remains unknown and should be studied.
- The creep and relaxation of PVC foam may be significant factors to consider under long term loadings and should be studied.
- The environmental effects on the response of epoxy resins may be of great importance, in case such resins are to be employed in the joining of sandwich panels to each other.

REFERENCES

ABAQUS/CAE User's Manual Version 6.7, SIMULIA, 2007.

Adams, R.D. and Singh M.M. (1995), "The effect of immersion in sea water on the dynamic properties of fibre-reinforced flexibilised epoxy composites," *Composite Structures*, Vol 31, No. 2, pp. 119-127.

Anderson, T.L. (2004). "Fracture Mechanics: Fundamentals and Applications." Third Edition, (CRC).

Ashyby, M.F. (2005): "The properties of foams and lattices." *Phil. Trans. R. Soc. A*, Vol. 364, pp. 15–30.

ASTM C 273/C 273M, "Standard test method for shear properties of sandwich core materials."

ASTM D 3039 "Standard test method for tensile properties of polymer matrix composite materials."

ASTM D 5229 "Standard test method for moisture absorption properties and equilibrium conditioning of polymer matrix composite materials."

Broek, D. (1982). Elementary engineering fracture mechanics, 2nd ed. (Springer).

Camps, G.V., Carlsson, L.A., Li, X. (2000) "Factor influencing face/core debond toughness." In: Rajapakse Y.D.S, Kardomateas G.A., Birman V., editors Proceedings of 2000 ASME International Mechanical Engineering Congress and Exposition, Orlando, Florida. AD-Vol62/AMD-Vol 245, Mechanics of Sandwich Structure, p. 79-87.

Chang, T.W., Wang C.H., and Tsai, C.L. (2008). "Advancing Boundary Model for Moisture Diffusion in A Composite Laminate.: *Journal of Composite Materials*,Vol. 42, No. 10 (May 1), pp. 957-973.

Chung, D. (1994). "Carbon fiber composites." Butterworth-Heinemann, September 23.

Cox, H.L. (1952), "The elasticity and strength of paper and other fibrous materials," *British Journal of Applied Physics*, Vol. 3, pp. 72-79.

Crank, J. (1980), "The mathematics of diffusion," 2nd ed. (Oxford University Press, USA).

Cussler, E. L. (1997). "Diffusion: mass transfer in fluid systems." 2nd ed. Cambridge University Press, January 15.

Daniel, I.M. and Abot, J.L. (2000). "Fabrication, testing and analysis of composite sandwich beams," *Composites Science and Technology*, Vol. 60, No. 12-13, pp. 2455-2463.

Daniel, I.M., and Ishai, O. (2005). "Engineering mechanics of composite materials," 2nd ed. (Oxford University Press, USA).

DERAKANE (2004), "Technical Specification", Ashland Inc.

Frostig, Y. (1997). "Hygothermal (Environmental) Effects in High-Order Bending of Sandwich Beams with a Flexible Core and a Discontinuous Skin." *Composite Structures*, Vol. 37, No. 22, pp. 205-221.

Gates, T.S., Whitley, K.S., Grenoble, R.W., and Bandorawalla, T. (2003). "Thermal/mechanical durability of polymer-matrix composites in cryogenic environments." In *44th AIAA/ASME/ASCE/AHS/ASC Structures, Structural Dynamics, and Materials Conference, Apr 7-10 2003*, 3:1783-1794. Collection of Technical Papers - AIAA/ASME/ASCE/AHS/ASC Structures, Structural Dynamics and Materials Conference. American Inst. Aeronautics and Astronautics Inc.

Gin-Boay C., Leong-Keey S., and Lee-Soon C. (1999), "Stress distribution in sandwich beams under tension," *Composite Structure 45* 195-204, no. 3: 195-204.

Gopalan, R., Rao, R.M.V.G.K., Murthy, M.V.V., and Dattaguru, B. (1986). "Diffusion Studies on Advanced Fibre Hybrid Composites." *Journal of Reinforced Plastics and Composites*, Vol. 5, No. 1 (January 1), pp. 51-61.

Grant, T. S., and Bradley, W.L. (1995). "In-Situ Observations in SEM of Degradation of Graphite/Epoxy Composite Materials due to Seawater Immersion." *Journal of Composite Materials*, Vol. 29, No. 7 (May 1), pp. 852-867..

Harper, B.D. (1987). "The effects of moisture induced swelling upon the shapes of anti-symmetric cross-ply laminates." *Journal of Composite Materials*, Vol. 21, No. 1 (January 1), pp. 36-48.

Ionita, A., and Y.J. Weitsman. (2007). "A model for fluid ingress in closed cell polymeric foams," *Mechanics of Materials*, Vol. 39, No. 5, pp. 434-444.

Kang, S.G, Kim M.G., and Kim, C.G. (2007). "Evaluation of cryogenic performance of adhesives using composite-aluminum double-lap joints." *Composite Structures*, Vol. 78, No. 3 (May), pp. 440-446.

Kelly A. (1994). Concise encyclopedia of composite materials, Rev Sub. (Pergamon).

Kim, M.G., Kang S.G., Kim, C.G., and Kong, C.W. (2007) "Tensile response of graphite/epoxy composites at low temperatures," *Composite Structures*, Vol. 79, No. 1 (June), pp. 84-89.

Kim, M.G., Kang, S.G., Kim, C.G., and Kong, C.W (2008). "Thermally induced stress analysis of composite/aluminum ring specimens at cryogenic temperature," *Composites Science and Technology*, Vol. 68, No. 3-4 (March), pp. 1080-1087.

Kolat, K., Neser, G., and Ozes, C. (2007): 'The effect of sea water exposure on the interfacial fracture of sandwich systems in marine use," *Composite Structures*, Vol 78, No. 1 (March), pp. 11-17.

Kootsookos, A., and Mouritz A.P. (2004). “Seawater durability of glass- and carbon-polymer composites.” *Composites Science and Technology*, Vol. 64, No. 10-11 (August), pp. 1503-1511.

Kuhn, P. (1956). Stresses in aircraft and shell structures.

Lee, M.C. and Peppas, N.A. (1993). “Models of Moisture Transport and Moisture-Induced Stresses in Epoxy Composites.” *Journal of Composite Materials*, Vol. 27, No. 12 (January 1), pp. 1146-1171.

Li, X. (2000). “Debonding fracture of foam core sandwich structure.” Ph.D. Dissertation, Department of Mechanical Engineering, Florida Atlantic University.

Li, X., and Carlsson L.A. (1999). “The tilted sandwich debond (TSD) specimen for face/core interface fracture characterization.” *Journal of Sandwich Structures and Materials*, Vol. 1, No. 1, pp. 60-75.

Li, X., and Weitsman, Y.J., (2004): “Sea water effects on foam cored composite sandwich layups,” *Composites, Part B.*, Vol. 35, pp. 451-459.

Megson, T.H.G (1999). Aircraft structures for engineering students.

Mouritz, A.P., Kootsookos, A., Mathys, G. (2004). "Stability of polyester- and vinyl ester-based composites in seawater." *Journal of Materials Science*, Vol. 39, No. 19, pp. 6073-6077.

Nordin, C.P. (2008). “Effect of combined loading and low-temperature on the stiffness of GFRP laminates.” Master. Thesis, Department of Civil and Environmental Engineering, University of Tennessee, Knoxville.

Papanicolaou G.C. and Bakos D. (1996): “Interlaminar fracture behaviour of sandwich structures,” *Composites Part A: Applied Science and Manufacturing*, Vol. 27, No. 3, pp. 165-173.

Penumadu, D., Weitsman, Y.J., and Siriruk, A. (2007). "Effect of Sea Water on Interfacial Delamination Behavior of Sandwich Layups." *16th International Conference on Composite Materials*, July 8 – 13, Kyoto, Japan.

Prasad, S., and Carlsson L.A. (1994). "Debonding and crack kinking in foam core sandwich beams--I. Analysis of fracture specimens." *Engineering Fracture Mechanics*, Vol. 47, No. 6 (April), pp. 813-824.

Prasad, S., and Carlsson L.A. (1994). "Debonding and crack kinking in foam core sandwich beams--II. Experimental investigation." *Engineering Fracture Mechanics*, Vol.47, No. 6 (April), pp. 825-841.

Rice J.R. (1968). "A Path-independent Integral and The Approximate Analysis of Strain Concentration by Notches and Cracks." Trans ASTME, Ser. D *Journal of Mech*. Vol. 35, pp. 379-385.

Roy, S., Xu, W., Patel, S., and Case, S. (2001). "Modeling of moisture diffusion in the presence of bi-axial damage in polymer matrix composite laminates." *International Journal of Solids and Structures*, Vol. 38, No. 42-43 (October), pp. 7627-7641.

Sala, G. (2000). "Composite degradation due to fluid absorption." *Composites Part B: Engineering*, Vol. 31, No. 5 (July): pp. 357-373.

Selvarathinam, A. and Weitsman Y.J. (1998). "Transverse cracking and delamination in cross-ply gr/ep composites under dry, saturated and immersed fatigue." *International Journal of Fracture*. Vol 91, No. 2 (May 1), pp. 103-116.

Shen, C.H., and Springer, G.S. (1977). "Moisture Absorption and Desorption of Composite Materials." *Journal of Composite Materials*. Vol. 10, No. 1 (January 1), pp. 2-20.

Shen, C.H., and Springer, G.S. (1977). "Environmental Effects on the Elastic Moduli of Composite Materials." *Journal of Composite Materials*, Vol. 11, No. 3 (July 1), pp. 250-264.

Shivakumar, K.N., Swaminathan, G., and Sharpe, M. (2006). "Carbon/Vinyl Ester Composites for Enhanced Performance in Marine Applications." *Journal of Reinforced Plastics and Composites*, Vol. 25, No. 10 (July 1), pp. 1101-1116.

Siriruk, A., Penumadu, D., and Weitsman, Y.J. (2008). "Effect of sea environment on interfacial delamination behavior of polymeric sandwich structures," *Composites Science and Technology*.

Siriruk, A., Penumadu, D., and Weitsman, Y.J. (2008). "Effect of sea water on mechanical properties of polymeric foam and sandwich composites" *8th International Conference on Sandwich Structures*, FEUP, Porto, Portugal.

Siriruk, A., Weitsman, Y.J., and Penumadu, D. (2008). "Polymeric foams and sandwich composites: Material properties, environmental effects, and shear-lag modeling," *Composites Science and Technology*.

Swaminathan, G., Shivakumar, K.N., and Sharpe, M. (2006). "Mechanical properties of glass and t700 carbon vinyl ester composites." *Journal of Advanced Materials*, Vol. 38, No. 2.

Timoskenko S.P. and Goodier J.N (1951). "Theory of elasticity." 2nd Edition, McGraw Hill, New York.

Tucker, W.C. and Brown, R. (1989): "Moisture absorption of graphite/polymer composites under 2000 feet of seawater." *Journal of Composite Materials*, Vol. 23, No. 8, pp. 787-797.

Upadhyay, P.C., and Prucz, J. (1992). “Parametric damage modelling of composites due to moisture absorption.” *Journal of Reinforced Plastics and Composites*, Vol 11, No. 2 (February), pp. 198-210.

Wan, Y.Z., Wang, Y.L., Luo, H.L., Dong, X.H., and Cheng, G.H. (2002). “Moisture absorption behavior of C3D/EP composite and effect of external stress.” *Materials Science and Engineering A*, Vol. 326, No. 2 (March 31), pp. 324-329.

Weitsman, Y. J. and M. Elahi (2000). "Effects of fluids on the deformation, strength and durability of polymeric composites - an overview." *Mechanics Time-Dependent Materials*, Vol. 4, No. 2, pp. 107-126.

Weitsman, Y.J. (1976). “Diffusion With Time-Varying Diffusivity, With Application to Moisture-Sorption in Composites.” *Journal of Composite Materials* , Vol. 10, No. 3 (July 1), pp. 193-204.

Weitsman, Y.J. (2000). "Effects of fluids on polymeric composites—A review." *Comprehensive composite materials, polymer matrix composites*, Vol. 2, R. Talreja and J.-A. E. Manson, eds., Elsevier Science, New York, pp. 369–401. Oxford, Pergamon.

Weitsman, Y.J. (2006). “Anomalous fluid sorption in polymeric composites and its relation to fluid-induced damage.” *Composites Part A: Applied Science and Manufacturing*, Vol. 37, No. 4 (April), pp. 617-623.

Weitsman, Y.J., and Guo, Y.J. (2002). “A correlation between fluid-induced damage and anomalous fluid sorption in polymeric composites.” *Composites Science and Technology*, Vol. 62, No. 6 (May), pp. 889-908.

Weitsman, Y.J., Siriruk, A., and Penumadu, D. (2007). “Sea Water Effects on Polymeric Composites: Comparative Study” *16th International Conference on Composite Materials*, July 8 – 13, Kyoto, Japan.

Wiesenburg, D.A. and Little, B.A. (1987): “A synopsis of the chemical/physical properties of sea water” *Ocean Physics and Engineering*, Vol. 12, pp. 127-165.

Wood, C.A., and Walter, L.B. (1997). “Determination of the effect of seawater on the interfacial strength of an interlayer E-glass/graphite/epoxy composite by in situ observation of transverse cracking in an environmental SEM.” *Composites Science and Technology*, Vol. 57, No. 8, pp. 1033-1043.

APPENDICES

Appendix 1: Summary of H100 foam core characterization

Property	Foam	Dimension
Longitudinal modulus, *E* (Dry)	60	MPa
Longitudinal modulus, *E* (Wet) due to sea water*	22	MPa
Shear modulus, *G* (Dry)	25	MPa
Shear modulus, *G* (Wet) due to sea water*	7.3-23	MPa
Shear modulus, *G* (Wet) due to combined sea water and low temperature	22	MPa
Shear modulus, *G* (Wet) due to hydrostatic pressure*	23	MPa
Shear modulus, *G* (Wet) due to hydrostatic pressure and low temperature*	22	MPa
Coefficient of thermal expansion, α	70	$\mu\varepsilon/^{\circ}C$
Moisture expansional strain at saturation, ε_H	2200	$\mu\varepsilon$ at saturation
Poisson's ratio, *v* (Dry)	0.13	
Poisson's ratio, *v* (Wet)	0.50*	

* Implied from data by means of analysis

Appendix 2: Summary of carbon reinforced vinyl ester facing characterization

Property		Dimension
Longitudinal modulus E of $[0/90]_{2s}$	80	GPa
Longitudinal modulus E of $[\pm 45]_{2s}$	15	GPa
Longitudinal modulus E of $[0/90]_{2s}$ due to sea water	80	GPa
Longitudinal modulus E of $[\pm 45]_{2s}$ due to sea, tap, distilled water	15	GPa
Longitudinal modulus E of $[\pm 45]_{2s}$ at -15 ˚C	16	GPa
Coefficient of thermal expansion, α	11.5	με/˚C
Moisture expansional strain at saturation, ε_H	450	με at 0.5 % saturation wt gain

Vita

Akawut (O) Siriruk was born in Nakhonrajsima, Thailand on July 17, 1980. Following high school, he enrolled at Kasetsart University in Bangkok and received a Bachelor of Engineering degree in Civil Engineering in 2001. He attended the University of Dayton, Ohio in 2002 and received a M.S in Civil Engineering with a structural emphasis in 2004. In 2005, Akawut started to pursue a Ph.D degree in Civil Engineering at University of Tennessee under the supervision of Dr. Penumadu and Dr. Weitsman. He obtained his doctoral degree in May 2009. Upon completion of Ph.D he intends to continue post-doctoral research at U.T., directed by Dr. Penumadu and Dr. Weitsman.